Journal of Energy

ISSN 1849–0751 (On–line)
ISSN 0013–7448 (Print)
UDK 621.31
https://doi.org/10.37798/EN2024733

VOLUME 73 Number 3 | 2024

ENERGIJA

Journal of Energy

Scientific Professional Journal Of Energy, Electricity, Power Systems
Online ISSN 1849–0751, Print ISSN 0013–7448, VOL 73
https://doi.org/10.37798/EN2024733

Published by
HEP d.d., Ulica grada Vukovara 37, HR–10000 Zagreb
HRO CIGRÉ, Berislavićeva 6, HR–10000 Zagreb

EDITORIAL

The paper “Testing of Insulation Systems in Accelerated Aging Conditions” outlines the test procedure for insulation systems in electrical rotating machines with form wound windings. The study compares reference and candidate insulation systems by simulating accelerated aging to evaluate their reliability. The tests were performed with reduced coil models placed in stator core simulators. The thermal evaluations include thermal aging, capacitance and insulation resistance measurements, partial discharge detection, mechanical stress, moisture exposure and dielectric strength tests. The tests continue until all Formette coils in a test object fail. Subsequent IEC 60034-18-42 tests include insulation tests on the main wall to determine the electrical life curve, while interturn insulation results are derived from previous tests. The voltage stress control system will also be evaluated. While the preliminary results provide insight, further testing is required for final conclusions.

The second paper, “Development of Electrolyser Projects for Production of Renewable Hydrogen«,” examines electrolyser plants from a technical, environmental and regulatory perspective and highlights the key challenges in their implementation. The paper discusses the additional complexity and safety risks associated with installations beyond the electrolyser stack, such as rectifiers, cooling systems, water demineralization units, and high-pressure tanks. From an environmental perspective, green hydrogen can significantly reduce greenhouse gas emissions. However, blending with natural gas is associated with technical difficulties and uncontrolled leakage of hydrogen is a concern. The paper also provides an overview of existing electrolysis projects and development plans and argues for locally adapted solutions rather than replicating one-size-fits-all solutions for all regions.

The third paper, “Evaluation and Modelling the Performance of Rice Husk Gasifier Cook Stove for Household Energy Use” evaluates the Belonio type rice husk gasifier cook stoves as sustainable energy sources and waste management solutions for Ethiopian households. Biomass gasification is a promising technology for developing countries like Ethiopia as it is easy to build, install and operate. The study compares the performance of insulated and non-insulated rice husk gasifiers, focusing on fuel consumption, water boiling tests and thermal efficiency. Non-insulated stoves produced a higher maximum flame temperature and a higher average temperature than insulated stoves. Operating time significantly affected fuel consumption, gasification rate and combustion zone rate. The maximum fuel consumption was higher for non-insulated furnaces. The study found that non-insulated stoves produced more biochar per rice husk. A multiple regression analysis showed that the cubic polynomial model most accurately predicted the relationship between time, temperature and heat energy.

The article “Review of Supercapacitor Equivalent Circuit Models” provides a systematic overview of five commonly used equivalent circuit models for supercapacitors. It compares three predominant types and discusses the metrics used to determine the parameters of the supercapacitor model. The models discussed include the RC model, the »classical« model, the simplified theoretical model, the Zubieta-Bonert model and the Tironi-Musolino model. The literature review shows that the models or their variations are often referred to by different names and that the criteria for model comparisons are inconsistent and poorly defined. The model parameters are usually determined by experimental measurements, but the lack of data makes it difficult to evaluate the accuracy of the models.

Finally, the paper “Impact of Climate Change on Transmission System Operator Assets: Experiences from Croatia and the Need for a Resilience Plan” discussed the impact of two consecutive storms in July 2023 that severely affected the Croatian transmission grid. A total of 59 overhead lines were shut down and 51 transmission towers were damaged. To restore the affected grid, 22 modular emergency power pylons were deployed. The article provides an overview of climate change forecasts in Croatia. It assesses whether the current requirements for new overhead lines need to be revised and emphasizes the need to create resilience mechanisms to withstand the effects of climate change and global warming. Based on experience, the paper offers lessons learned and recommendations for improving resilience and preparing for future extreme weather events.

Igor Kuzle
Editor–in–Chief

Journal of Energy
VOLUME 73 Number 3 | 2024
journal homepage: http://journalofenergy.com/

Testing of Insulation Systems in Accelerated Aging Conditions

Slaven Nađ, Josip Treger, Stjepan Car

***Summary* — The paper describes the testing procedure of the insulation system of electrical rotating machines with form-wound windings in accordance with the standards IEC 60034-18-31 and IEC 60034-18-42. Testing is based on a comparison of reference insulation system which has given satisfactory service experience and candidate insulation system which is intended to be used instead of existing insulation system. To prove or disprove the reliability of candidate systems in reasonable time, the accelerated aging test is carried out, considering various factors that reduce the life of the insulation system in greater or lesser extent: heat, exposure to mechanical vibrations and moisture (according to IEC 60034-18-31) and voltage (according to IEC 60034-18-42). In order to save materials and easier handling of test samples, tests are carried out on reduced models of coils (so-called formette coils) that are placed in frames imitating the stator core. The purpose of the test is to verify the potential contributions of a new impregnating resin, as well as the addition of nanoparticles in a new impregnating resin in a condition of increased voltage stress due to machine connection to the grid via frequency converter. In addition to the test procedure, the paper presents the results obtained so far.**

***Keywords* — insulation system, electrical rotating machines, form-wound winding, thermal classification, life curve, formette**

I. Introduction

As a part of research project named "Development of submerged aggregate for small hydroelectric power plant with low water head" launched in 2020 in Končar – Generators and motors, investigation of generator insulation system, which is vital part of submerged unit, is taking a place. Overall insulation system of generator is consisting of mica-based mainwall and inter-turn insulation. The voltage stress control system is performed in two variants: with just a conductive slot-part layer or with both a conductive slot-part layer and a semi-conductive layer in the end-winding region. Conductive layer is based on glass fabric impregnated with an electrically conductive varnish, while semi-conductive layer consists of polyester fabric, impregnated with a silicon carbide. Rated voltage is 690 V. Due to fact that generator is connected to grid via frequency converter with impulse repetition rate 2 kHz and impulse rise time equal 0,12 μs, insulation system will be exposed to higher voltage stress in comparison with insulation system of directly grid connected generator. In order to ensure capability of withstanding higher voltage stress and better thermal conductivity of insulation system, new polyamide-based impregnating resin is applied as well as the addition of nanoparticles in new impregnation resin [1], [2]. Main purpose of this research is to determine the influence of those two new elements to the insulation system lifetime comparing existing end new insulation system. To achieve reliable results of comparison in reasonable time, accelerated aging tests are performed with purpose to consider factors which can reduce the lifetime of insulation systems in a greater or lesser extent: heat, mechanical vibrations, humidity (in accordance with IEC 60034-18-31 standard) and voltage (in accordance with IEC 60034-18-42 standard).

(Corresponding author: Slaven Nađ)

Slaven Nađ, Josip Treger and Stjepan Car are with the Končar - Generators and Motors Ltd., Zagreb, Croatia (e-mails: snad@koncar-gim.hr, jtreger@koncar-gim.hr, scar@koncar-gim.hr)

II. Thermal Evaluation and Classification of Insulation Systems

A. Introduction

Thermal evaluation and classification of insulation systems is carried out in accordance with IEC 60034-18-31:2012 [3] and some practical solutions form [4]. Object of testing is insulation systems with form-wound windings used in rotating electrical machines in conditions of accelerated thermal ageing. Test procedure is based on comparison between existing insulation system, which gave reliable service life (so-called "reference insulation system") and new insulation system which is intended to replace the existing insulation system (so-called "candidate insulation system"). Reference and candidate system are compared under the same test conditions.

Testing is performed on coils with shorten slot-part (so-called "formette coils" – figure 1) which are inserted in special frame (so-called "formette frame") which simulates stator core. Formette coils with formette frame constitute the test object - formette.

Fig. 1. Coil with shorten slot part – so-called "formette coil"

Slaven Nađ, Josip Treger, Stjepan Car, Testing of Insulation Systems in Accelerated Aging Conditions, Journal of Energy, vol. 73 Number 3 (2024), 3–8
https://doi.org/10.37798/2024733517

In this specific case, test object consists of 5 complete formette coils and 8 half-formette coils (coil legs with shorten slot part) which is intendent to fill the empty upper/lower layers as shown on picture 2. All provided test procedures are performed on complete formette coils which are not electrically connected between themselves. Purpose of half-formette coils is to provide fixture of complete formette coils and imitation of real condition in stator core.

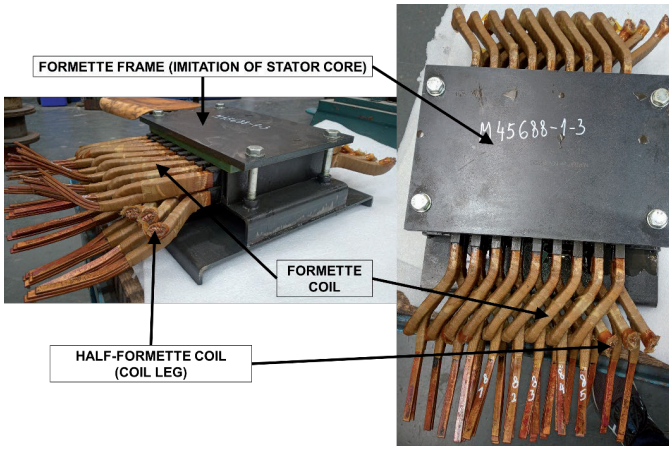

Fig. 2. Test object (formette) and its main parts

Sequence of test procedure is shown on figure 3. At the beginning of test procedure, first step is so-called "zero-cycle" or "initial diagnostic cycle" which has a purpose to determine initial state of insulation system. It considers test of mainwall and inter-turn insulation which is following with informative tests (measuring of capacitance, insulation resistance and possible occurrences of partial discharges). After successful implementation of zero-cycle, next step is cycle which consist of series of sub-cycles: thermal aging, informative tests (measuring of capacitance, insulation resistance and possible occurrences of partial discharges), mechanical stress, exposure to moisture and diagnostic sub-cycle (voltage withstand test of mainwall and inter-turn insulation). The specified cycle is repeated until insulation breakdown on all formette coils is recorded in diagnostic sub-cycle, which means end of testing. Insulation system is intended for thermal class H (180 °C).

Thermal evaluation and classification of insulation systems will be carried out on 6 different insulation systems shown in table 1. Insulation systems 1 and 2 are references, while systems 3-6 are candidates.

TABLE I:

INSULATION SYSTEMS PREPARED FOR TESTING

No.	Voltage stress control system	Impregnating resin	Insulation system
1	Only conductive	Existing	Reference
2	Conductive and semiconductive		
3	Only conductive	New	Candidate
4	Conductive and semiconductive		
5	Only conductive	New + nanoparticles	Candidate
6	Conductive and semiconductive		

B. THERMAL AGEING

Sub-cycle of thermal ageing is conducted at three different temperatures. For thermal class H, in accordance with standard [3], temperatures are following: 200 °C, 220 °C and 240 °C. Thermal aging time is reverse proportional to aging temperature. From proposed interval following aging times are chosen:

- 29 days for temperature 200 °C
- 8 days for temperature 220 °C
- 2 days for temperature 240 °C

Each of the listed insulation systems in table 1 is tested at the three specified temperatures with the corresponding exposure time using one test object (formette coils + formette frame) per temperature and per insulation system, which means that a total of 18 test objects - formettes required for testing.

An oven (figure 4) is used to heat the test objects in a way that all parts of the insulation system are equally exposed to the selected aging temperature, which was controlled on the oven control device screen during the entire exposure time and was kept at a

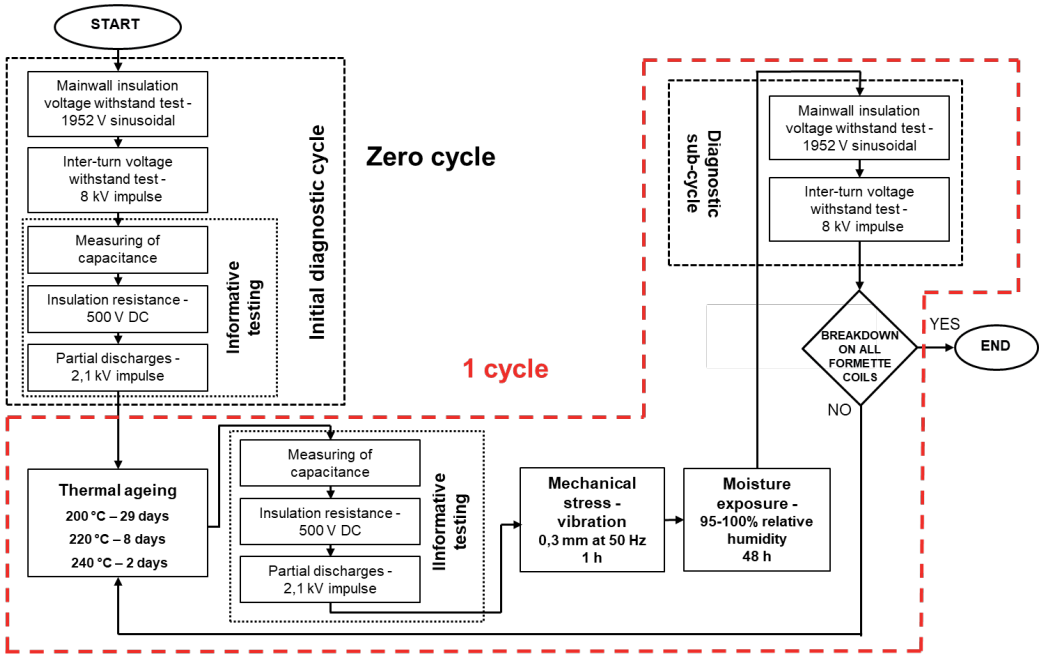

Fig. 3. Sequence of test procedure for thermal evaluation and classification of insulation systems

Slaven Nad, Josip Treger, Stjepan Car, Testing of Insulation Systems in Accelerated Aging Conditions, Journal of Energy, vol. 73 Number 3 (2024), 3–8
https://doi.org/10.37798/2024733517

constant interval of ± 3 K.

The sub-cycle of thermal aging of the test objects begins when the calibrated temperature detector reaches the aging temperature, while the end of the cycle represents turning off the oven and opening the door to cool the test objects to the ambient temperature. After cooling down the test objects, a sub-cycle of informative tests follows.

Fig. 4. Oven for thermal aging (left) and test objects inside of the oven (right)

C. Informative tests

Non-destructive informative tests are carried out after the thermal aging sub-cycle. They consist of the following tests:

- Measuring of insulation resistance 500 V DC, according to standard [5]
- Measuring of capacitance
- Partial discharge measurement with impulse voltage 2,1 kV according to standard [6]

D. Exposure to mechanical vibrations

After conducting informative tests, the test objects are exposed to mechanical stress at room temperature without applying voltage.

Each test object is mounted on a horizontal shaking table (figure 5) and subjected to oscillation at 50 Hz. The movements of the vibrating table are in the direction normal to the plane of the test specimens so that the coil ends will vibrate radially, which is consistent with the end winding forces that typically occur on an actual rotating machine. The peak-to-peak vibration amplitude value is about 0,3 mm.

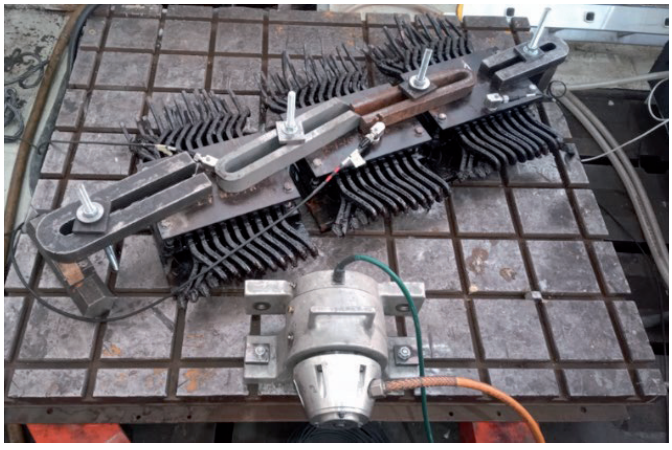

Fig. 5. Horizontal shaking table with test objects

E. Exposure to moisture

After mechanical conditioning, test objects are exposed to moisture. A visible and continuous moisture deposit is achieved by enclosing the test object in a condensation chamber (figure 6). Each test object is exposed to moisture for 48 hours, with temperature range 25°C ± 10°C. According to IEEE standard [7] which deal with the same test, the requirement for relative humidity is 95-100 %.

Fig. 6. Condensation chamber with (left) and without (right) cover

F. Diagnostic sub-cycle

Diagnostic sub-cycle is based on elevated voltage withstand tests which are used for check condition of the specimens and to determine the end of test life. The test is performed immediately after the end of the moisture exposure cycle, while the test objects are still wet.

Each part of the insulation system is tested separately to identify location that may contain cracks and/or separation of layers caused by thermal aging and mechanical stress. The voltage was applied as follows:

- Between the test specimens and the frame - **test of mainwall insulation** - voltage waveform: sinusoidal, amplitude: 1952 V, frequency: 50 Hz, duration: 1 min
- Between turns of test specimen - **inter-turn insulation test** - voltage waveform: impulse, amplitude: 8 kV, impulse rise time: 0,2 ± 0,1 μs, duration: 1 min

After completion of diagnostic sub-cycle, one complete cycle ends and the next one begins in the same sequence of sub-cycles: thermal aging, informative tests (measuring of capacitance, insulation resistance and possible occurrences of partial discharges), mechanical stress, exposure to moisture and diagnostic sub-cycle (voltage withstand test of mainwall and inter-turn insulation) until a breakdown is determined on all formette coils that consist one test object, which designate the end of the test.

G. First results

Since this is a long-term testing, only part of the results is available. Thermal aging at the highest temperature (240 °C) started first, because it takes the shortest time. Despite that fact, the test on highest temperature is still ongoing, and the results obtained so far are shown in table 2. The change of capacity and insulation resistance through the cycles measured as part of informative tests is shown in figures 7 and 8. Partial discharges with impulse voltage of 2,1 kV were not recorded in any cycle.

Slaven Nad, Josip Treger, Stjepan Car, Testing of Insulation Systems in Accelerated Aging Conditions, Journal of Energy, vol. 73 Number 3 (2024), 3–8
https://doi.org/10.37798/2024733517

TABLE II:

THE RESULTS OF THERMAL AGEING CARRIED OUT SO FAR AT 240 °C

No.	Total completed cycles	The number of cycle in which the failure was recorded					90% - CONFIDENCE LIMIT OF FAILURE OCCURRENCE					
		No. of formette coil					5% - value		MEDIAN		95% - value	
		1	2	3	4	5	*No. of cycles*	*Hours*	*No. of cycles*	*Hours*	*No. of cycles*	*Hours*
1	**21**	20	19	21	19	20	19	912	**20**	**960**	20,8	998,4
2	**21**	21	21	21	19	18	18,2	873,6	**21**	**1008**	21	1008
3	**21**	15	21	21								
4	**21**					18						
5	**18**	18	18	18	18	18	18	864	**18**	**864**	18	864
6	**20**	20				17						

Testing at the highest temperature (240 °C) was completed for insulation systems 1, 2, and 5 because breakdown occurred on all formette coils. Failure is determined on each formette coil separately, so table 2 shows the median and 90% confidence limit of failure occurrence for each insulation system. According to the test results obtained so far, insulation system 1 (reference) and insulation system 5 (candidate) can be tentatively compared. Comparing their confidence intervals and medians (table 2), it is evident that the reference insulation system (No. 1) withstood more cycles of exposure to heat compared to the corresponding candidate system (No. 5), but for a final conclusion, test needs to be carried till the end, which means breakdown of all formette coils of insulation systems 3, 4 and 6. After that, it is necessary to carry out the same test for lower temperatures (220 and 200 °C) with appropriate thermal aging times and make a mutual comparison of the corresponding reference (1 and 2) and candidate insulation systems (3-6).

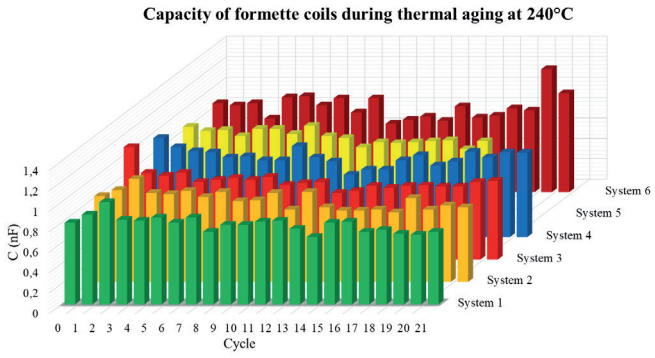

Fig. 7. Change of formette coils capacity during thermal aging cycles implemented so far at 240 °C

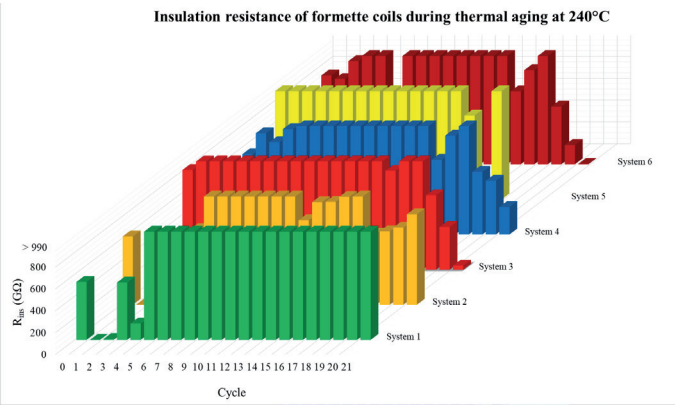

Fig. 8. Change of formette coils insulation resistance during thermal aging cycles implemented so far at 240 °C

If the insulation systems capacity (determined as the median of five formette coils for each system) is observed during the thermal aging cycles (Figure 7), a slight drop in capacity can be observed as the cycles progress. A similar occurrence happens with the insulation resistance, which is also represented by the median of five formette coils per insulation system. At the very beginning, the resistance is lower, after which it reaches a level that exceeds the measuring range of the instrument (indicated in Figure 8 with > 990 GΩ). This phenomenon can be attributed to the additional curing of the insulating layers during heating to a temperature higher than the temperature class. Around the fifteenth cycle, the majority of insulation systems experience a drop in resistance. That tendency continues in the following cycles, and the final result is the breakdown of certain formette coils.

Slaven Nad, Josip Treger, Stjepan Car, Testing of Insulation Systems in Accelerated Aging Conditions, Journal of Energy, vol. 73 Number 3 (2024), 3–8
https://doi.org/10.37798/2024733517

III. Testing of Insulation Systems According to Standard IEC 60034-18-42

A. Introduction

Standard [8] and its amendment [9] define the necessary voltage tests for the qualification of the partial discharge resistant electrical insulation systems used in rotating electrical machines fed from voltage converters. The standard includes the testing of three basic elements of the insulation system: mainwall insulation, inter-turn insulation and voltage stress control system (so-called conductive and semi-conductive layers). Similar for the previous group of tests, formette coils with associated formette frames (so-called test objects) are used, whereby the execution of the formette coils and frame is adapted to the needs of the individual test.

Mainwall insulation test consists of the life curve reconstruction using voltage aging. In the case of inter-turn insulation, the presence of partial discharges when exposed to impulse voltage is checked and, if necessary, the life curve is reconstructed, also using voltage aging. Voltage stress control system is tested using a combination of sinusoidal and impulse voltage, and the presence of partial discharges and possible damage is checked after the test.

The purpose of those voltage tests is to determine the level of resistance of the insulation system to the occurrence of partial discharges and to associate corresponding IVIC (Impulse Voltage Insulation Class) class. According to simulated operating conditions of the voltage converter, the test parameters were adapted for testing in accordance with the IVIC 5.

As in the previous case, the test is carried out on 6 different insulation systems, which are shown in table 1.

B. Mainwall insulation test

The test is carried out on coil legs with a shortened slot part (so-called „half-formette coils“) that are inserted into formette frame, imitating the presence of a stator core. According to the amendment [9] for testing the mainwall insulation, the test object consists of a frame with two slots filled with four half-formette coils (Figure 9). The half-formette coils are connected in parallel that each is exposed to an equal voltage, while the formette frame is grounded.

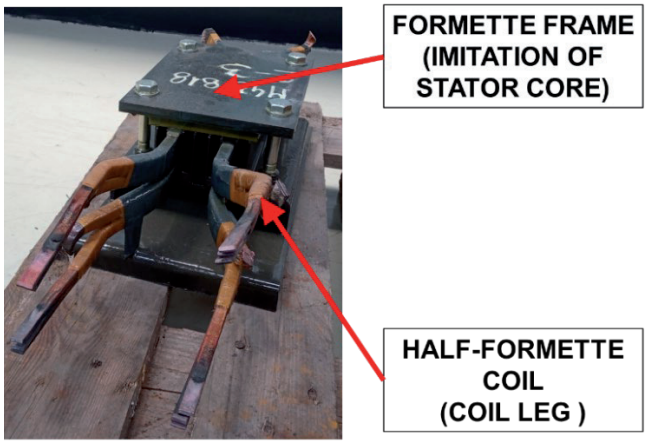

Fig. 9. Parts of formette for mainwall insulation test

The purpose of testing is to determine the electrical life curve of the mainwall insulation of both systems (reference and candidate) and compare their life curves in a way that the candidate system can be qualified. The reconstruction of the life curve is done under conditions of accelerated voltage aging, while the voltage levels are determined using the life curve of the mainwall insulation given in annex E of the standard [8], considering the IVIC 5 classification. According to the requirements stated in standard [8], it is necessary to choose at least three voltage levels, whereby the predicted average time to failure at the highest voltage level should be around 50 h, and at the lowest voltage level it should be over 5000 h. Taking in consideration that requirements voltage levels were calculated and are listed in table 3. The voltage has a sinusoidal waveform.

Table III:

Test voltage levels for reconstruction of mainwall electrical life curve

Predicted average time to electrical failure	Peak to peak test voltage
50 h	11,58 kV
2500 h	7,83 kV
5000 h	7,31 kV

According to table 3, insulation system 1 was subjected to the highest test voltage with an expected time to failure of 50 h. However, named insulation system has lasted 860 hours without electrical breakdown so far, and the test is still ongoing. This phenomenon indicates that the mainwall insulation of system 1 exceeds the IVIC 5 classification and that it can potentially be assigned a numerically higher IVIC level. Therefore, for the expected time to failure of 50 h, it is necessary to select a higher test voltage. In addition, it can be assumed that the initially selected amount of voltage (11.58 kV) will result in a failure time that is in the middle of the interval [50, 5000] h. Remaining insulation systems (2-6) will be tested after the completion of insulation system 1 testing.

C. Inter-turn insulation test

The inter-turn insulation is tested with an impulse voltage in accordance with standard [6], and the possible presence of partial discharges is determined. Since the mentioned test was already carried out as part of the zero or initial diagnostic cycle (informative tests) within the Thermal evaluation and classification of insulation systems (chapter 2.A), and according to the standard [8] the test objects are equal to the test objects shown in Figure 2, the results were taken over from that test. During the test, the presence of partial discharges was not found on any of the insulation systems, therefore the inter-turn insulation is considered qualified, which means that the test of the inter-turn insulation was successfully carried out.

D. Test of voltage stress control system

Testing of the voltage stress control system consists of three cycles: exposure to impulse voltage at the beginning and at the end of test and exposure to sinusoidal voltage. The test parameters are listed in Table 4.

Slaven Nad, Josip Treger, Stjepan Car, Testing of Insulation Systems in Accelerated Aging Conditions, Journal of Energy, vol. 73 Number 3 (2024), 3–8
https://doi.org/10.37798/2024733517

TABLE IV:

PARAMETERS FOR VOLTAGE STRESS CONTROL SYSTEM TESTING

Cycle	1	2	3
Duration	100 h	1000 h	100 h
Voltage waveform	Impulse	Sinusoidal	Impulse
Peak to peak test voltage	$1{,}3 \cdot U_{j\,max} = 1430$ V	$1{,}3 \cdot U_{pg} = 2860$ V	$1{,}3 \cdot U_{j\,max} = 1430$ V
Frequency	2 kHz	50 Hz	2 kHz
Impulse rise time	0,12 µs	-	0,12 µs

Acceptance criteria [8]: There are no partial discharge activity visible to the unaided eye in a darkened room or with a UV detector during the final stage of testing with impulse voltage. There is no visible (to the unaided eye) outer surface damage of the voltage stress control system (conductive and semi-conductive layer) in the endwinding region.

For testing the voltage stress control system, the test object consists of 3 formette coils, 6 half-formette coils and a formette frame with 9 slots as shown in Figure 10 on the left. The three slots inside the frame remain unfilled, while purpose of half-formette coils is to provide fixture of complete formette coils and imitation of real condition in stator core. Half-formette coils are not exposed to the test voltage.

Fig. 10. Parts of formette for voltage stress control system test (left) and

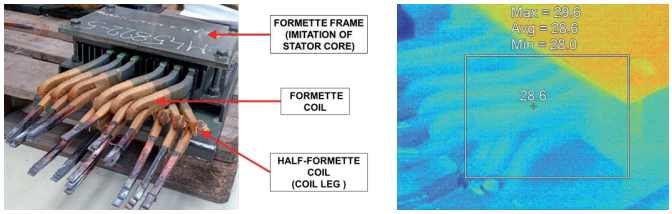

temperature distribution of insulation system 1 formette at the beginning of testing (right)

Additionally, the test object is inspected with a thermal camera at the beginning and at the end of the test to determine the possible presence of temperature increase, and to detect possible damage more easily on the conductive and semi-conductive layers. For now, the first test cycle of the voltage stress control system (impulse voltage exposure) has been successfully carried out on insulation system 1. At the very beginning of the test, the initial heating of the conductive and semi-conductive layers was determined with a thermal camera (Figure 10 right). The second test cycle (exposure to sinusoidal voltage) is currently underway. The testing of the other insulation systems (2-6) follows after the successfully completed testing of the insulation system 1.

CONCLUSION

The paper describes the construction of test objects and procedure for testing insulation systems under conditions of accelerated thermal and voltage aging in accordance with the relevant IEC standards. Due to the duration of the study, only the partial results are listed. Thermal aging for the highest temperature has been completed for half of the intended insulation systems. The first results indicate a slightly higher endurance of the reference systems compared to the candidate systems, but for concrete conclusions it is necessary to carry out the test till the end. Informative tests performed during thermal aging (slight drop in capacity and insulation resistance) correspond to the progressive degradation of the insulation system caused by delamination and the accumulation of moisture between the insulation layers. The mainwall insulation voltage test, according to the first results, indicates a slightly higher voltage endurance of insulation system 1 compared to IVIC classification 5, but for final conclusion the test should be completed. The inter-turn insulation, from a voltage endurance perspective, is considered qualified, while testing of the voltage stress control system is ongoing.

REFERENCES

[1] P. Gröpper, T. Hildinger, F. Pohlmann, J.R. Weidner: Nanotechnology in high voltage insulation systems for large electrical machinery - First results, CIGRE 2012.

[2] T. Hildinger, P. Gröppel, M. Weil, J. R. Weidner: Improved generator performance with a nanocomposite high voltage insulation system for stator windings – A status report, CIGRE 2017.

[3] HRN EN 60034-18-31:2012: Functional evaluation of insulation systems - Test procedures for form-wound windings - Thermal evaluation and classification of insulation systems used in rotating machines, 2012.

[4] M. Farahani, E. Gockenbach, H. Borsi, K. Schäfer and M. Kaufhold: Behavior of machine insulation systems subjected to accelerated thermal aging test, IEEE Transactions on Dielectrics and Electrical Insulation, vol. 17, no. 5, pp. 1364-1372, October 2010.

[5] HRN EN IEC 60034-27-4:2018: Measurement of insulation resistance and polarization index of winding insulation of rotating electrical machines, 2018.

[6] IEC TS 61934: Electrical insulating materials and systems - Electrical measurement of partial discharges (PD) under short rise time and repetitive voltage impulses, 2011.

[7] IEEE 1776: IEEE Recommended Practice for Thermal Evaluation of Unsealed or Sealed Insulation Systems for AC Electric Machinery Employing Form-Wound Pre-Insulated Stator Coils for Machines Rated 15 000 V and Below, 2008.

[8] HRN EN 60034-18-42:2017: Partial discharge resistant electrical insulation systems (Type II) used in rotating electrical machines fed from voltage converters - Qualification tests, 2017.

[9] HRN EN 60034-18-42:2017/A1:2020: Partial discharge resistant electrical insulation systems (Type II) used in rotating electrical machines fed from voltage converters -- Qualification tests (IEC 60034-18-42:2017/am1:2020; EN 60034-18-42:2017/A1:2020), 2020.

Slaven Nad, Josip Treger, Stjepan Car, Testing of Insulation Systems in Accelerated Aging Conditions, Journal of Energy, vol. 73 Number 3 (2024), 3–8
https://doi.org/10.37798/2024733517

Journal of Energy
VOLUME 73 Number 3 | 2024
journal homepage: http://journalofenergy.com/

Development of Electrolyser Projects for Production of Renewable Hydrogen

Martina Mikulić, Martina Rubil, Ivan Andročec

***Summary* — Hydrogen is one of the important factors in reaching climate neutrality from the European Green Deal, particularly hydrogen made from renewable energy sources. The paper describes electrolysis plants in technical, environmental and regulatory aspects and presents obstacles that need to be overcome for the successful implementation of electrolyser projects, looking at the bigger picture of the energy sector. Part of the paper is dedicated to the research of existing projects and the plans for the development of electrolysers. Possible contribution of the development of electrolysis plants is in the application at the locations of existing thermal power plants that are no longer suitable for operation due to technological, economic or environmental reasons, which would take advantage of the existing location of the power plant for the installation of new technology that meets the concept of low-carbon development.**

***Keywords* — electrolyser, hydrogen, low-carbon development.**

I. Introduction

Given that it does not cause carbon emissions when used, hydrogen can be an important factor in achieving the goal of climate neutrality from the European Green Plan until 2050, especially in the sectors that represent the biggest challenge – energy-intensive industry and transport. The greatest potential for decarbonisation is in hydrogen from renewable energy sources (RES), the so-called clean or green hydrogen.

New circumstances in the energy sector and the expected development, which includes a fall in the price of electricity from renewable sources and technological progress, provide opportunities for increasing the use of hydrogen as a raw material, fuel and energy carrier in different parts of the energy sector.

Hydrogen can be produced in different ways - by catalytic oxidation of hydrocarbons, partial oxidation of heavy hydrocarbons, production from refinery gases and methanol, electrolysis of water, and advanced technologies such as thermochemical gasification of biomass or photobiological production using algae and similar, whereby the creation of different types and the amount of greenhouse gas emissions and costs. The focus of this work is the production of hydrogen by electrolysis of water in electrolysis plants using electricity. Emissions resulting from the production of hydrogen using electricity depend on the method of electricity production. If the electricity is obtained from renewable energy sources, we call such hydrogen renewable, clean or green hydrogen.

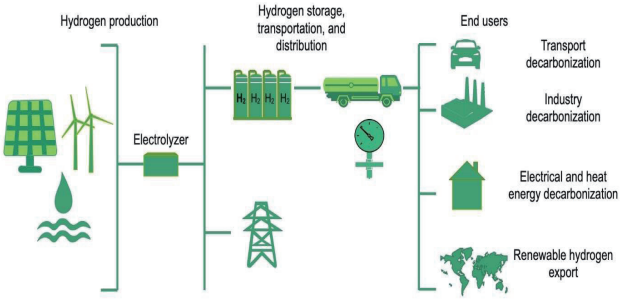

Fig. 1. General scheme of the hydrogen value chain, from production to end-use [1].

As is shown in the paper, the decarbonization of hydrogen production is still in its infancy, but with a strategy goal to support energy transition. Benefiting from a wide variety of production pathways, research and financing policies are needed to accelerate the penetration and cost effectiveness measures to ensure a tangible effect is achieved in a timely manner.

As of December 2022, 97 water electrolysis hydrogen production projects (67 with a minimum capacity of 0.5 MW) were in operation in Europe, totaling 174.28 MW of production capacity. A further 46 projects were under construction (i.e., construction work has begun) and are expected to deliver an additional 1,199.07 MW of water electrolysis capacity once operational (between January 2023 and 2025). In 2022, hydrogen export from Belgium to the Netherlands (25.737 tonnes, or 75% of all the hydrogen traded in Europe) was the single biggest hydrogen flow to and between European countries. [32]. The European goal is production of 10 million tonnes of renewable hydrogen till 2030 (see chapter IV).

The paper is divided into several chapters focusing on concept and different aspects of electrolyser facilities, describing several existing electrolyser projects, presenting different development plans and finally showing some obstacles and guidelines for the way forward.

II. Concept and Aspects of Electrolyser Facilities

The chapter describes the concept of electrolyser facilities and analyzes the technical, environmental and regulatory aspects of the construction of electrolyser projects and hydrogen production.

(Corresponding author: Ivan Andročec)

Martina Mikulić, Martina Rubil and Ivan Andročec are with the HEP, Inc., Zagreb, Croatia (e-mail: martina.mikulic@hep.hr, martina.rubil@hep.hr, ivan.androcec@hep.hr)

Martina Mikulić, Martina Rubil, Ivan Andročec, Development of Electrolyser Projects for Production of Renewable Hydrogen, Journal of Energy, vol. 73 Number 3 (2024), 9–16
https://doi.org/10.37798/2024733518

A. The Concept of Electrolyser Facilities

An electrolyser is an electrochemical device in which hydrogen and oxygen are produced in gaseous phases by means of water electrolysis. The process is called electrochemical because direct electrical energy is used to obtain chemical energy that is stored in the resulting hydrogen. The electrolyser consists of two electrodes that are connected to an external direct current circuit. Between the electrodes, there is a voltage drop that causes the bipolar electrodes to charge so that the part of the electrode that receives electricity is charged positively (anode), and the part that transmits it is negatively charged (cathode). For the electrolysis process, the DC voltage on the electrodes must be equal to or greater than the reversible voltage, which is 1.23 V. As a result of the voltage drop, redox reactions take place on the electrodes - reduction of water (H_2O) takes place at the cathode, and a hydrogen molecule (H_2) is formed, and at the anode, oxidation occurs and an oxygen molecule (O_2) is formed. The amount of hydrogen production is directly related to the number of cells in the electrolyser, that is, the greater the number of cells, the greater the production of hydrogen, provided that a higher voltage is supplied. The chemical reaction of the electrolysis process is shown by (1).

$$2\,H_2O \rightarrow 2\,H_2 + O_2. \quad (1)$$

Three types of electrolysers are mostly used: alkaline electrolyser (AE), proton exchange membrane electrolyser (PEM) and solid oxide electrolysis (SOE). Currently, the most developed and cheapest technology for hydrogen production is with the help of an alkaline electrolyser, in which the membrane is selective and allows only hydroxide ions to pass through. PEM electrolysers use a membrane as an electrolyte, where polymer materials are used to build the membrane. The advantage of this type of electrolyser is greater stability with non-uniform sources of electricity, compactness, greater purity of hydrogen and lower electricity consumption. Electrolysers that use solid oxides as a membrane work at a temperature of 700-800°C, and use the hot water vapor that is created in the process, thus reducing the amount of electricity needed for hydrogen production. [2]

Traditionally, electrolysers are made in small quantities for specific market niches. Despite the fact that some electrolysers are used commercially (alkaline and PEM), traditional hydrogen production technologies are still preferred due to incomparably lower costs. Innovations in electrolyser technologies, greater efficiency and cost reduction (including a drop in the price of electricity from RES) are needed for this technology to play its key role in decarbonisation. According to A Hydrogen Strategy for a climate neutral Europe [3], the price of hydrogen produced from fossil fuels is currently about 1.5 €/kg (about 2 €/kg taking into account the price of released CO_2 into the atmosphere), and the price of renewable hydrogen production is in range from 2.5 till 5.5 €/kg. Price competitiveness of renewable hydrogen production with other forms of hydrogen production is expected in the period from 2025 to 2030 [3].

B. Technical, Environmental and Regulatory Aspects

The decision to invest in electrolyser facilities is preceded by a review of a whole series of technical, environmental and regulatory aspects, which are described in the following chapter.

B.I. Technical Aspects

In addition to the electrolyser stack itself (or several stacks), electrolyser plants include accompanying equipment necessary for operation. The electrolyser is a set of electrolyser stacks, and the stack contain anode, cathode and proton or anion exchange membrane. A schematic view of the electrolysis facility with all the necessary systems can be found in Figure 2.

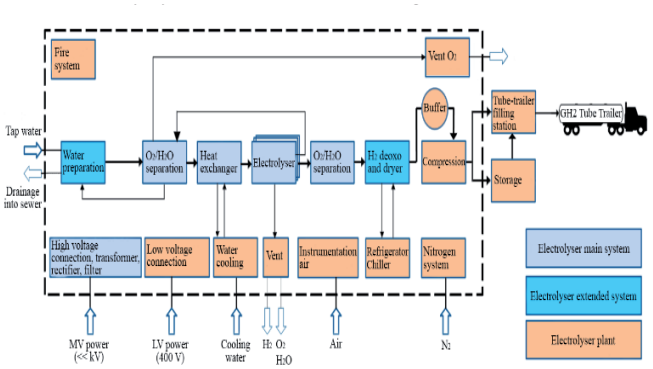

Fig. 2. Schematic representation of the electrolyser facility with all necessary systems [4]

Since direct current is used in the electrolysis process, the basic system of the electrolyser facility includes mains switches, filters, a transformer and a rectifier. Each plant must be equipped with a system for purification and demineralization of water for use in the electrolyser. An essential part of the facility is the cooling system, which is required to maintain the desired operating temperature of the electrolyser (60-75°C), due to heat generation in the electrolysis process, and systems for separating water from the produced hydrogen and oxygen. To achieve the desired purity of hydrogen, a special cooling system for drying hydrogen is required. Additional elements of the system are a hydrogen intermediate tank at the plant exit, a compressor to achieve the desired delivery pressure (up to max. 380 bar) and a high-pressure hydrogen tank. For the safe operation of the electrolysis plant, a system of compressed air required for instrumentation, a system of compressed nitrogen for flushing the system, and a fire alarm and fire protection system are also required.

On the side of safety and technical aspects, it is important to note that a mixture of hydrogen and oxygen can occur in the electrolyser (firecracker gas), which is why manufacturers of electrolysers take precautionary measures. When using hydrogen, there is no risk of the formation of a mixture of hydrogen and oxygen, but hydrogen may leak into the air. However, in an open or closed space with ventilation, there is a low probability of generating the critical amount of hydrogen necessary for ignition (4%), except immediately (up to 30-40 cm) above the point of hydrogen leakage due to the weight of hydrogen, which is 13 times lighter than air.

B.II. Environmental Aspects

The use of hydrogen as a low-carbon form of energy should lead to significant reductions in carbon dioxide and greenhouse gas emissions, as well as significant climate benefits. Hydrogen is the most widespread element in nature and makes up about 90% of all atoms. Its extreme chemical reactivity is the reason why it is not found as a free element in nature, but is bound in compounds, so it must be produced for use.

The method by which hydrogen will be produced for industrial use determines how much positive impact or possible damage there is to the environment. Excess renewable energy can be used

Martina Mikulić, Martina Rubil, Ivan Andročec, Development of Electrolyser Projects for Production of Renewable Hydrogen, Journal of Energy, vol. 73 Number 3 (2024), 9–16
https://doi.org/10.37798/2024733518

for production, so such energy is not wasted, but is used to produce hydrogen that can be successfully stored. In addition to gas pipelines, hydrogen can also be stored in fuel cells. Hydrogen fuel cells, unlike batteries, do not need to be recharged and last longer allowing them to be used to power vehicles offering zero emissions and are two to three times more efficient than gasoline internal combustion engines.

Adding hydrogen to the natural gas network results in changes in the physical and chemical properties of the fuel mixture - this mixture is lighter with a higher diffusion coefficient and higher volumetric flow compared to pure methane for the same pressure and flow rate. Following on from the conducted research, if we replace 10% of natural gas with hydrogen, taking into account losses in the distribution network of around 1%, the impact of the newly created mixture on the climate will be reduced due to the weaker GWP (Global Warming Potential) of hydrogen (4.3) in comparison on the GWP of methane (25) over a 100-year period [5].

However, uncontrolled leakage of hydrogen into the atmosphere during its production, storage, distribution and use could reduce the positive environmental impacts achieved by its use and have a detrimental impact on air quality and climate. More than 50% of hydrogen comes from burning fossil fuels and burning biomass, and the rest includes the oxidation of methane and volatile organic compounds. Although it is not a greenhouse gas in itself, hydrogen can participate in chemical reactions in the lower and upper atmosphere that can lead to a harmful effect on the environment. An increase in the concentration of H_2 in the atmosphere leads to a series of chemical reactions that, as a result, have negative effects on air quality, global warming and the destruction of the ozone layer, as well as prolonging the life cycle of methane, which is a greenhouse gas [6]. Changes in H_2 concentration also affect atmospheric water vapor, and the increase in H_2 and H_20 in the stratosphere leads to the production of hydrogen radicals responsible for the destruction of the ozone layer.

The impact of hydrogen on climate change has not been sufficiently investigated, there is only one study that provides an estimate of the GWP for hydrogen, which can be shown as 4.3 t of equivalent CO_2 emissions per ton of hydrogen over a 100-year period, i.e. the GWP for hydrogen is estimated at 4.3 with a relatively large uncertainty. From this it can be concluded that the influence of hydrogen on the global climate is relatively small [7]. Given that we cannot predict the amount of hydrogen that would flow out into the soil uncontrollably, it is difficult to determine the ratio of benefits and harm to the environment. There is a possibility that the increased use and possible leakage of hydrogen will have a negative effect on the climate, but the available results from the conducted studies show that the harmful global atmospheric impact of hydrogen on the climate will be small. The production of hydrogen should be in an environmentally friendly manner with maximum precautions.

B.III. Regulatory Aspects

The legislative framework of the Republic of Croatia (ROC) includes ensuring the transfer of EU legislation into national legislation in accordance with the goals set at the EU level. At the EU level, rules for the production of hydrogen from RES were adopted in June of this year, and steps were taken to establish a hydrogen bank that combines demand and production for hydrogen.

In addition to the Croatian strategy for hydrogen until 2050, laws were passed that regulate the possibilities of using hydrogen, i.e. the introduction of hydrogen on the Croatian market, and define the technical specifications of filling stations:

- Act on Amendments to the Act on Biofuels for Transportation (Official Gazette, No. 52/21),
- Act on the Establishment of Infrastructure for Alternative Fuels (Official Gazette, No. 120/16).

In order to obtain permits for construction projects of electrolyser facility, it is necessary to create project documentation for the installation of the electrolyser with all subsystems, for connection to the power system and potentially for connection to the gas system. The necessary documentation includes the decision of the competent ministry on the need to carry out an assessment procedure on the need to assess the impact of the intervention on the environment, an energy permit and a building permit. As a regulatory obstacle, a certain confuse was observed regarding the way electrolysers are treated as other production facilities and the need for an environmental permit, which is not clearly defined either at the level of the European Union (EU) or Croatia.

B.III. Comparison of different hydrogen production methods

Electrolysis techniques can be categorized based on the electrolytes employed: alkaline electrolysis (AE); polymer electrolyte membrane (PEM) electrolysis; solid oxide electrolysis (SOE); and anion exchange membrane (AEM) electrolysis. For electrolysis efficiency, many internal and external variables can affect both the electrical behavior and efficiency of electrolysis cells, including the concentration and purity of the electrolyte, the type and shape of the electrodes, and the cell temperature and pressure. Table I compares the main characteristics of AE, PEM, and SOE system [29].

Table I

Comparison of Different Characteristics of Water Electrolysis-Based Hydrogen Production Technologies

	AEC[a]	PEM[a]	SOE[a]
TRL[a]	9	8	6
Expected TRL 2050	9	9	9
Typical electrolyte	Aqueous potassium hydroxide (20–40 wt% KOH)	Polymer membrane (e.g. Nafion) [	Yttria Stabilised Zirconia (YSZ)
Anode	Ni or Ni–Co alloys	RuO_2 or IrO_2	LSM/YSZ
Cathode	Ni or Ni–Mo alloys	Pt or Pt-Pd	Ni/YSZ
Cell voltage (V)	1.8–2.4	1.8–2.2	0.7–1.5
Current density (A cm^{-2})	0.2–0.4	0.6–2.0	0.3–2.0
Cell area (m^2)	<4	<0.3	<0.01
Voltage efficiency (%)	62-82	67-82	77-85
Operating temperature (^{0}C)	60-80	50-80	650-1000
Operating pressure (bar)	<30	30-80	<25
Production rate ($m^3H_2h^{-1}$)	<760	<40	<40
Stack energy ($kWh_{el}m^3H_2^{-1}$)	4.2–5.9	4.2–5.5	>3.2
System energy ($kWh_{el}m^3H_2^{-1}$)	4.5–6.6	4.2–6.6	>3.7
Gas purity (%)	>99.5	99.99	99.9
Cold-start time (min.)	<60	<20	<60
System response	Seconds	Milliseconds	Seconds
Stack lifetime (h)	60,000–90,000	20,000–60,000	<10,000

Martina Mikulić, Martina Rubil, Ivan Andročec, Development of Electrolyser Projects for Production of Renewable Hydrogen, Journal of Energy, vol. 73 Number 3 (2024), 9–16
https://doi.org/10.37798/2024733518

Capital cost per stack 2020 (€$_{2021}$/kW)	1000-1200[d]	1860-2320[d]	>2000[d]
Capital cost per stack 2030 (€$_{2021}$/kW, estimated)	611	978	1902
Stack efficiency (LHV) range 2020 (%)	58–70%	58–65%	81–83%
Stack efficiency (LHV) range 2050 (%, estimated)	61–80%	70–74%	88–90%
Advantages	Long life span	High current density	High system efficiency
	Minimal expense	Compact system layout	Less electricity utilization
	High technology readiness level	Fast response to current change	Expected cost reduction
	Large stack size		Integration with other technologies
Disadvantages	Low current density	Noble metal material requirement	Extraction and utilization of cathodic Lanthanide rare earth elements may cause environmental damage
	Corrosive electrolyte	Short life span	Unstable electrodes
		High membrane expense	Sealing problems
Barriers for large-scale application	Accessibility to low cost and abundant electricity	Accessibility to low cost and abundant electricity	Accessibility to low cost and abundant electricity; immaturity of technology

a: AEC: alkaline electrolysis cell; GHG: greenhouse gas; LHV: Low heating value; LSM: $La_{0.8}Sr_{0.2}MnO_3$; PEM: polymer electrolyte membrane; SOE: solid oxide electrolysis; TRL: technology readiness level; wt: weight.

b: The global share of renewable electricity in total electricity output was approximately 27% at the end of 2019, including 11% produced by wind turbines and solar photovoltaic, which potentially can be used to produce sustainable hydrogen.

c: Adequate renewable electricity for large-scale deployment of electrolysis is assumed to be available based on the existing net-zero commitments.

d: Updated capital cost according to Chemical Engineering Plant Cost Index (CEPCI). $CEPCI_{2020}$ = 596.2; $CEPCI_{2021}$ = 708.0. Calculation formula: cost at 2021 = cost at 2020 · $CEPCIindexat2021CEPCIindexat2020$).

III. Existing Electrolyser Facility Projects

Installed capacities in electrolyser facilities have been growing at an accelerated pace for the past few years, but precise data on total world capacities are currently not readily available. According to a report by the International Energy Agency (IEA) [8], electrolysis capacity for dedicated hydrogen production has been growing in the past few years, but the pace slowed down in 2022 with about 130 MW of new capacity entering operation, 45% less than the previous year. However, electrolyser manufacturing capacity increased by more than 25% since last year, reaching nearly 11 GW per year in 2022. Global electrolyser capacity additions slowed in 2022 despite strong momentum, but installed capacity could reach almost 3 GW in 2023. On the other hand, data from the European Commission (EC) from the Hydrogen Strategy [3] and other documents show that only in the European Economic Area (EEA) the total installed capacity of electrolysers is about 1 GW. Examples of interesting and significant electrolyser facility projects in the world are presented below.

In December 2021, the world's largest 150 MW alkaline electrolyser facility powered by a 200 MW solar power plant was put into operation in the Ningxia region, in central China. Although the idea of the electrolyser is to be powered by solar energy, there is the possibility of taking electricity from the grid. The investment in the electrolyser facility amounted to about 200 million euros with a planned production of 27,000 tons of pure hydrogen per year, however, the realistic possibilities are somewhat lower and it is possible to achieve a production of 23,700 tons per year [10]. It is a project of the company that produces coal-based chemicals, Ningxia Baofeng Energy Group, which announced at the beginning of 2023 the construction of the world's largest plant for the production of olefins, i.e. synthetic polypropylene fibers, from pure hydrogen and coal, for which the investment will amount to around 6.5 billion euros. Olefins are widely used raw materials in the chemical industry, in the field of packaging, furniture, household appliances, cars, medicine and aviation. For the production of synthetic fibers, coal and pure hydrogen will be used as raw materials, while oxygen as a by-product will replace part of the coal as fuel. The planned production of 3 million tons of olefins per year would be achieved from 2.6 million tons of coal and 400 thousand tons of pure hydrogen. Compared to pure hydrogen plants, such projects should produce an additional 1.2 million tons of methanol, save more than 2.5 million tons of coal, and reduce carbon emissions by 6.3 million tons every year [11].

Fig.3. Hydrogen Pro Elektrolyser [12]

At the end of 2022, the company Hydrogen Pro installed the world's largest electrolyser with a diameter of 2 m and a weight of more than 80 t in a test facility on the Herøya peninsula in Norway, which was manufactured in a factory in Tianjin, China. A high-pressure alkaline electrolyser can produce 1100 m3/hour of hydrogen, which corresponds to the production of 100 kg of pure hydrogen per hour [12]. With the exception of the project in Norway, there are mostly smaller capacity electrolysis plants in Europe.

As part of the EU-funded GrInHy2.0 project, a demonstration plant for the production of pure hydrogen by steam electrolysis using waste heat from the Salzgitter Flachstahl GmbH iron and steel plant, in the city of Salzgitter in northern Germany, was developed in 2020. The facility is presented as the world's largest high-temperature electrolyser (HTE) for energy-efficient hydrogen production. The nominal power of the electrolyser is 720 kW, and it can produce 200 m3/hour of hydrogen under normal conditions. By the end of 2022, the plant is expected to operate for at least 13,000 hours, producing about

Martina Mikulić, Martina Rubil, Ivan Andročec, Development of Electrolyser Projects for Production of Renewable Hydrogen, Journal of Energy, vol. 73 Number 3 (2024), 9–16
https://doi.org/10.37798/2024733518

100 tons of high-purity hydrogen (99.98%), which will be used for annealing processes in integrated steel plants as a substitute for hydrogen produced from natural gas [13]. The Salzgitter Group has selected technology group ANDRITZ to supply one of Europe's largest green hydrogen plants for the SALCOS® program, which aims to achieve virtually CO2-free (green) steel production. ANDRITZ will build a 100 MW electrolysis plant at the Salzgitter Flachstahl GmbH site on an EPC basis, incorporating pressurized alkaline electrolyser technology from HydrogenPro. Starting in 2026, the plant will produce around 9,000 tons of green hydrogen per year, which will be used to produce green steel. [28] The conversion to a virtually CO2-free steel production at the Salzgitter site is to be completed by the end of 2033, well ahead of the statutory requirements.

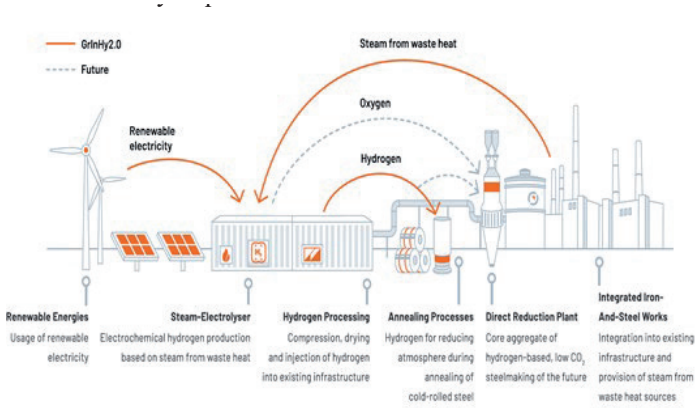

Fig. 4. Project GrInHY 2.0 – process [13]

The Danish company Green Hydrogen Systems designs and manufactures standardized, modular, pressurized alkaline electrolysers intended for the production of hydrogen exclusively from renewable energy sources. With the aim of accelerating the production of pure hydrogen on a large scale, within the GreenHyScale project, funded by Horizon 2020, it is planned to build a 100 MW electrolyser in the GreenLab Skive energy park in Denmark. The project started in 2021 and will last until 2026, the costs amount to 53 million euros, of which 30 million euros are financed from EU funds. In March of this year, the prototype of the electrolyser with a capacity of 6 MW, weighing 70 tons, was completed and testing began, which will last until the end of the year [14].

Apart from the examples of projects shown, the EU finances numerous other projects with the aim of solving the problem of hydrogen production and facilitating the decarbonisation of Europe, whereby the funding from the 2020 Green Deal Call for the development of a 100 MW electrolyser alone amounted to 90 million euros [15]. Examples of supported projects are shown in the following table.

TABLE II

EXAMPLES OF SUPPORTED HYDROGEN PROJECTS FROM EU FUNDS [15]

Acronym	Cost (€)	EU funds (€)	Project (Country)
REFHYNE II	147.365.995	32.431.618	Clean Refinery Hydrogen for Europe (Germany)
GreenHyScale	52.982.524	30.000.000	Production of green hydrogen with a capacity of 100 MW in an industrial environment (Denmark)
GREENH2SINES (GREENH2-ATLANTIC)	76.614.020	30.000.000	Flexible green hydrogen production process with a capacity of 100 MW with hybrid RES (Portugal)

IV. ELECTROLYSER DEVELOPMENT PLANS

According to the IEA report, the realization of all electrolyser projects in preparation could lead to an installed global capacity of 170-365 GW by 2030 [8]. Although the overlooked figures seem large, such a pace of growth, in relation to the currently installed capacities, is not fast enough to achieve the IEA "Net Zero Emissions by 2050" scenario with the goal of zero rate of CO2 emissions in the global energy sector - installed capacities should be above 560 GW by 2030.

Hydrogen valleys are being established around the world to help develop hydrogen projects, and there are currently more than 80 potential hydrogen valleys on five continents (Europe, Asia, North America, South America and Australia), of which the largest number is in Europe (74%) [9]. Hydrogen valley projects cover all the necessary steps in the hydrogen value chain, from production to storage and transportation / distribution of hydrogen to end users. Also, incentive programs for pure hydrogen are being established, such as the program in the United States of America (USA) where there is support for the production costs of pure hydrogen of 3 USD/kg, which makes the USA an attractive market for hydrogen production [16].

The announced significant worldwide development projects include electrolysis plants with the capacity of:

- 260 MW for the production of 20,000 tons of hydrogen per year in the town of Kuqa, on the territory of Xinjiang, Northwestern China (Chinese oil giant Sinopec) – the construction of the electrolyser began in 2021 and is in operation from July 2023, and the construction of the storage tank is also planned for hydrogen storage and pipelines for transporting hydrogen to the nearby oil refinery [17],
- for the production of 30,000 tons of hydrogen and 240,000 tons of oxygen per year in the Inner Mongolia Autonomous Region (Sinopec) - the construction of the electrolyser began in early 2023, the products will be used for carbon reduction in the neighboring pilot project of energy-intensive coal processing [18], and it is planned the construction of a pipeline with a length of more than 400 km from Inner Mongolia to Beijing for long-distance hydrogen transport with an annual capacity of 100,000 tons [19],
- about 840 MW in Louisiana, USA (DG Fuels, HydrogenPro partner) [16].

The announcement of the construction of a global gigafactory of electrolysers in Massachusetts, USA, which should correspond in price and size to a quarter of the cost of comparable PEM or alkaline electrolysers, is interesting, given that they are electrolysers with anion exchange membrane (AEM) designed with the aim of cheap mass production, without precious metals [20]. Factories for the production of electrolysers are being built or are being planned all over the world.

As for European goals, in July 2020 the EC presented the Hydrogen Strategy for a climate-neutral Europe, in which pure hydrogen is highlighted as one of the key levers for a successful energy transition. The strategy expects a gradual development:

- Phase 1 from 2020 to 2024 – increasing the capacity of the electrolyser by at least 6 GW with the production of up to one million tons of renewable hydrogen (compared to the current capacity of about 1 GW),
- Phase 2 from 2025 to 2030 – increase in electrolyser capacity by at least 40 GW of electrolysers with the production of up to 10 million tons of renewable hydrogen (requiring an additional 80 GW of RES),
- Phase 3 from 2030 to 2050 – reaching maturity of renewable hydrogen technologies and wide application.

Martina Mikulić, Martina Rubil, Ivan Andročec, Development of Electrolyser Projects for Production of Renewable Hydrogen, Journal of Energy, vol. 73 Number 3 (2024), 9–16
https://doi.org/10.37798/2024733518

The EU strategy for hydrogen also mentions investment plans at the gigawatt level and that the list of global investments includes around 8.2 GW of electrolysers by 2030, of which 57% are in Europe, or 4.7 GW. As in the case of world plans, the European development plans have lagged behind the necessary pace of growth to achieve the goals set out in the strategic documents. However, later reports provide more optimistic indicators of the growth of hydrogen projects. The proposed electrolyser projects that should be in operation in 2024 have a total capacity of 5.2 GW, which is within reach of the set goal of 6 GW by 2024 [21].

The EU has developed several different financial instruments to help finance hydrogen projects, which can be reviewed through the Hydrogen Public Funding Compass, and are structurally divided into EU funding programs and national funding programs [22].

A. The Croatian Hydrogen Strategy and Project Example

The Croatian hydrogen strategy until 2050 [1] was adopted in March 2022, and the basis for its preparation is based on the National Development Strategy of the Republic of Croatia until 2030 and the Energy Development Strategy of the Republic of Croatia until 2030 with a view to the year 2050 . The Croatian strategy has set the goal of reaching 70 MW of electrolysers by 2030 and 2750 MW by 2050, and the movement of the required capacities of electrolysers by year is shown graphically in Figure 5. The figure shows the required capacities of electrolysers that obtain electricity for hydrogen production from network and exclusively from RES. The strategy also sets goals for the share of hydrogen in total energy consumption (0.2% by 2030, 11% by 2050), the number of hydrogen filling stations (15 by 2030, 100 by 2050) and the number of patents related to the economy based on hydrogen (5 by 2030, 50 by 2050), whereby the initial value for all performance indicators is zero (0) according to the situation in 2021/2022 years.

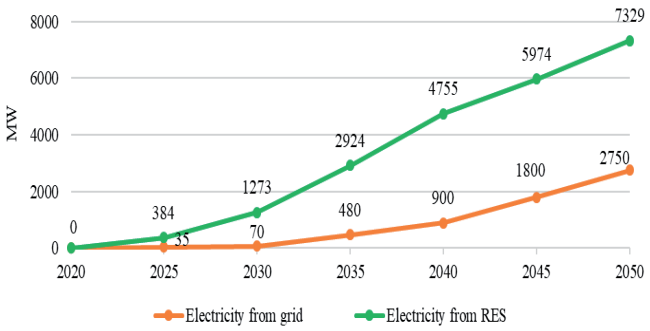

Fig. 5. Projected capacities of electrolysers in Croatia until 2050

The establishment of hydrogen valleys at the world level was mentioned, and one of the potential hydrogen valleys is the Northern Adriatic Hydrogen Valley, for which 25 million euros have been allocated with the aim of developing a transnational hydrogen valley between the Autonomous Region of Friuli Venezia Giulia (Northeastern Italy), Slovenia and Croatia [23]. Key stakeholders from the three countries will develop pilot projects for the production of more than 5,000 tons of renewable hydrogen per year and deal with its storage, distribution and use for the decarbonisation of important industrial sectors (including transport).

In the territory of the Republic of Croatia, INA d.d. started the procedures for the realization of a plant for the production of pure hydrogen with two photovoltaic power plants at the location of the Refinery in Kostrena. The proposed project envisages the construction of an electrolyser with a capacity of 10 MW for the production of 4.5 tons of hydrogen per day, or about 1,500 tons per year, and will be intended for the transport sector of Croatia and for own consumption in INA's refinery. Co-financing of the project is expected from the funds of the National Recovery and Resilience Plan (NRRP), but according to the available information, the project began to be conceived before the preparation of the RRP, i.e. in 2018 [24].

Another well-known project for the construction of a hydrogen production facility in Croatia exists in the HEP group, and it refers to the use of the existing location of KTE Jertovec for the installation of a battery system and an electrolyser for the production of hydrogen with associated systems. According to the environmental permit, the planned exit from KTE Jertovec is on December 31, 2023, which opens up new possibilities for using the location. With regard to the current conditions in the EES, the construction of the infrastructure and the transition to low-carbon energy sources, in December 2021 a conceptual solution and techno-economic analysis of the installation of the battery system and electrolyser with associated systems at the KTE Jertovec location was prepared. The next steps in the development of the project relate to the creation of project documentation for obtaining a building permit, which is expected to be by the end of 2025. Current project plan is 16 MW/16 MWh capacity of battery system and 9 MW electrolyser capacity with storage for at least two day production of hydrogen (at least 4 hours per day in periods of low wholesale electricity prices).

V. Problems, Obstacles and Guidelines

The application of renewable hydrogen is expected mostly to balance the power system based on RES, providing the necessary flexibility, for daily or seasonal storage with the aim of increasing security of supply in the medium term and in traffic [3]. The EC intends to use hydrogen as the main solution for reducing greenhouse gas emissions in sectors that are difficult to decarbonize and where electrification is difficult or impossible (for example, steel production or heavy goods vehicle transport) [25].

The issue of the development of hydrogen projects was addressed through the analysis of technical, environmental and regulatory aspects in chapter 2.2, and various issues were also addressed through several reports at the HRO CIGRE 15th Symposium on the power system management in November 2022, which is also an indicator of interest and topicality topics.

Levačić and Teklić in their report [26] state the main obstacles in the development of hydrogen production according to the document of the International Renewable Energy Agency (IRENA) [27], namely: high production costs, lack of necessary infrastructure for production and further use, significant energy losses (30-35%), lack of recognition of value and benefits and the need to ensure long-term sustainability.

Keeping in mind the development of the circular economy, additional obstacles and issues are:

- where to use waste heat,
- where to use oxygen - release into the atmosphere or additional systems for drying and compressing oxygen required in case of preparation for sale,
- water availability – the problem of water poverty,
- how to solve the problem of transportation and the energy needed for transportation – problems with compression and use of hydrogen in another (remote) location and the consequent increase in the carbon footprint.

Questions that seem to be partially resolved:

- availability of cheap clean electricity for electrolysis - from RES sources, but consequently the problem of increasing inflexibility and intermittency of the system - electrolysis systems with higher operating ranges and faster response

Martina Mikulić, Martina Rubil, Ivan Andročec, Development of Electrolyser Projects for Production of Renewable Hydrogen, Journal of Energy, vol. 73 Number 3 (2024), 9–16
https://doi.org/10.37798/2024733518

times are better suited for providing operational flexibility, and systems with higher efficiencies/capacity factors are better suited for providing longer duration flexibility, such as seasonal storage,

- technical and safety obstacles due to the easy flammability of hydrogen - setting safety standards during production, transport and storage, as well as for the monitoring and verification system,
- infrastructure development required for further development – construction of local networks and new transport options, including conversion of existing gas infrastructure.

Further to the described obstacles, guidelines for increasing the production of pure hydrogen include [26]: development of a model for the use of hydrogen in the power system work support functions, removal of regulatory obstacles, establishment of a common market and further development of technology at lower prices.

From the point of view of running the power system as a potential location for the production of pure hydrogen, locations are proposed where more electricity will be produced in relation to the required consumption [26], however, considering that these are usually areas of low level of consumption and other forms of energy / energy sources, thereby increasing the problem of hydrogen transport. The guideline for the development of hydrogen projects, based on the analysis done in this report, would be the development of such projects based on the principles of the circular economy and looking at the wider picture of the utilization of products created by electrolysis. In doing so, priority should be given to existing plant locations that are no longer suitable for operation for technological, economic or environmental reasons, and have a certain part of the infrastructure built that can be used for the production and transport of hydrogen.

Given potential uncertainties—such as the availability of renewable energy sources, the future cost of electricity, policy decisions, techno-economics of hydrogen facilities, or the performance of electrolysers—modeling efforts may include multiple scenarios or probabilistic techniques to capture the range of possibilities. To accurately capture the flexibility of electrolysis-based hydrogen production as a flexible load, modelers need to accurately represent (1) the operating characteristics of hydrogen production, and (2) the flexibility of hydrogen end uses, which also depend on the availability of hydrogen storage buffers. It is crucial to take into consideration the operating regime and goals of the electrolysis plant, recognizing that hydrogen production facilities are unlikely to treat the provision of electricity and flexibility as their primary objectives [33]. Robust business models for both the production and use of clean hydrogen and its derivatives can develop only if the necessary infrastructure is available with sufficient lead time. The techno-economic optimization of hydrogen production plants with water electrolysers is based on a complex system model and depends highly on the boundary conditions and the input parameter. Oversizing the capacity of a plant becomes less attractive except in cases of exceptionally low-cost electricity.

The Commission Delegated Regulation 2023/1184 contains detailed rules on the conditions under which electricity used to produce hydrogen may be counted as fully renewable according to European Union (EU) law [30]. Renewable hydrogen producers will have the possibility to sign long-term renewable power purchase agreements with existing installations (until 1 January 2028) or to conclude power purchase agreements (PPAs) with new and unsupported renewable electricity generation capacity. Fuel producers may count electricity taken from the grid as fully renewable if the installation producing the renewable hydrogen is located in a bidding zone where the average proportion of renewable electricity exceeded 90% in the previous calendar year and the production of renewable hydrogen does not exceed a maximum number of hours set in relation to the proportion of renewable electricity in the bidding zone. Otherwise, in the bidding zone the emission intensity of electricity needs to be lower than 18 gCO_2eq/MJ.

The EU Hydrogen Bank, a pillar of said hydrogen strategy, serves as a bridge between wary investors and, still as of yet, high CAPEX marred projects with stiff commercial competition. Based on an open auction system with a fixed premium for renewable hydrogen production within the EU, the Bank has already implemented its first trial auction with a budget 800 million Euros and the contracts set were awarded in May 2024. The exact consequences of the initial auctions will be hard to determine for some time until a tangible effect can be felt and quantified, however there is available information about the immediate consequences of these auctions. Out of 132 bids, 119 proposals were considered eligible and admissible. The final tally of projects selected amounted to 7 projects located in 4 European nations as shown in Table III. The selected projects have cumulatively been awarded a little under 720 million Euros and are expected to mitigate 10 million tonnes of CO2 emissions. The subsidies per project ranged from 8 million to 24 million Euros [31].

TABLE III

PROJECTS THAT WERE AWARDED FUNDING UNDER THE HYDROGEN BANK'S PILOT AUCTION [31]

Project	Coordinator	Country	Bid volume [ktH_2/10 yrs]	Bid capacity [MWel]	Expected GHG mitigation [ktCO_2/10 yrs]	Build price [EUR/kg]
eNRG Lahti	Nordic Ren - Gas Oy	Finland	122	90	836	0,37
El Alamillo H_2	Benbros Energy S.L.	Spain	65	60	443	0,38
Grey2Green-II	Petrogal S.A.	Portugal	216	200	1477	0,39
Hysencia	Angus	Spain	17	35	115	0,48
Skiga	Skiga	Norway	169	117	1159	0,48
Catalina	Renato Ptx Holdco	Spain	480	500	3284	0,48
MP2X	Madošuapower 2x	Portugal	511	500	3494	0,48

VI. CONCLUSION

According to the research of existing projects of electrolysis facilities in the world, it can be concluded that most of them are pilot or test projects financed from research and development projects, or projects of large companies that have factories or industrial facilities where they can use hydrogen or use existing resources (for example waste heat). Examples of projects in the world can be used to acquire new information and ideas, but the construction and application of electrolysis plants should be adapted to the conditions of a certain area, and not blindly copy solutions that are not universally applicable, but specific to a certain area. A good direction is the utilization of existing resources, for example the location of existing facilities that are no longer suitable for operation due to technological, economic or environmental reasons, but even in this case a detailed technological-technical concept is required looking at the broader picture of the energy sector and an economic-financial analysis of the profitability of the investment. Announced clean hydrogen supply globally has reached significant amount of renewable hydrogen production through 2030. However, only 7% of investments in clean hydrogen overall have passed final investment decision (as of December 2023). Continued efforts are nee-

Martina Mikulić, Martina Rubil, Ivan Andročec, Development of Electrolyser Projects for Production of Renewable Hydrogen, Journal of Energy, vol. 73 Number 3 (2024), 9–16
https://doi.org/10.37798/2024733518

ded to foster the faster maturing of projects from announcement to deployment. The current support schemes are complex, partly tailor-made and seem to lack simplicity and scalability. Improving feasibility of business models in all techno-economic-regulator aspects are crucial for ambitious renewable hydrogen production deployment.

References

[1] Narodne novine, br. 40/2022, Hrvatska strategija za vodik do 2050. godine, ožujak 2022.

[2] Office of Energy Efficiency & Renewable Energy, Hydrogen Production: Electrolysis, Available: https://www.energy.gov/eere/fuelcells/hydrogen-production-electrolysis

[3] European Commission, A hydrogen strategy for a climate-neutral Europe, July 2022.

[4] EIHP i FER, Tehno-ekonomska analiza postavljanja baterijskog sustava i elektrolizatora s pripadajućim sustavima na lokaciji KTE Jertovec, December 2021.

[5] Messaoudani, Rigas, Binti Hamid i Che Hassan, Hazards, safety and knowledge gaps on hydrogen transmission via natural gas grid: A critical review, International Journal of Hydrogen Energy, 2016.

[6] Howarth, Santoro i Ingraffea, Methane and the greenhouse-gas footprint of natural gas from shale formations, Climatic Change, 2011.

[7] D. OBE, Hydrogen for Heating: Atmosferic impacts, BEIS Research Paper, Newbury, 2018.

[8] IEA, Electrolysers, Tracking report – July 2023, Available: https://www.iea.org/energy-system/low-emission-fuels/electrolysers s

[9] Clean Hydrogen Partnership, Hydrogen valleys, Available: https://h2v.eu/hydrogen-valleys

[10] Fuel Cells Works, The World's Largest Green Hydrogen Project With a 150MW Electrolyser Comes Online in China, Available: https://fuelcellsworks.com/news/the-worlds-largest-green-hydrogen-project-with-a-150mw-electrolyser-comes-online-in-china-el-periodico-de-la-energia/

[11] Yicai Global, China's Baofeng Starts Building World's Largest Plant for Making Olefins From Green Hydrogen, Coal, Available: https://www.yicaiglobal.com/news/china-baofeng-starts-building-world-largest-plant-producing-olefins-from-green-hydrogen-coal

[12] PV Magazine, The Hydrogen Stream: World's largest electrolyzer to be deployed in Norway, September 2022., Available: https://www.pv-magazine.com/2022/09/13/the-hydrogen-stream-worlds-largest-electrolyzer-to-be-deployed-in-norway/

[13] Salzgitter AG, SALCOS, Project GrInHy2.0, Available: https://salcos.salzgitter-ag.com/en/grinhy-20.html

[14] GreenHyScale, Available: https://greenhyscale.eu/

[15] European Commission, EU funding programmes and funds 2021-2027, Horizon Europe: Available: https://single-market-economy.ec.europa.eu/industry/strategy/hydrogen/funding-guide/eu-programmes-funds/horizon-europe_en

[16] Hydrogen Central, HydrogenPro ASA – Fourth quarter 2022 results, February 2023., Available: https://hydrogen-central.com/hydrogenpro-asa-fourth-quarter-2022-results/

[17] Hydrogeninside, World's largest green hydrogen project — China's 260MW Kuqa facility — to be commissioned at the end of May, Available: https://www.hydrogeninsight.com/production/world-s-largest-green-hydrogen-project-chinas-260mw-kuqa-facility-to-be-commissioned-at-the-end-of-may/2-1-1457242

[18] Global Construction Review, Sinopec launches world's biggest green hydrogen project in Inner Mongolia, Available: https://www.globalconstructionreview.com/sinopec-launches-worlds-biggest-green-hydrogen-project-in-inner-mongolia/

[19] Offshore Technology, China's Sinopec to build 400km west-to-east hydrogen transmission line, Available: https://www.offshore-technology.com/news/chinas-sinopec-hydrogen-transmission-line/

[20] Hydrogen Insight, EXCLUSIVE | 'World's biggest hydrogen electrolyser factory will be a quarter the cost and size of a comparable PEM or alkaline plant', Available: https://www.hydrogeninsight.com/innovation/exclusive-worlds-biggest-hydrogen-electrolyser-factory-will-be-a-quarter-the-cost-and-size-of-a-comparable-pem-or-alkaline-plant/2-1-1412223

[21] S&P Global, Hydrogen fever in EU puts 2024 target of 6-GW electrolyzer capacity in reach, July 2021., Available: https://www.spglobal.com/commodityinsights/en/market-insights/latest-news/electric-power/070721-hydrogen-fever-in-eu-puts-2024-target-of-6-gw-electrolyzer-capacity-in-reach

[22] European Commission, Hydrogen Public Funding Compass: Available: https://single-market-economy.ec.europa.eu/industry/strategy/hydrogen/funding-guide_en

[23] MINGOR, Vijesti, Available: https://mingor.gov.hr/vijesti/projektu-dolina-vodika-sjeverni-jadran-dodijeljeno-25-milijuna-eura/9120

[24] Poslovni dnevnik, Ina kreće s pripremama za proizvodnju u sklopu novog vrijednog mega-projekta, Available: https://www.poslovni.hr/hrvatska/ina-krece-s-pripremama-za-proizvodnju-zelenog-vodika-4362904

[25] European Commission, Pitanja i odgovori: Strategija za vodik za klimatski neutralnu Europu, Available: https://ec.europa.eu/commission/presscorner/detail/hr/qanda_20_1257

[26] Levačić i Teklić, Zeleni vodik i prijenosna elektroenergetska mreža - prilika budućnosti kao potpora razvoju projekata OIE, HRO CIGRE 15. simpozij o vođenju EES-a, November 2022.

[27] IRENA, Making the breakthrough: Green hydrogen policies and technology costs, 2021.

[28] Salzgitter orders one of Europe's largest green hydrogen plants from ANDRITZ, September 2023, Available: https://www.salzgitter-flachstahl.de/en/news/details/salzgitter-orders-one-of-europes-largest-green-hydrogen-plants-from-andritz-21046.html

[29] Yunfei Li, Richen Lin, Richard O'Shea, Vaishali Thaore, David Wall, Jerry D. Murphy: A perspective on three sustainable hydrogen production technologies with a focus on technology readiness level, cost of production and life cycle environmental impacts, Heliyon, Volume 10, Issue 5, 15 March 2024, e26637, https://www.sciencedirect.com/science/article/pii/S2405844024026689

[30] Commission Delegated Regulation (EU) 2023/1184 of 10 February 2023 supplementing Directive (EU) 2018/2001 of the European Parliament and of the Council by establishing a Union methodology setting out detailed rules for the production of renewable liquid and gaseous transport fuels of non-biological origin, C/2023/1087, OJ L 157, 20.6.2023, p. 11–19

[31] European Hydrogen Bank auction provides €720 million for renewable hydrogen production in Europe, press release, 30 April 2024, Brussels, https://ec.europa.eu/commission/presscorner/detail/en/IP_24_2333

[32] The European hydrogen market landscape, November 2023, Clean Hydrogen Joint Undertaking, European Hydrogen Observatory, https://observatory.clean-hydrogen.europa.eu/.

[33] Assessing the Flexibility of Green Hydrogen in Power System Models, ESIG, A Report by the Energy Systems Integration Group's Flexibility Resources Task Force, April 2024

Martina Mikulić, Martina Rubil, Ivan Andročec, Development of Electrolyser Projects for Production of Renewable Hydrogen, Journal of Energy, vol. 73 Number 3 (2024), 9–16
https://doi.org/10.37798/2024733518

Journal of Energy

VOLUME 73 Number 3 | 2024

journal homepage: http://journalofenergy.com/

Evaluation and Modeling the Performance of Rice Husk Gasifier Cook Stove for Household Energy Use

Mersha A. Fetene, Dessye B. Tikuneh

***Summary* — The study evaluates the Belonio-type gasifier stoves with rice husk as sustainable energy sources and waste management options for Ethiopian households. It compares the performance of insulated and non-insulated types to determine reactor design parameters. It predicts a mathematical model for the optimal performance of the gasifier stoves, where the insulated stove showed a lower start-up time. Still, there was no significant difference at a 5% probability level. The temperature change was also insignificant, as heat transfer and temperature change started when the husk was ignited. At room temperature, the maximum and minimum flame temperatures were 1,190.30 °C and 27.33 °C respectively, whereas the average temperature was 758.916 °C for the non-insulated gasifier stove. The insulated gasifier stove also observed maximum and average temperatures of 518.30 °C and 289.014 °C, respectively, at the same room temperature. The fuel consumption rate has a significant effect on the type of gasifier stove, with the maximum rates being 3.820 and 2.099 kg/hr for non-insulated and insulated types of gasifier stoves, respectively. The average specific gasification rates for insulated and non-insulated types of stoves are 106.45 and 120.63 kg/m2h, respectively. The fuel or rice husk holding capacity of each type of stove is significant at a 5% level, with the amount of rice husk and biochar produced being 1.18 kg and 0.27 kg for insulated stoves, and 2.511 kg and 0.688 kg for non-insulated stoves, respectively. Multiple regression analysis was used to model the relationship between time elapsed and temperature and heat energy. The cubic polynomial model was found to be the best predictive model for all variables that can be used to predict the optimal combination of variables. Hence, it can be concluded that the stove is very acceptable with a high prospect for adoption for household energy use.**

***Keywords* — Energy, Insulated, Non-Insulated, Heat, Temperature, Time, Boiling, Relation**

I. Introduction

Rice milling generates a byproduct known as husk, with 78% of the weight being head rice, broken rice, and bran during the milling process of paddy. According to the Central Statistics Agency (CSA), the Ethiopian rice production has increased from 170,630.101 tons to 268, 223.514 tons of paddy in 2019/2020 to 2020/2021 cropping season [1]. Hence, during milling an average of 22% of the paddy is received as husk [2]. Rice mills in Ethiopia, are situated in rice-producing areas in Fogera, Gurafarda, and Gambella [3]. These mills produce rice from dry paddy through various processes including cleaning, parboiling, drying, milling, polishing, and packaging. Recently, rice husk biomass waste has been common in those rice-producing regions considered as waste material and has generally been disposed of by dumping or burning, although some have been used as a low-grade fuel. This has led to environmental problems such as pollution resulting in a refuse heap on streets, drainage systems, and waterways, which has resulted in flooding on rainy days due to the blockage of waterways [4]. On the other hand, Ethiopia has one of Africa's fastest-growing economies but has one of the world's poorest access to modern renewable energy supplies. Biomass accounts for approximately 87% of the total energy supply in rural areas for lighting and cooking [5].

However, this waste can be converted into fuel for domestic cooking, benefiting many households and achieving more forest savings for the country [6]. Rice husk can be a solution for renewable energy promotion and an alternative for the reduction of greenhouse gas emissions by being an alternative to fast-declining wood fuels. Energy remains essential for development, but the exploitation of energy sources needs to be carried out with sustainability in mind. Rice husk has a higher ash content (20-22.4%), 1.0% crude protein, 0.3% crude fat, and 30% carbohydrate with exceptional biomass with good flow ability, availability with 10-12% moisture, and fewer alkaline minerals [7]. It can be used for household fuel, with 25% of the weight converted into ash during the firing process. Using rice husk as a useful household energy source has the advantages of cleanliness, ease of handling, and igniting, producing a small volume of smoke. Its ash content is rich in potash and phosphate, which can be used as fertilizer on unfertile soil. Hence, rice husk dumps can be properly recycled into useful products, more goods will be made available to society, and environmental pollution and other disease attacks will be greatly reduced [7]. Rice husk ash can be used as organic fertilizer, pest or insect repellent, or for eco-friendly construction. Rice husk accumulation is challenging to eradicate; instead, it is a situation that must be continually managed and controlled by utilization and specifically by household fuel and energy branding remains the sustainable option for dealing with husk accumulation, as this takes up a long time [8].

Research trials and emerging evidence suggest that sustainable approaches help increase yields while making production systems more resilient and economically accessible [9]. The developed Belonio-type rice husk stoves are available in countries where rice growing is a major economic activity, such as India, Indonesia, and the Philippines [8]. This simple stove requires no installation and is ready for use by end-users with basic instructions. Rice husk gasifier stoves reduce the accumulation of rice husks in riverbanks

(Corresponding author: Dessye Belay Tikuneh)

Mersha A. Fetene and Dessye B. Tikuneh are with the Ethiopian Institute of Agricultural Research, Agricultural Engineering Research, Bahir Dar, Ethiopia (e-mail: dessyebelay20@gmail.com)

Mersha A. Fetene, Dessye B. Tikuneh, Evaluation and Modeling the Performance of Rice Husk Gasifier Cook Stove for Household Energy Use, Journal of Energy, vol. 73 Number 3 (2024), 17–35
https://doi.org/10.37798/2024733521

and along roadsides, utilization to reduce the wild dumping of rice husks in Ethiopia's Fogera plain, going a long way in reducing the cutting of trees for fuel wood, which in turn will cause desertification. This rice husk stove was introduced recently and refabricated in Ethiopia and was evaluated and predicted model as a major research activity that needs further adoption. Hence, this research report was initiated with the following objectives.

- To evaluate the Belonio-type gasifier stoves with rice husk as a sustainable energy source and waste management options for Ethiopian household energy use
- To investigate and compare the performance of the Belonio-type insulated and non-insulated types of gasifier stoves for the determination of appropriate design parameters of the reactor
- To predict an appropriate mathematical model estimating the optimum performance of the Belonio-type gasifier stoves

II. Materials and Methods

Study Area

The research was conducted in Fogera National Rice Research and Training Center (FNRRTC), Wereta, Ethiopia, which is one of the federal research centers of the Ethiopian Institute of Agricultural Research (EIAR) found in Fogera Wereda, south Gondar zone of Amhara Regional State, Ethiopia. It is located at 11° 58' N latitude, 37° 41' E longitude, and at an elevation of 1810 m above sea level. Based on ten years' average meteorological data, the annual rainfall, and mean annual minimum, maximum, and average air temperatures are 1300mm, 11.5°C, 27.9°C, and 18.3°C, respectively (Abebe et al., 2019). FNRRTC is located 625 km from Addis Ababa and 55 km from the regional capital of Bahir Dar, Ethiopia.

Description of the Rice Husk Gasifier Stove

The rice husk gasifier stove is a recently developed device for domestic cooking that utilizes rice husks as fuel. Primarily, the stove was developed by [8] that used to burn rice husk using a limited amount of air for combustion to produce a luminous blue flame, which is almost similar to that of the liquid petroleum gas (LPG) stove. Then the model of the gasifier stove was redesigned and remanufactured in Ethiopia for utilization of rice husk for household energy and then evaluated and modeled its performance in the Ethiopian condition. According to [8], the details of the gasifier stove components are explained below:

- **Gasifier stove reactor:** It is the part of the gasifier stove, where rice husks are put and burned while breathing in very little air. This cylindrical reactor can range in diameter from 0.10 to 0.30 meters, depending on how much electricity the stove requires. Depending on the needed working period, the cylinder's height ranges from 0.4 to 1.0 m. The cylinder is constructed from gauge no. 18 regular galvanized iron on the outside and gauge no. 20 stainless steel on the interior. The burned rice husks or any other materials are placed in this 2-cm cylinder area, which acts as insulation to stop heat loss in the gasifier. Rice husks are held in place during gasification by a stainless steel fuel grate located at the reactor's bottom end. This grate is angled so that, following each operation, it may be readily released. To keep the grate in the right position while in use, a lock or spring is used. To prevent hands from unintentionally contacting the hot reactor while it is operating, an aluminum screen is held in place by circular rings around the exterior of the reactor (Fig. 1).
- **The char chamber:** It stores the char that is left over from each operation. Its placement underneath the reactor makes it convenient to collect any char that may fall from the reactor. The door to this chamber can be opened for convenient charcoal disposal, but it must always be kept closed while running the gasifier. To minimize excessive airflow loss in the system during fuel gasification, the char chamber is firmly fitted on all sides to keep air released by the fan from exiting the chamber. To hold the entire stove, the chamber has four (4) support legs with rubber coverings underneath (Fig. 1).
- **Air blower:** during gasification, the fan assembly supplies the air required by the fuel. To force air into the reactor's rice husk column directly, it is often connected to the char chamber at either the chamber's entrance or its interior. The standard model's fan is an axial-type fan with a 3-inch diameter, which is frequently found in computer systems. It uses a 220-volt AC line with a rated power input of 16 watts. During operation, the fan's speed is managed by a manually operated rotary switch, which also regulates the gas supply to the burner. The burner (Fig. 1) transforms the gas exiting the reactor into a blue flame.
- **Burner:** It is made up of a series of 3/8-inch-diameter holes that allow flammable gas to flow through. The air required for gas combustion is supplied by the secondary holes around the burner's perimeter. A pot support sits atop the burner, keeping the pot steady as it cooks. The burner is fixed in place during operation and is detachable for simple fuel loading into the reactor (Fig. 1).

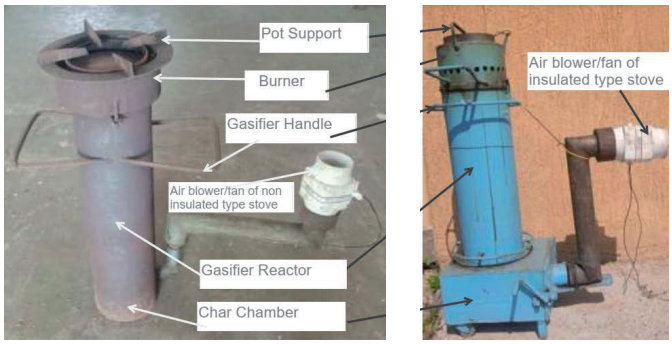

a) b)

Fig. 1. Parts of the rice husk gasifier stove (a) the non-insulated type and (b) insulated type gasifier stoves

Materials Used

The following are the materials and instruments used to test the performance of the stove:

1. **Fresh, dried rice husk** – This will be used as fuel in testing the performance of the stove. It was freshly obtained from the rice husk and dried to be 9.97% moisture content.
2. **Volumetric flasks and beaker** - This glassware was used to measure the volume of water before and after the boiling test. The change in the volume of water after the test indicates the power output of the stove per load.
3. **Stop Watch** – This was used to record the time of each of the different activities both cooking and boiling) during the tests.

Mersha A. Fetene, Dessye B. Tikuneh, Evaluation and Modeling the Performance of Rice Husk Gasifier Cook Stove for Household Energy Use, Journal of Energy, vol. 73 Number 3 (2024), 17–35
https://doi.org/10.37798/2024733521

4. **Thermometer** - This equipment is used in the measuring of the gas temperature leaving the combustion chamber was a universal thermometer, 0-250 °C (model: Bengt Ek Design/ 209007).
5. **Sensitive Weighing Balance** - This device with the model WT6002N was used to measure the weight of rice husk fuel as well as the weight of food to be cooked and the weight of water to be boiled.
6. **The data logger** – was used to measure the temperature produced by burning rice husks in the reactor of the stove as well as related generated and losses of heat. The data loggers with the Squirrel 2020 with SQ2020/2F8 model were used in this research with high-performance universal data loggers with fast, and PC-linked data acquisition systems in this research. It used this device for that maximum temperature with twin processors, multiple 24-bit analog-to-digital converters, up to 16 universal channels, and a choice of communications methods to ensure that the Squirrel 2020 series provides state-of-the-art data logging and communication capability for sophisticated applications needs.

The procedure of the Experiment

In this study, the rice husks were collected from the FNRRTC rice-processing workshop. The guidelines for the performance evaluation and operation of the stove used were based on standard procedures recommended by [8]. The raw material, the rice husk was collected and cleaned to avoid foreign matters such as stone, soil, and other foreign matters. The collected raw material was then sun-dried to remove excess moisture and make it easy to handle, transport, and store. After maintaining husk moisture at 9.97%, it was evaluated as an energy source for cooking using a gasifier stove. The rice husk gasifier stove was a recently developed device to utilize rice husk as a fuel that was used for evaluating rice husk for household fuel with minor modifications [8]. The char is a carbonized raw material that was taken out of the reactor and cooled. Some pictures taken during the experiment are illustrated in Fig. 2 and 3 below. The burner, grate, and ash chamber door are set in their proper position during the performance evaluation. The fan was plugged into a full outlet after checking the working condition when the switch was in the ON or OFF position.

The load of rice husk fuel into the reactor is by directly pouring the fuel from the container with one full load of fuel used per replication. Pieces of paper were used for easy start-up by pouring drops of it on the fuel column. The water-boiling test was conducted as illustrated in Fig. 2 and 3 below.

a)

b)

Fig. 3. Water boiling test using a data logger for non-insulated type gasifier

a)

b)

Fig. 2. Water boiling test using a data logger with the computer for insulated type gasifier

Mersha A. Fetene, Dessye B. Tikuneh, Evaluation and Modeling the Performance of Rice Husk Gasifier Cook Stove for Household Energy Use, Journal of Energy, vol. 73 Number 3 (2024), 17–35
https://doi.org/10.37798/2024733521

The reactor was closed by placing the burner on top of it when the rice husk in the reactor was observed to be burning. After allowing the rice husk to burn for a minute, the gas was ignited at the burner. The startup time was recorded until a luminous blue flame was produced. Then the operation time was started to record both with place a casserole and with an aluminum pot on top of the burner and without a pot. When all the rice husk is completely burned or when the stove stops producing gas, it means that the operation is finished; the total operation time was recorded, and shut OFF the fan with the SEAFLO Inline blower, model: SFLB1-270-02. The burned rice husk (bio-char) was immediately discharged cooled and weighed bio-char.

Fig. 4. The rice husk gasifier stove (a) the non-insulated type and (b) insulated type gasifier stoves

Experimental Design

The experiment design for the performance evaluation and modeling of the rice husk gasifier stove was a completely randomized design (CRD) having two stove types viz: non-insulated and insulated gasifier stoves as treatments on the cooking of boiling water and with no-cooking with three replications. The material properties of the gasifier stoves are the basic characteristics used to determine the heat transfer property. The gasifier stove reactor is the component of the stove where rice husks are placed and burned with a limited amount of air. The details of the two treatments are illustrated here below.

1. **The insulated type gasifier stoves:** The mild steel reactor of the insulated stove type has an annular spacing of 2cm and measures 3 cm on the outside and 2 cm on the inside. This reactor is cylindrical in shape, having a diameter of 0.15 m, height of 0.565 m, and volume of 0.010 m^3. Unlike the non-insulated one, it is the burned biochar or rice husk ash acts as a heat-retaining barrier in the annular space between the inner and outside of the reactor to reduce heat loss. This cylinder of the insulated one is provided with an annular space of 2 cm, where the burned rice husks or ash is placed to serve as insulation to prevent heat loss in the gasifier for the insulated type of stove (Fig. 4a). The burning layer of rice husks, also known as the combustion zone, descends the reactor when the fuel is ignited from the top, depending on how much air is provided by the fan [8]. At the lower end of the reactor is a fuel grate made of stainless steel material, which is used to hold the rice husks during gasification.
2. **The non-insulated type gasifier stoves:** The non-insulated type stove has a reactor with a cylinder shape made up of 3mm mild steel. It was made up of mild steel of 3mm thickness and was only one-sided. This reactor is cylindrical in shape, having a diameter of 0.19 m, height of 0.665m, and volume of 0.019 m^3. Hence, during burning, it has not a heat-retaining barrier on the reactor to keep heat from escaping the gasifier. The burning layer of rice husks, also known as the combustion zone, descends the reactor when the fuel is ignited from the top, depending on how much air is provided by the fan [8]. In addition, the outside parts of the reactor or combustion zone are very hot during burning because of heat loss through the outside of the reactor (Fig. 4b). At the lower end of the reactor is a fuel grate made of stainless steel material, which is used to hold the rice husks during gasification for both insulated and non-insulated types of gasifiers.

Data Collected

The multiple regression analysis was made to analyze and establish a relationship between the heat energy and the operating time of both gasifier stoves for both heat energies produced and lost. The heat energy provided by the burning of the rice husk in the reactor of the stove and associated heat losses at the outside of the reactor were estimated for both types of stoves through the change in temperature concerning operating time using the Squirrel 2020 SQ2020/2F8 data logger. The regression analysis using the relationship between heat energy produced and the operating time of both types of stoves was expressed using a polynomial regression model using the equation and fitting curve. The variables/parameters described below were recorded in each three replications along with the treatments of both gasifiers. Hence, the following parameters are used during evaluating the rice husk for energy:

1. **Start-Up Time:** It is the time required to ignite the rice husk and consequently produce combustible gas. The start-up time was measured using a stop watch where the time burning pieces of paper are introduced to the fuel in the reactor until combustible gas is produced at the burner and repeated three times.
2. **Operating Time:** It is the duration from the time of gasifier produces a combustible gas until no more gas is obtained from the burning of the rice husk and measured using a stopwatch with three replications.
3. **Fuel Consumption Rate (FCR):** FCR is the amount of rice husk fuel used in operating the stove divided by the operating time within three replications. The weight of dried rice husk was measured using a weight balance at 9.97%, average moisture content. The FCR was computed using the equation (1) below [8]:

$$FCR = \frac{\text{Weight of Rice Husk Fuel Used (kg)}}{\text{Operating Time (hr)}} \quad (1)$$

4. **Specific Gasification Rate (SGR):** SGR is the amount of Rice husk fuel used per unit time per unit area of the reactor. It was measured for treatments of both gasifiers per replications and computed using equation (2) [8]:

$$SGR = \frac{\text{Weight of Rice Husk Fuel Used (kg)}}{\text{Reactor area } (m^2) \times \text{Operating Time (hr)}} \quad (2)$$

5. **Combustion Zone Rate (CZR):** The time required for the combustion zone to move down through the reactor is Combustion Zone Rate (CZR). It was computed in each replication and computed using the equation (3) [8]:

Mersha A. Fetene, Dessye B. Tikuneh, Evaluation and Modeling the Performance of Rice Husk Gasifier Cook Stove for Household Energy Use, Journal of Energy, vol. 73 Number 3 (2024), 17–35
https://doi.org/10.37798/2024733521

$$CZR = \frac{\text{Length of the Reactor (m)}}{\text{Operating Time (hr)}} \quad (3)$$

6. **Boiling Time:** This is the time required for the water to boil starting from the moment the pot is placed on the burner until the temperature of the water reaches 100ºC [8]. It was replicated three times for 2 liters of water using a 2 mm thickness aluminum pot without a lid.

7. **Sensible Heat:** This is the amount of heat energy required to raise the temperature of the water. This is measured before and after the water reaches the boiling temperature. It was repeated for three replications and computed using the equation (4) [8]:

$$SH = Mw \times Cp \times (Tf - Ti) \quad (4)$$

Where:

SH = sensible heat, Kcal,
Cp = specific heat of water, 1 Kcal/kg-°C,
Tf = temperature of water at boiling, Approx. 100°C, Mw = the mass of water, kg (1kg/liter),
Ti = temperature of the water before boiling, 27-30°C

8. **Latent Heat:** This is the amount of heat energy used to evaporate water. The amount of evaporated water from the initial 2 liters of water was measured after completion of the complete burning of husk fuel from each replication and computed using the equation (5) [8]:

$$Lh = We \times Hfg \quad (5)$$

Where:

L_H = latent Heat, Kcal
H_{fg} = latent heat of water, 540 Kcal/kg
We = the weight of water evaporated, kg,

9. **Heat Energy Input:** It is the amount of heat energy available in the rice husk fuel. The heat energy input was estimated in three replications and computed using the equation (6) [8]:

$$QF = We \times Hfg \quad (6)$$

Where:

QF = heat energy available in the fuel, Kcal,
WFU = the weight of rice husk used in the stove, kg
HVF = the heating value of rice husk, Kcal/kg

10. **Thermal Efficiency:** This is the ratio of the energy used in boiling and evaporating water to the heat energy available in the fuel per each replication and computed using the equation (7) [8].

$$TE = \frac{\text{Sh} + \text{LH}}{\text{HF} + \text{WF}} x100 \quad (7)$$

Where:

TE = thermal efficiency, %
LH = latent heat, Kcal
Sh = sensible heat, Kcal,
HF = the heating value of fuel, Kcal/kg,
WF = the weight of fuel used, kg

11. **Input Power of Rice Husk:** This is the amount of energy supplied to the stove based on the amount of rice husk consumed in each replication and computed using the equation (8) [8].

$$Pi = 0.0012 \times FCR \times HVF \quad (8)$$

Where:

Pi = power input, Kw,
FCR = fuel consumption rate, kg/hr,
HVF = the heating value of fuel, Kcal/kg

12. **Input power of Fan:** The total consumed electric power in the working load of the air blower was measured in each replication. The SEAFLO Inline blower, model, SFLB1-270-02 was used and the input power of the fan was calculated by the following equation (9) [10]:

$$E_f = P \times I \quad (9)$$

Where:

I = line current strength (Ampere) and
V = potential difference (Voltage).

13. **Power Output:** This is the amount of energy released by the stove for cooking. It was computed using the equation (10) per each replication [8]:

$$Po = FCR \times HVF \times TE \quad (10)$$

Where:

Po = power output, kW,
FCR = fuel consumption rate, kg/hr.,
HVF = the heating value of fuel, Kcal/kg, TE = thermal efficiency and percentage

14. **Char Produced (%):** This is the ratio of the amount of char produced after the complete burning of rice husks. The char produced can be computed per each replication using the equation (11) [8]:

$$\%Char = \frac{Weight\ of\ char(kg)}{\text{Weight of dried Water Hyacinth used}(kg)} \quad (11)$$

15. **Heat Energy:** The heat energy produced at the burner of the stove and heat loss through the combustion zone of the stove to the outside environment where raising the temperature to a desired level was considered. The heat energy produced in the gasifier stove was calculated using the equation (12) provided by [11].

$$M_h C_p (T_i - T_f) \quad (12)$$

Where:

M_h = mass of husk, kg
C_p = the specific heat capacity of the produce, (kJ/kg°C)
T_i = the room temperature during the test, °C, T_f = the temperature produced by burning in the burner, °C

Data Analysis

The least significant difference (LSD) test was applied to determine differences between treatments using a 5% probability level. The significant difference in levels for each experiment was tested using the LSD test. A $p < 0.05$ was considered statistically significant. Data were subjected to analysis of variance (ANOVA) using statically producer as described by [12].

Mersha A. Fetene, Dessye B. Tikuneh, Evaluation and Modeling the Performance of Rice Husk Gasifier Cook Stove for Household Energy Use, Journal of Energy, vol. 73 Number 3 (2024), 17–35
https://doi.org/10.37798/2024733521

III. Result and Discussion

The performance evaluation of the gasifier stove was conducted at an average moisture content of husk on a wet basis of 9.97%, with both insulated and non-insulated types of gasifier stoves. The relative humidity and temperature of the testing room were 42.78% and 26.43 °C, respectively. Both gasifier stoves were evaluated in full load conditions where the husk was collected from local millers that are produced during usual milling with a bulk density of 130.05 kg/m^3.

A. Performance of Gasifier Stoves

Operations of both insulated and non-insulated gasifier stoves were initiated using small pieces of paper. The ignition time or the time required to start to ignite the insulated and non-insulated gasifier stoves are 3.86 and 4.65 minutes, respectively. The insulated gasifier has a relatively lower start-up time than the non-insulated type, but statistically, there is no significant difference at a 5% probability level. The change in temperature of the gasifier stoves concerning the start-up time was not significant and graphically showed that it is a straight line over time, as shown in Figs. 5 and 6 below. After the startup time of the stoves was recorded, it was operating time when it was fully in operation until the burning of rice husk was finished. The operation times in one batch feed of husk of both insulated and non-insulated gasifier stoves are 33.888 and 39.672 minutes, respectively, but there is no statistical difference. The amount of husk consumed per batch of insulated and non-insulated gasifier stoves was also 1.1802 and 2.5106 kg, respectively. As shown in Fig. 5, the maximum flame temperature was 1,190.30 °C at a room temperature of 27.33 °C, whereas the average temperature was 758.916 °C for the non-insulated type gasifier stove. On the other hand, the maximum and average temperatures of the insulated gasifier stove were also 518.300 °C and 289.014 °C, respectively, at the same room temperature as shown in Fig. 6, which was in line with similar findings [8].

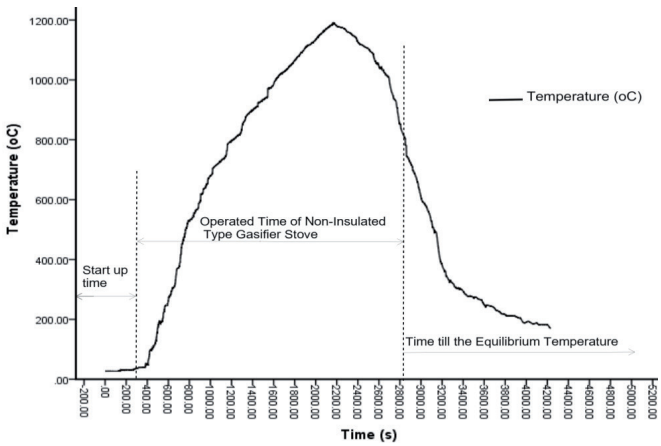

Fig. 5. The relationship between burning temperature (°C) and burning time (s) of a non-insulated type gasifier stove

On the other hand, the maximum and average temperatures of the insulated gasifier stove were 518.30 °C and 289.014 °C, respectively, at the same room temperature as indicated in Fig 6. Belonio (2006) found that insulated gasifier stoves produced flame temperatures ranging from 465 to 610 ºC, which was consistent with previous findings for the insulated type [8]. It was also observed that the Paul Oliver rice husk gasifier stove, which is very similar in design to the non-insulated type gasifier stove, has a maximum burning temperature of around 700 °C [13].

The insulated type gasifier stove reactor was insulated using biochar, which filled the annular space between the inside and outside mild steel sheet. This insulation resulted in lower temperatures and reduced heat expansion throughout the reactor wall to the outside environment, indicating that the insulated-type gasifier stove was more effective in preventing heat loss. The temperature of a gasifier stove increases from startup time to maximum values, where fuel ignites from the top to bottom of the reactor. The temperature declines with the amount of husk in the reactor, and when the rice husk is burned, the flame is stopped, and the temperature declines sharply to room temperature. The residual temperature of insulated and non-insulated gasifier stoves starts at 330.70 and 817.60 °C, respectively, after burning the husk as shown in Figs. 5 and 6. The temperature-time graph profile of the non-insulated type gasifier stove as shown in Fig. 5 is much more in line with other findings [13]. According to reports revealed, the flame temperature of rice husks for Rice Husk Gasifier Stoves (Belonio Type) starts to decline after around 800 °C, which was lower and higher than the non-insulated and insulated type gasifier stoves, respectively [13].

The residual temperature is also maximum for the non-insulated type gasifier stove, as shown in Fig. 5 and 6. The burning of fuel in the combustion zone moves downward along the height of the reactor, determining the operating time for the conversion of burned rice husks to biochar. The relationship between burning temperature and time shows a similar shape for both types of stoves, with sharp declines after burning the husk but slow cooling to room temperature. The fuel burning zone in stoves was moved downward along the reactor height, with the height of the reactor for both insulated and non-insulated gasifier stoves determining the operating time for the conversion of rice husks to biochar. Generally, the relationship between the burning temperature and time showed a relatively similar shape for both types of stoves, with sharp declines after burning of the husk but slow to reach an equilibrium temperature.

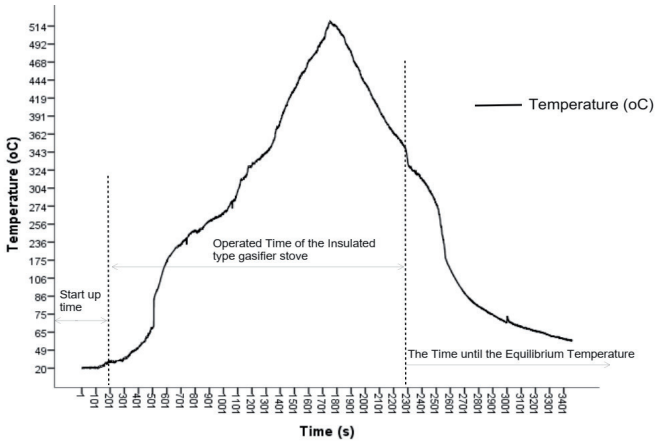

Fig. 6. The relationship between burning temperature (°C) and burning time (s) of the insulated type gasifier stove

B. Fuel consumption

As shown in Figs. 5 and 6, the operating time is the basic factor for the temperature change that indirectly influences some parameters like fuel consumption rate, specific gasification rate, and combustion zone rate of stoves. At a 5% significance level, the fuel consumption rate significantly influences the types of gasifier stoves, with the maximum fuel consumption rate for non-insulated and insulated types being 3.820 and 2.099 kg/hr, respectively. The observed result of an insulated type of gasifier stove is in line with the fuel consumption rate of the insulated type of stove, which ranges from 1.59 to 2.0 kg per hour, [8]. Moreover, the time to consume rice husks to completely gasify the rice husks in the reactor depends on the density of the rice husk, the volume of the reactor, and the fuel consumption rate, which determines the total time to consume the rice husk. The volumes of the reactors for non-insulated and insulated-type gasifier stoves are 0.019 and 0.010 m^3, respectively, and the rice husk consumption per batch was 2.512

Mersha A. Fetene, Dessye B. Tikuneh, Evaluation and Modeling the Performance of Rice Husk Gasifier Cook Stove for Household Energy Use, Journal of Energy, vol. 73 Number 3 (2024), 17–35
https://doi.org/10.37798/2024733521

and 1.180 kg, respectively. It was observed that the non-insulated type of gasifier stove has a higher fuel consumption rate than the non-insulated one. On the other hand, the amount of rice husk fuel used per unit time per unit area of the reactor *i.e.* specific gasification rate did not significantly differ on the types of stoves at a 5% significant level. The average specific gasification rate of insulated and non-insulated types of stoves was 106.45 and 120.63 kg/m^{2}h, respectively; however, it was higher than the 56.81 kg per hr-m^2 that was the same design with the insulated type observed by [8].

The volume of the reactor and the amount of rice husk held per batch of the insulated type are nearly half of the non-insulated type of the stove; however, despite this size, it does not show significant differences in the specific gasification rate. The time required for the combustion zone to move downward to the reactor of the stove's so-called combustion zone rate on the type of stove was not significant at a 5% level of significance. The combustion zone rates of the insulated and non-insulated types of stoves were 1.015 and 1.004 m/h, respectively. The combustion zone rate was also directly proportional to the length of the reactor, where it was 0.665 and 0.565 m for non-insulated and insulated-type gasifier stoves, respectively. However, the size of the reactor of the insulated type is significantly smaller than the non-insulated type of the stove. The same conditions with the volume of the reactor were 0.019 and 0.010 m^3 for the non-insulated and the insulated types of the stoves, respectively, which directly influenced the values of the fuel consumption rate, specific gasification rate, and combustion zone rate of the stoves but did not significantly affect the insulation property of the stove due to the difference in volume and length of the reactors between the stoves. This showed that the fuel (rice husk) holding capacity of the reactor of each type of stove is significant at a 5% level, where the amount of rice husk and biochar produced was 1.18kg and 0.27kg for the insulated type and 2.511kg and 0.688kg for the non-insulated type of stoves, respectively.

C. Water Boiling Test

The time required for the water to boil starts from the moment that the pot is placed on the burner until the temperature of the water reaches 100 °C, which is a significant difference between the insulated and non-insulated types of gasifier stoves at a 5% level of significance. Boiling time using 2 liters of water, boiling from 26°C to 100°C, the time consumed ranges from 8.51 and 12.80 minutes for the non-insulated and insulated types of gasifier stoves, respectively, which indicates the water boiling time for the non-insulated type of gasifier stove is shorter than the non-insulated one while it was much lower than 16- 25 minutes for insulated types of stove obtained to boil the same amount of water [8].

As shown in Fig. 7, after the startup time, the temperature of the water sharply increased up to 207.70 °C, and then it became constant at 205–207 °C for 26.36 minutes. It is in line with the measured gas temperature of water boiling ranges from 160 to 210 °C [8]. The maximum temperature recorded during the boiling of the water was 208.80 °C, which gradually declined until the end of the burning of the husk and the residual temperature of the water reached equilibrium to room temperature (Fig. 7). On the other hand, the amount of water boiled from boiling of two liters of sample water was significant at a 5% level of significance, where the average water boiled for insulated and non-insulated was 1.077 and 0.950 liters, respectively. Unlike the boiling time, the amount of water boiled for the insulated type gasifier stove is higher than the non-insulated type gasifier stove.

The time required to boil water in the insulated-type rice husk gasifier stove to boil two liters of water took 12.80 minutes, which is less than the same stove boiling time of 16–21 minutes [8]. As shown in Fig. 8, the shape of the time versus temperature graph was a dome shape where the temperature increased sharply to the

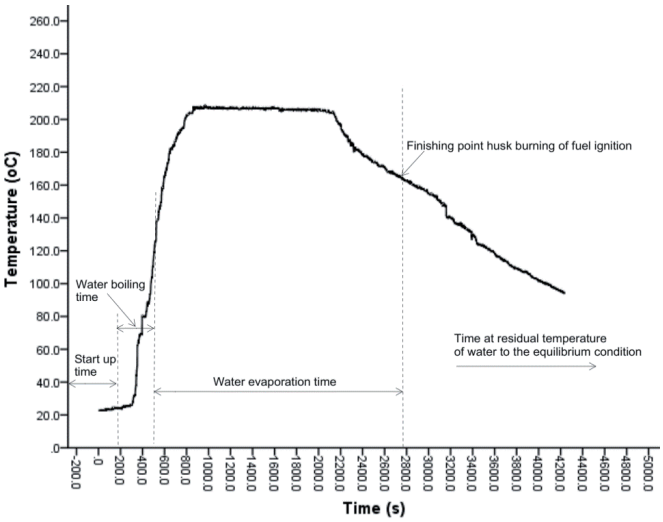

Fig. 7. The boiling temperature (°C) and time (s) of a non-insulated type gasifier stove

maximum range of 124.9 °C. The maximum and average temperatures recorded were 124.9 and 92.99 °C, respectively. Unlike the average and maximum temperature, the amount of water boiled for an insulated gasifier stove is greater than the non-insulated type.

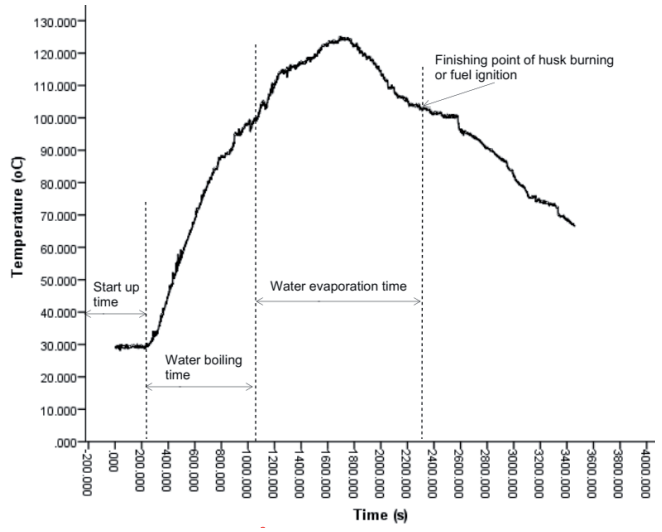

Fig. 8. The boiling temperature (oC) and time (s) of the insulated-type gasifier stove

Moreover, the sensible heat (KJ) is not significantly different between the types of gasifier stoves at a 5% significant level. The average sensible heat of insulated and non-insulated gasifier stoves is 299.96 and 305.11 KJ, respectively. Sensible heat is the product of mass, specific heat, and the temperature difference of water. Hence, the sensible heat of the insulated gasifier stove is relatively lower than that of the non-insulated stove because, to estimate the gasifier stoves, the factors caused by temperature differences are higher on non-insulated gasifier stoves, which is why mass and specific heat are common for both types of gasifier stoves. On the other hand, the latent heat (kJ) is a significant difference in the types of gasifier stoves at a 5% level. The average latent heat of insulated and non-insulated types of gasifier stoves is 2424.4 and 2139.2 kJ, respectively. Unlike the sensible heat of the gasifiers, the latent heat of the insulated type is greater than the non-insulated one, where it mainly depends on the water evaporated during the boiling of the water. In this condition, latent heat depends on the amount of water boiled. It was observed that the average water boiled for insulated and non-insulated types of gasifier stoves is 1.065 and 0.95 liters, respectively. This showed that with these results, the insulated rice husk gas stove is sufficient to provide energy for

Mersha A. Fetene, Dessye B. Tikuneh, Evaluation and Modeling the Performance of Rice Husk Gasifier Cook Stove for Household Energy Use, Journal of Energy, vol. 73 Number 3 (2024), 17–35
https://doi.org/10.37798/2024733521

a family for cooking, and some excess energy can be used to heat water for bathing [8].

D. Thermal Efficiency of the Stove

The amount of energy supplied to the stoves depends on the amount of fuel consumed and air supplied by the fan. This energy depends on the heating value and the amount of husk and energy needed to drive the fan, *i.e.,* the input power source for the gasifier stoves. Based on the data observed on the performance of gasifiers, it was indicated that the biochar conversion rate (%) has shown a significant difference among the types of gasifiers at a 5% significance level. The mean biochar conversion rates of non-insulated and insulated gasifier stoves are 27.337% and 22.854%, respectively, which is lower than the 35% found by Belonio, (2005). It indicated that the mass of biochar produced per rice husk of the non-insulated type is higher than the insulated one, which shows that the insulated gasifier stove was better at burning the husk completely. Hence, the input power supplied was 13.389 kW and 7.4151 kW for non-insulated and insulated gasifier stoves, respectively, which showed the maximum input power was 13.389 kW for non-insulated type gasifier stoves, while the power input for the insulated type of stove was similar, with 5.724 to 7.200 kW for the insulated type of stove observed by Belonio (2005). However, the insulated and non-insulated gasifiers estimated thermal efficiency (%) was 18.469% and 7.8025%, respectively, with highly significant differences among the stoves at a 5% level, which showed the insulated gasifier stove recorded higher thermal efficiency, while the thermal efficiency found by Belonio (2005) was in the range of 12.28 to 13.83%. Moreover, the output powers (kW) for insulated and non-insulated gasifier stoves are 1.3440 and 1.0344, respectively; hence, it is higher for the insulated stove, ranging from 0.749 to 0.909 kW [8]. Therefore, it can be recommended that the stove be insulated with rice husk ash as a good insulating material to obtain higher thermal efficiency. On the other hand, due to its high silica content and being very cheap, since it can be easily obtained from the burned rice husks found on roadsides or in the field, rice husk ash is a good choice for insulation with higher thermal efficiency.

E. Analysis of the Multiple Regression Model

The heat energy in the reactor of gasifier stoves from the burning of rice husks was estimated using the recorded temperature concerning the operating time. Before developing the polynomial regression models, the experimental temperature or heat energy data were plotted against the time-elapse parameters separately for each sampling point to get a visual insight into the relationship between the time and the temperature or heat energy (Figs. 5-8). Those figures revealed the dependency of heat energy and temperature over time. The multiple regression analysis was used to model this relationship between burning time and temperature/heat energy during the evaluation of gasifier stoves. The result from polynomial regression of linear, quadratic, and cubic analysis was the three models used to explain the relationship between times elapsed, or the independent variable, and temperature or heat energy, or the dependent variable, which was used as a criterion for inclusion in the model. Therefore, the relationship between changes in heat energy throughout the operating time was analyzed through a polynomial regression model using the equation and fitting curve.

E. I. Analysis of Heat Energy

The heat energy generated per unit of time is a variable entered into multiple regressions that are used to analyze and establish a relationship between the time (t) in seconds and heat energy (Q) in joules for both insulated and non-insulated types of gasifier stoves.

E..1.1. Heat Generation of the Insulated Type Gasifier Stove

The polynomial regression to model the relationship between the heat energy or dependent variable and multiple explanatory variables *i.e.* time of the insulated type of gasifier stove was made using linear, quadratics, and cubic equations at the coefficient of determination (R^2) of 0.09, 0.90, and 0.95 respectively as shown in Eq. 13, Eq. 14 and Eq. 15 below. The analysis of models to build and select the variable to decide if a variable term can be removed or added without affecting the model significantly. In this case, the larger model or full model is Eq.3 or a cubic polynomial model whereas the remaining Eq. 1 and Eq. 2 are linear and quadratics models respectively. Among the polynomial models, which one significantly, decreased the error and significantly increased the predictive power of the model or improved the model expression is the main thing that makes sense in this concept.

$$Q = 0.083t + 270.950, \qquad R^2 = 0.09 \tag{13}$$

$$Q = 144.43 + 1043t - 0.0004t^2, \qquad R^2 = 0.90 \tag{14}$$

$$Q = -23.192 + 0.483t + 2\times10\text{-}4t^2 - 1.386\times10^{-7}\, t^3, \; R^2 = 0.95 \tag{15}$$

Hence, an analysis of variance (ANOVA) of the three models was made to conclude on the idea of how far the observed heat generated (Q) is from the predicted or fitted heat generated value. On the other hand, adding or reducing the model to make it either significantly better or significantly worse is essentially determined using the partial F test and the sum of squares error. The regression model of linear, quadratic, and cubic functions residual standard error (RSE) and coefficient of determination (R^2) was shown in Table 1 below, which revealed that the cubic model was highest in R^2, lowest in RSE with 0.951, and 45.594, respectively. It can be concluded that the lowest RSE showed the model predicted heat generated (Q) value is closest to the observed heat generated (Q) values or the model most wisely fits than the remaining linear and quadratic models. Besides, to check whether at least one model is significantly better or there is no difference between the three polynomial models, the ANOVA, or partial F-test, was applied. Hence, the ANOVA between linear, quadratics, and cubic models indicated that the full model, or cubic model, is significantly better than the remaining reduced models (linear and quadratics) at $P > 0.001$, as shown in Table 1.

Table 1.
Polynomial Regression Summary Using Linear, Quadratics and Cubic Model (Standard eError is in Parenthesis) of Heat Generated within Time Elapse for Insulated Type Gasifier Stove

	Coefficients				R- Square
Model	Constant	t	t^2	t^3	
Linear	270.30*** (7.72)	0.083*** (0.005)	-	-	0.090 (196.525)
Quadratic	-144.42*** (3.81)	1.043*** (0.007)	-3.7e-4*** (8.39e-20)		0.902 (64.55)
Cubic	-23.20*** (1.659)	0.483*** (0.012)	-2.01e-4*** (4.96e-19)	-1.386e-7* (1.24e-22)	0.951 (45.594)

Significance codes: 0.0001***, 0.001**, 0.01*, 0.05, 0.1,

Mersha A. Fetene, Dessye B. Tikuneh, Evaluation and Modeling the Performance of Rice Husk Gasifier Cook Stove for Household Energy Use, Journal of Energy, vol. 73 Number 3 (2024), 17–35
https://doi.org/10.37798/2024733521

The graphical presentation of the observed heat generated compared with the three models (linear, quadratics, and cubic) to show how well it fits or predicts the observed data is shown in Fig 9 below. The lines colored black, blue, and red with green in the graph are linear, quadratic, and cubic models with observed heat-generated values, respectively. The visualizations of the polynomial model fit for the heat generated in the insulated type gasifier stove are shown in Figure 6 below. On the graph in Fig 9, the observed heat generated after 2600 seconds was heat energy generated by the residual temperature, which remains until the equilibrium condition with room temperature or until no heat energy is generated.

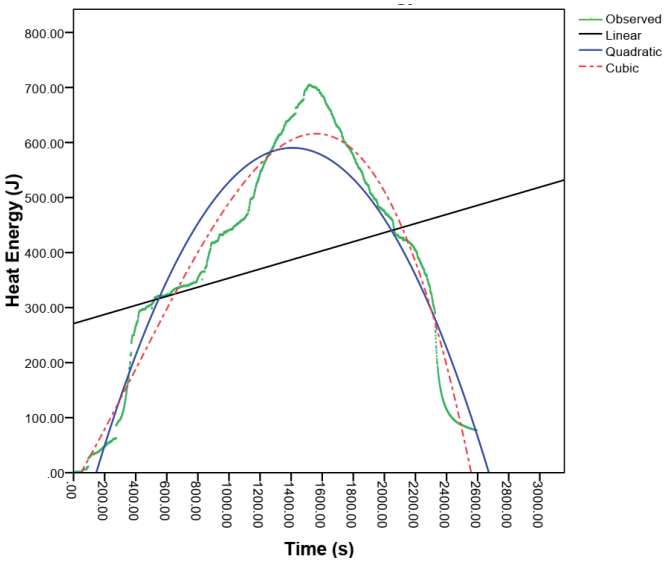

Fig. 9. Visualizations of the polynomial model fit for the heat generated in the insulated type gasifier stove

As shown in Fig. 10a, the 95% confidence interval (CI) for the fit provides a range of likely values for the mean generated heat energy (J) given the specified settings of the elapsed time (s). It is 95% confident that the confidence interval contains the population means for the heat-generated values of the variables in the model. The prediction interval (PI) is a range that is likely to contain a single future response for determining the heat energy generated and the time (s) of the insulated-type gasifier stove. The 95% PI is always wider than the CI due to the added uncertainty involved in predicting a single response of heat energy versus the mean response (Fig. 10a). Fig. 10b is the best-fit model for heat generation in the insulated type gasifier stove that was the cubic polynomial model, which was the normal probability plot that was approximately normally distributed. The data were plotted against a theoretical normal distribution, which forms an approximate straight line. Departures from this straight line indicate departures from normality, as shown in Fig. 10b. Fig. 10c, is also the residuals versus fits graph plots of the residuals on the y-axis and the fitted values on the x-axis, verifying the assumption that the residuals are randomly distributed and have constant variance. The points fell randomly on both sides of zero, with no recognizable patterns in the points. The histogram of the residuals shows the distribution of the residuals for all observations to determine whether the data are skewed or include outliers (Fig. 10d). Fig. 10e, residuals versus order in the plot displays the residuals in the order that the data were collected, verifying the assumption that the residuals are independent of one another. Independent residuals show no trends or patterns when displayed in time order, and the residuals on the plot should fall randomly around the centerline (Fig. 10e). In general, the best-fit model is a cubic model where the regression equation is:

$$Q = -23.192 + 0.483t + 2\times10^{-4}t^2 - 1.386\times10^{-7}t^3$$

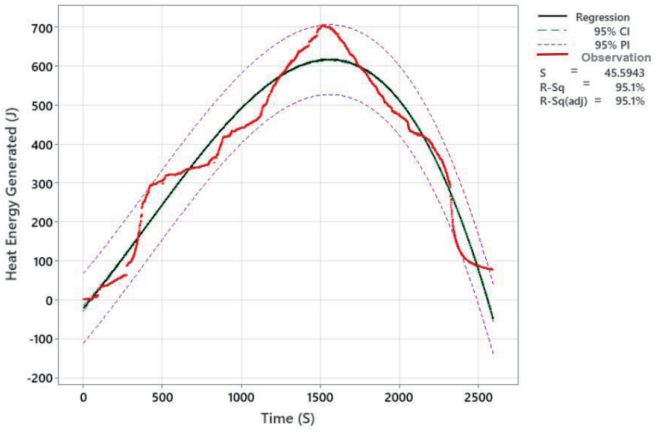

a)

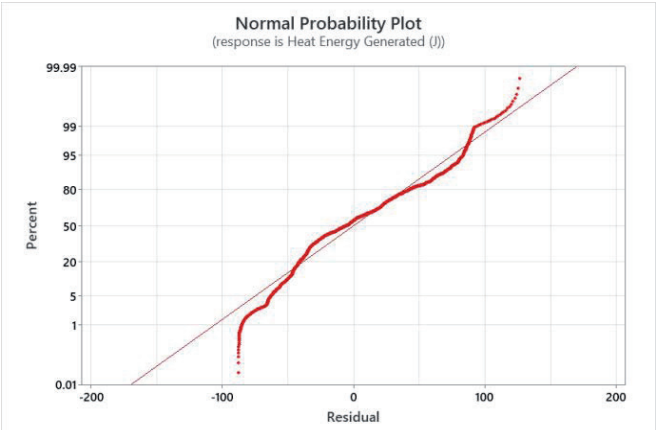

b)

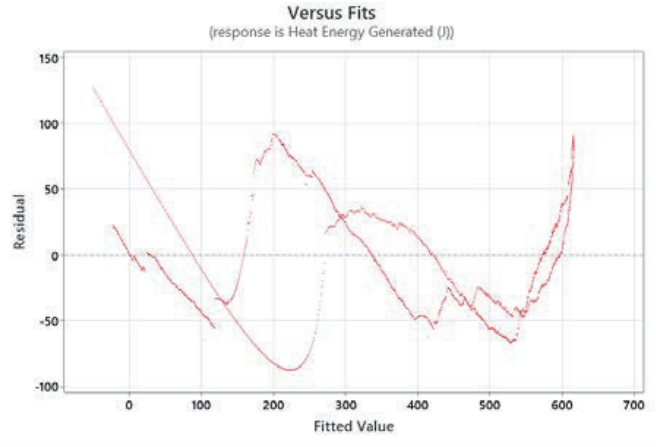

c)

Mersha A. Fetene, Dessye B. Tikuneh, Evaluation and Modeling the Performance of Rice Husk Gasifier Cook Stove for Household Energy Use, Journal of Energy, vol. 73 Number 3 (2024), 17–35
https://doi.org/10.37798/2024733521

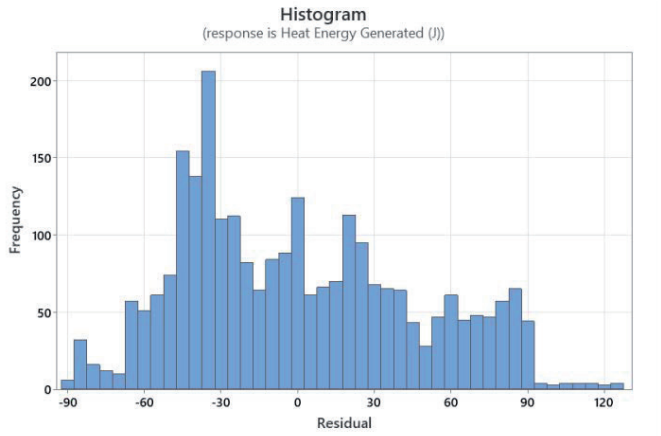

d)

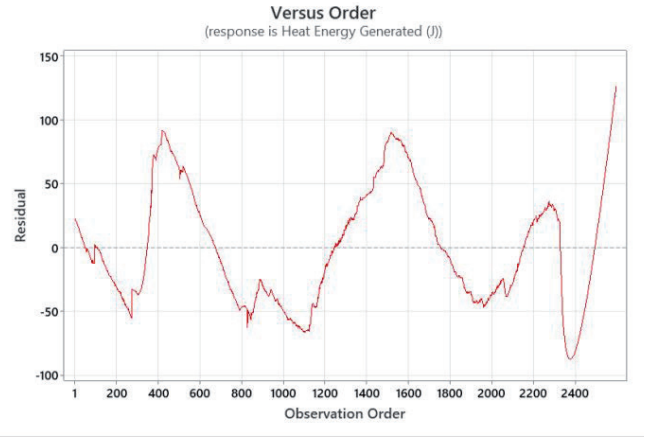

e)

Figure 10. The Polynomial Regression Analysis: Heat Energy Generated (J) versus Time (S) of the cubic regression model fit (a), Normal probability plot of residuals (b), Residuals versus fits (c), Histogram of residuals (d), and Residuals versus order (e) of the insulated type gasifier stove.

E .1.3. Heat Generation of the Non-Insulated Type Gasifier Stove

The heat energy generated by the non-insulate type gasifier stove within time was estimated using the model of the multiple polynomial regressions for linear, quadratic, and cubic equations at the coefficient of determination (R^2) of 0.023, 0.90, and 0.95, respectively, as shown in Eqs. 16, 17, and 18 below. The regression model to determine the fit for the heat generated in the non-insulated type gasifier stove was estimated using three models, but the important thing is which model perfectly fits the observed values of heat generated. Among the polynomial models, which one significantly decreased the error, significantly increased the predictive power of the model, or improved the model expression? The equations of the three polynomial models are shown in Eqs. 4, 5, and 6 below.

$$Q = 0.163t + 1958.39, \quad R^2 = 0.023 \quad (16)$$

$$Q = -233.19 + 4.345t - 0.001t^2, \quad R^2 = 0.968 \quad (17)$$

$$Q = -25.23 + 3.55t - 1.33\times10^{-3}t^2 - 1.33\times10^{-7}t^3, \quad R^2 = 0.974 \quad (18)$$

The coefficient of determination (R^2), residual standard error (RSE), and ANOVA between the models were used to determine the visualizations of the polynomial model fit of the model predicted value to the observed data of heat generated in the non-insulated type gasifier stove. Hence, the residual standard errors (RSE) of linear, quadratic, and cubic models are 996.142, 181.463, and 163.637, respectively. The cubic polynomial model is the list standard error, indicating that the predicted values are closer to the observed values than the other models. The coefficients of determination (R^2) of linear, quadratic, and cubic models were also 0.023, 0.968, and 0.974, respectively, as shown in Table 2 below. The cubic polynomial model has the highest values, revealing that the model could explain around 97.4% of variations in the heat generated. The analysis of variance (ANOVA) or the partial F-test between the three models also indicated that the full or cubic model is significantly better than the remaining models at P >0.001. Hence, the cubic polynomial model provides a significant best fit with a significantly lower sum of square error, as shown in Table 2.

Table II.

Polynomial Regression Summary Using Linear, Quadratics and Cubic Model (Standard Error is in Parenthesis) of Heat Generated within Time Elapse for Non-insulated Type Gasifier Stove

	Coefficients				R-Square
Model	Constant	t	t^2	t^3	
Linear	1958.39*** (35.53)	0.168*** (0.020)	-	-	0.023 (996.14)
Quadratic	-233.19*** (9.712)	4.345*** (0.014)	-0.001*** (3.213e-19)		0.968 (181.46)
Cubic	-25.23 (11.68)	3.55*** (0.032)	-1.33e-3*** (1.828e-18)	-1.33e-7* (4.82e-22)	0.974 (163.64)

Significance codes: 0.0001***, 0.001**, 0.01*, 0.05, 0.1.

Figure 11, displays a graph illustrating the polynomial model fit for heat generated in a non-insulated gasifier stove. The predicted lines are red, blue, and black, while the observed heat-generated data plot is green. The cubic and quadratic models are better-fitted than the linear model. The heat generated after 3000.00 seconds is due to the residual stove temperature until equilibrium conditions are reached, or heat energy generation decreases until zero or no heat transfer occurs.

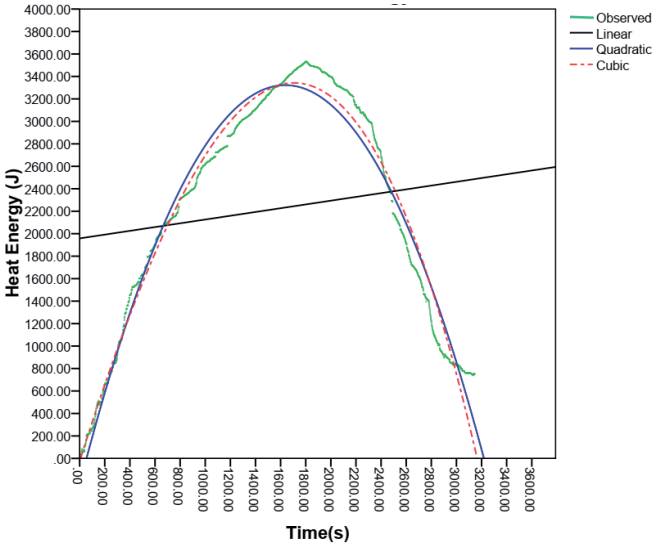

Fig. 11. Visualizations of the polynomial model fit for the heat generated in the non-insulated type gasifier stove

Mersha A. Fetene, Dessye B. Tikuneh, Evaluation and Modeling the Performance of Rice Husk Gasifier Cook Stove for Household Energy Use, Journal of Energy, vol. 73 Number 3 (2024), 17–35
https://doi.org/10.37798/2024733521

As shown in Fig. 12a, the 95% confidence interval (CI) for the cubic polynomial model fit provides a range of possible values for the mean heat energy generation at the designated burning period. This indicates that the population mean for the model's specified values of heat generation and time spent burning is contained within the confidence interval. For a given determination of heat energy generation and duration of burning variable settings, the 95% prediction interval (PI) is expected to include a single future response. The standard deviation of the distance between data values and fitted values measured in units of the response was 163.639 (Fig. 12a). Fig. 12b also, the normal probability plot of residuals displays the residuals versus their expected values when the distribution is normal, indicating a distribution with short tails (Fig. 12b). The residuals versus fits graph plots the residuals on the y-axis and the fitted values on the x-axis, verifying the assumption that the residuals are randomly distributed and have constant variance (Fig. 12c). Besides, as shown in Fig. 12d, the histogram of residuals shows the distribution of the residuals for all observations determined based on the number of intervals used to group the data, assessing the normality of the residuals. A histogram is most effective when there are approximately 20 or more data points (Fig. 12d). Fig. 12e, is the residuals versus order plot displays the residuals in the order in which the data were collected, verifying the assumption that the residuals are independent of one another. The independent residuals showed no trends or patterns when displayed in time order, suggesting that the residuals near each other may be correlated and thus not independent (Fig. 12e).

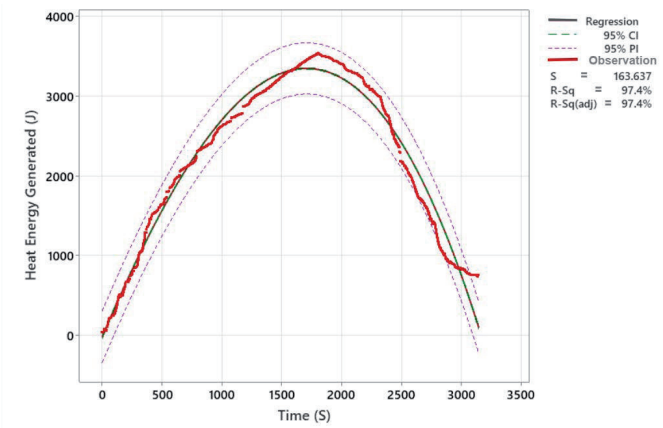

a)

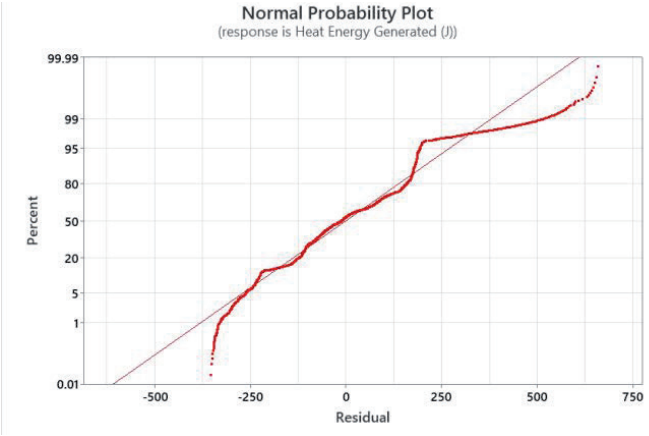

b)

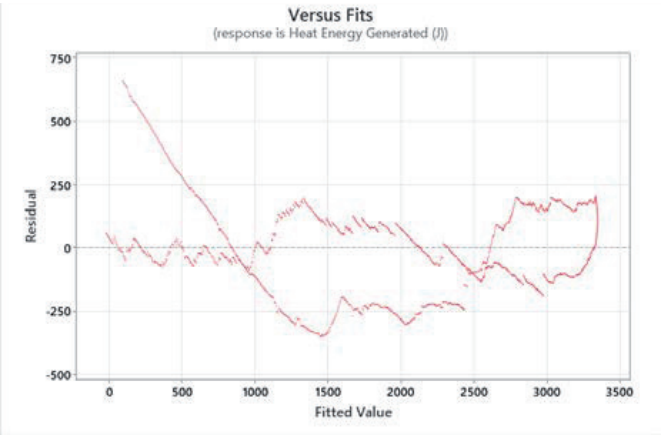

c)

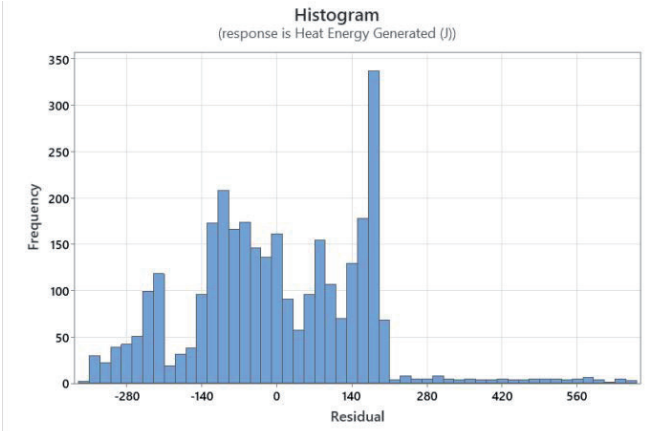

d)

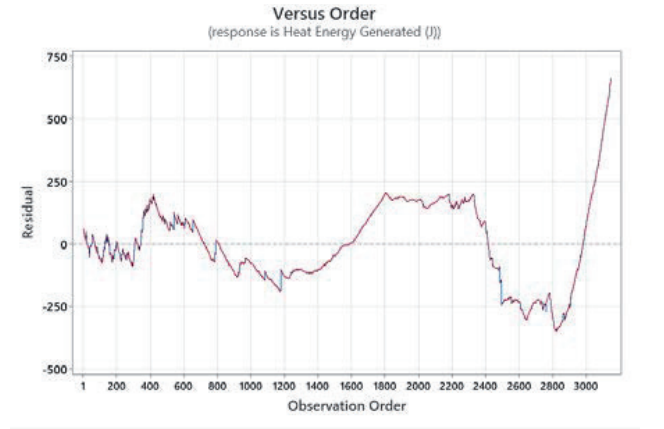

e)

Fig. 12. The Polynomial Regression Analysis: Heat Energy Generated (J) versus Time (S) of the cubic regression model fit (a), Normal probability plot of residuals (b), Residuals versus fits (c), Histogram of residuals (d), and Residuals versus order (e), of the non-insulated type gasifier stove.

E.1.4.1. Analysis of Heat Energy Loss

The energy loss through the reactor to the outside environment was recorded as the heat energy loss of the stoves. The relationship between the heat energy loss and the time elapsing, either going up and down together or not without causing one another, is an approach considered to be analyzed. The relation between energy loss and time was analyzed using the multiple regression model through polynomial regression using linear, quadratic, and cubic functions for both insulated and non-insulated gasifier stoves. The

Mersha A. Fetene, Dessye B. Tikuneh, Evaluation and Modeling the Performance of Rice Husk Gasifier Cook Stove for Household Energy Use, Journal of Energy, vol. 73 Number 3 (2024), 17–35
https://doi.org/10.37798/2024733521

residual standard errors (RSE), the coefficient of determination (R^2), and the partial F-test are used to test or determine whether a variable can be removed or added from a model without making a model significantly better or worse.

E.1.5. Heat Energy Loss of the Insulated Type Gasifier Stove

The loss of heat energy of the insulated type gasifier stove was analyzed through the linear, quadratic, and cubic model functions as shown in Eqs. 19, 20, and 21 below, respectively. The residual standard error (RSE) of models was 6.794, 1.215, and 1.044 for linear, quadratic, and cubic models, respectively, to determine relationships among the models as shown in Table 3. It indicated that the quadratics and cubic models have a lower RSE than the linear model, for the closest models well-fit the predicted values to the observed heat loss data. The coefficients of determination (R^2) of linear, quadratic, and cubic models are also 0.641, 0.989, and 0.992, respectively. The R^2 of the two models revealed that they are well predicted, and the heat loss model fits very closely as compared to the reduced model or linear model. A simple model is always preferable if the reduced (quadratic) model is significantly better compared to the full model or cubic model.

$$Q = 0.011t - 10.769, \quad R^2 = 0.641 \tag{19}$$

$$Q = -1.157\times10^{-5}t^2 + 0.044t - 4.187, \; R^2 = 0.989 \tag{20}$$

$$Q = -1.526\times10^{-9}t^3 - 5.201\times10^{-6}t^2 + 0.036t - 2.539, \; R^2 = 0.992 \tag{21}$$

Moreover, the analysis of variance (ANOVA) using a partial F-test was used to determine if the models were significantly better; it checked for significant differences either for the determination of the models to improve or reduce the predictive power. The ANOVA indicated that there is a significant difference between a linear model with quadratics and a linear model with cubic models. However, there is not a significant difference between quadratics and cubic models at $P > 0.01$. Hence, a simple model is always preferable, where the full (cubic) model is not significantly better than the reduced (quadratic) model or if it is not necessary to include the cubic time of the model without making the model significantly worse or not significantly better.

Table III.

Polynomial Regression Summary Using Linear, Quadratics and Cubic Model (Standard Error is in Parenthesis) of Heat Energy Loss Within Time Elapse for Insulated Type Gasifier Stove

	Coefficients				R- Square
Model	Constant	t	t^2	t^3	
Linear	10.769*** (0.258)	0.011*** (10^{-4})	-	-	0.641 (6.794)
Quadratic	-4.187*** (0.069)	0.044*** (1.15e-4)	-1.16x10^{-5}*** (10^{-6})		0.989 (1.215)
Cubic	-2.539*** (0.079)	0.036** (10^{-4})	-5.20x10^{-6}** (10^{-4})	1.526x10^{-9} (1x10^{-4})	0.992 (1.044)

Significance codes: 0.0001***, 0.001**, 0.01*, 0.05, 0.1.

The graph in Fig. 13 shows the visualizations of the polynomial model fit for the energy loss in the insulated type gasifier stove of all the observed heat energy loss data with predicted values of linear, quadratic, and cubic models. The maximum heat energy loss recorded on the insulated gasifier stove was 38.56J after 1919 seconds of operation, but steadily decreasing the heat loss up to the equilibrium condition of the room temperature, *i.e.,* 2783 seconds of operation time, the graph gradually approaches zero and declines slowly. As shown in the graph in Fig. 13, the cubic and quadratic polynomial models approach each other with the observed heat loss data but gradually separate and increase the gap at the heat loss during the residual temperature of the stove. The red, blue, and black lines on the graph are cubic, quadratic, and linear model fit curves, respectively, whereas the green ones are the observed heat loss values.

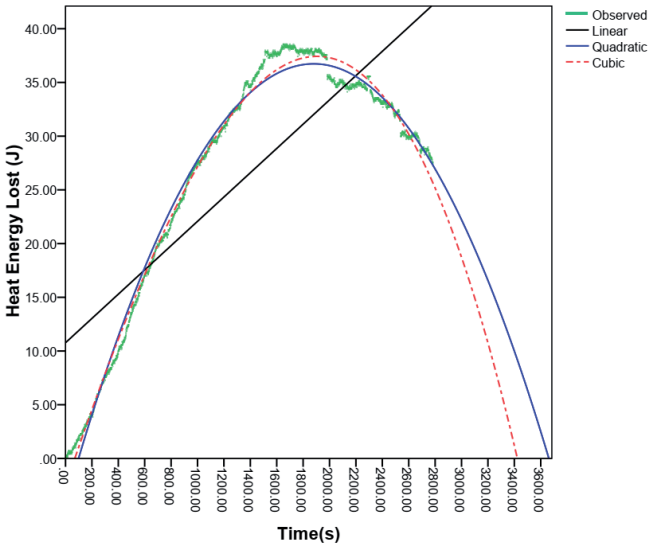

Fig. 13. Visualizations of the polynomial model fit for the heat energy loss in the insulated type gasifier stove

The cubic model is the best-fit polynomial model for determining heat energy loss and burning time variable settings. As shown in Fig. 14a, the 95% confidence interval (CI) provides a range of likely values for the mean response, while the 95% prediction interval (PI) is a range likely to contain a single future response. The confidence interval is 95% confident that the confidence interval contains the population mean for the specified values of variables in the model (Fig. 14a). Fig. 14b is also the normal probability plot of residuals displays the residuals versus their expected values when the distribution is normal, while the residuals versus fits graph plots show the residuals on the y-axis and the fitted values on the x-axis (Fig. 14b). The residuals versus fits plot confirm the assumption that the residuals are randomly distributed and have constant variance (Fig. 14c). The Fig. 14d is the histogram of residuals determines the appearance of the data, which depends on the number of intervals used to group the data. A histogram is most effective when there are approximately 20 or more data points (Fig. 14d). The residuals versus order plot (Fig. 14e) display the residuals in the order in which the data were collected, verifying the assumption that the residuals are independent of one another. Independent residuals show no trends or patterns when displayed in time order, where the residuals should fall randomly around the centerline (Fig. 14e).

Mersha A. Fetene, Dessye B. Tikuneh, Evaluation and Modeling the Performance of Rice Husk Gasifier Cook Stove for Household Energy Use, Journal of Energy, vol. 73 Number 3 (2024), 17–35
https://doi.org/10.37798/2024733521

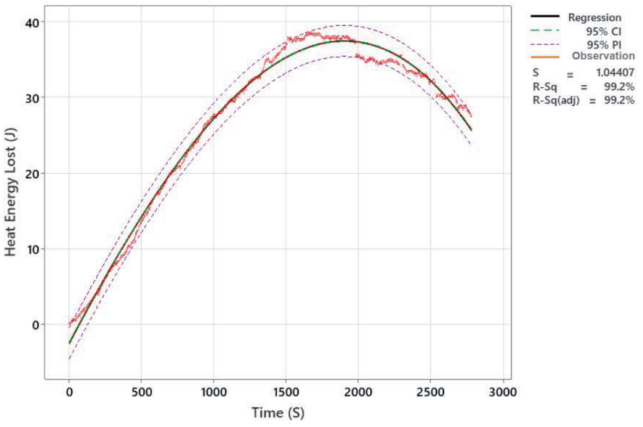

a)

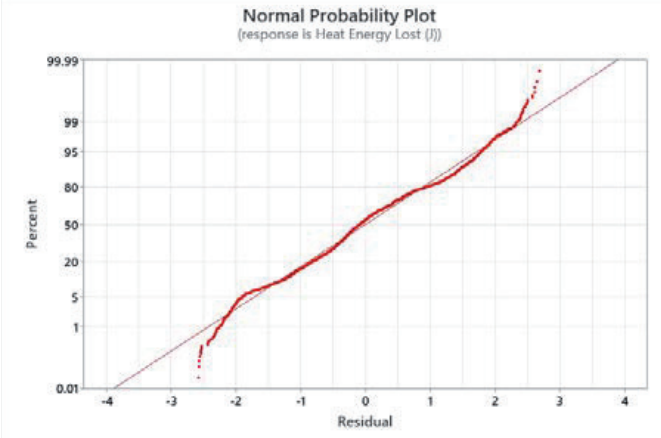

b)

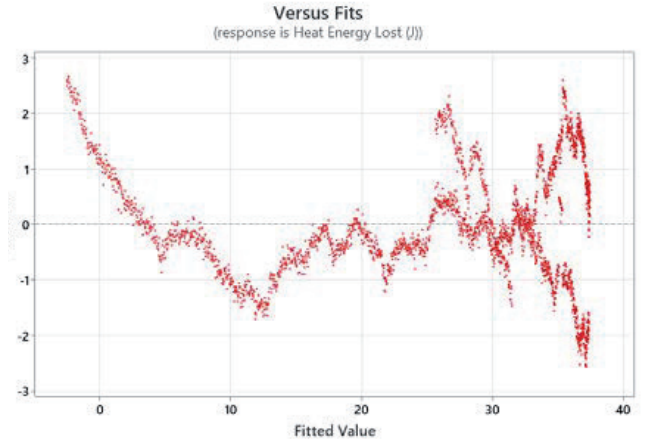

c)

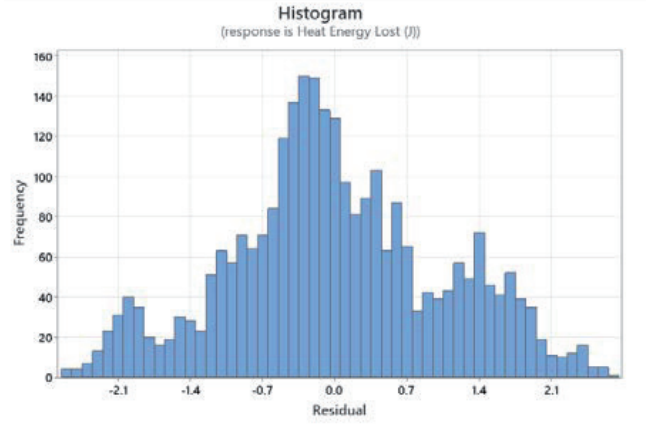

d)

e)

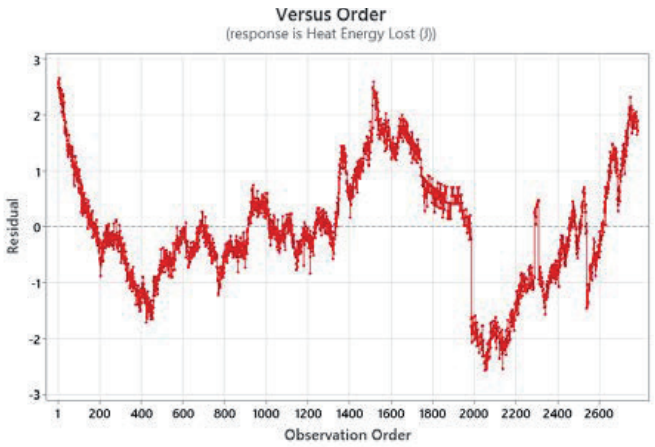

Fig. 14. The Polynomial Regression Analysis: The Heat Energy Loss by Insulated Type Gasifier Stove of the cubic regression model fit (a), Normal probability plot of residuals (b), Residuals versus fits (c), Histogram of residuals (d), and Residuals versus order (e) of the insulated type gasifier stove.

E.1.4.2. Heat Energy Loss in the Non-Insulated Type Gasifier Stove

The heat energy loss of the non-insulated type gasifier stove has been analyzed through the multiple regression model equations using the linear, quadratic, and cubic functions that are illustrated in Eqs. 22, 23, and 24, respectively. The determination of the best fit of the predicted values to the observed heat energy loss data was made among the models using residual standard error (RSE), coefficient of determination (R2), and ANOVA, or partial F-test. The RSEs of the linear, quadratic, and cubic models are 268.72, 130.54, and 122.323, respectively, indicating that the cubic polynomial model is relatively better predictively than the linear and quadratic models. Besides, the linear model has the highest RSE, which was the worst model and should be ignored in the prediction of the observed heat energy loss data of the non-insulated type gasifier stove. The coefficients of determination (R2) of the linear, quadratic, and cubic models are 0.04, 0.773, and 0.801, respectively, showing that the cubic model is relatively the best predictive model, where more than 80% of the heat energy loss data is explained by the model; however, the linear model has the least and worst predictive power, with only 4% of the data being fitted.

$$Q = 0.052t + 353.581, \qquad R^2 = 0.04 \tag{22}$$

$$Q = -2.340 \times 10^{-4} t^2 + 0.910t - 171.944, R^2 = 0.773 \tag{23}$$

$$Q = 4.886 \times 10^{-10} t^3 - 0.001t^2 + 1.305t - 292.807, R^2 = 0.801 \tag{24}$$

The partial F-test between the models also revealed that the quadratic and cubic models are significant at a significant level (P) of 0.001; however, the linear model is not significant enough to predict the observed data of the heat energy loss of the non-insulate type of gasifier stove, as shown in Table 4, below. Moreover, the ANOVA between the quadratic and cubic models is also significant, but the cubic models are relatively the best fit to predict the observation. In general, the heat energy loss of the non-insulated type of gasifier stove is greater than the heat loss of the insulated type of gasifier stove, where the gasifier is essentially insulated to reduce such energy loss.

Mersha A. Fetene, Dessye B. Tikuneh, Evaluation and Modeling the Performance of Rice Husk Gasifier Cook Stove for Household Energy Use, Journal of Energy, vol. 73 Number 3 (2024), 17–35
https://doi.org/10.37798/2024733521

TABLE IV.

POLYNOMIAL REGRESSION SUMMARY USING LINEAR, QUADRATICS AND CUBIC MODEL (STANDARD ERROR IS IN PARENTHESIS) OF HEAT ENERGY LOSS WITHIN TIME ELAPSE FOR NON-INSULATED TYPE GASIFIER STOVE

	Coefficients				R- Square
Model	Constant	t	t^2	t^3	
Linear	353.58** (8.875)	0.052** (0.004)	-	-	0.040 (268.721)
Quadratic	-171.944** (5.49e-14)	0.910** (9.772e-17)	-2.34e-04** (3.65e-20)		0.772 (130.54)
Cubic	-292.807*** (8.086)	1.305** (0.019)	0.001** ($1x10^{-4}$)	$4.886x10^{-8}$*** ($1x10^{-4}$)	0.801 (122.323)

Significance codes: 0.0001***, 0.001**, 0.01*, 0.05, 0.1.

The graph in Fig. 15 shows the visualizations of the polynomial model fit for the energy loss in the non-insulated type gasifier stove, where the linear, quadratic, and cubic model curves are black, blue, and red lines, respectively, concerning the green line of the observed data curve of the heat energy loss of the non-insulated gasifier stoves. The heat energy loss of a non-insulated type gasifier stove is the lowest fit with the irregular shape of the heat energy loss with time elapse among the models than the parameters. The maximum energy loss was 933.549J after 1468 seconds of gasification operation, whereas after 3400 seconds, the heat energy loss gradually declined concerning the residual temperature of the stove until the equilibrium condition of the room temperature was reached during the evaluation of the stove, as shown in the graph in figure 15.

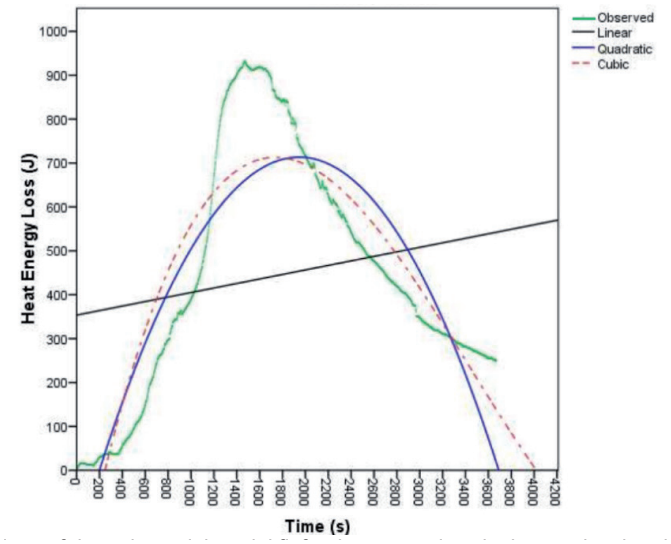

Fig. 15. Visualizations of the polynomial model fit for the energy loss in the non-insulated type gasifier stove

The study used a cubic polynomial model to analyze the heat energy generated and the burning time curve of a non-insulated type gasifier stove. The 95% confidence interval (CI) was aligned with the heat energy generated and burning time curve, providing a range of likely values for the mean response or heat energy loss given the specified settings of predictors or burning time. The confidence interval indicates confidence about the mean of future values, while the 95% prediction interval (PI) is a range likely to contain a single future response for a selected determination of variable settings of heat energy loss and burning time (Fig. 16a). The normal probability plot of residuals is illustrated in Fig. 16b, showing the residuals versus their expected values when the distribution is normal. The residuals versus fits graph, in Fig. 16c, plots the residuals on the y-axis and the fitted values on the x-axis, verifying the assumption that the residuals are randomly distributed and have constant variance. The histogram of the residuals, in Fig. 16d, shows the distribution of the residuals for all observations, which is most effective when there are approximately 20 or more data points without skewness or outliers. Fig. 16e is the residuals versus order plot displaying the residuals in the order that the data were collected, verifying the assumption that the residuals are independent of one another. The independent residuals showed no trends or patterns when displayed in time order, falling randomly around the center line.

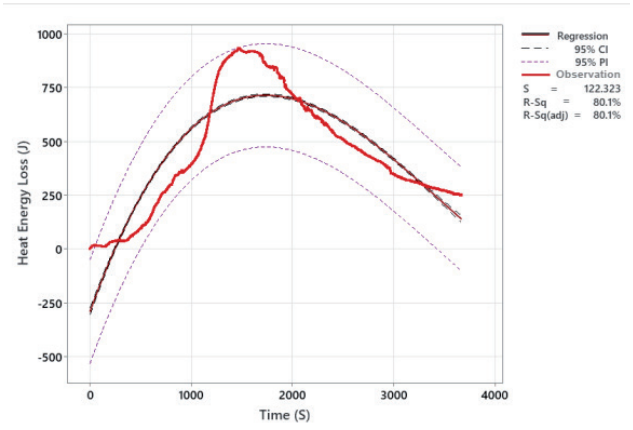

a)

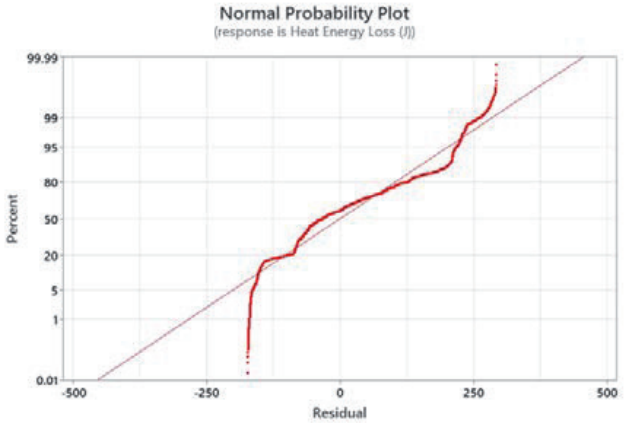

b)

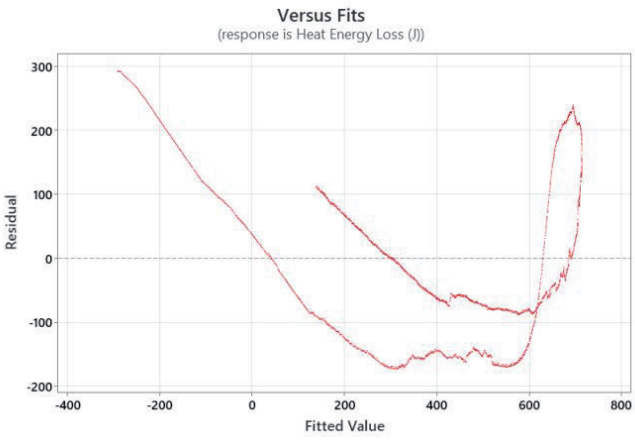

c)

Mersha A. Fetene, Dessye B. Tikuneh, Evaluation and Modeling the Performance of Rice Husk Gasifier Cook Stove for Household Energy Use, Journal of Energy, vol. 73 Number 3 (2024), 17–35
https://doi.org/10.37798/2024733521

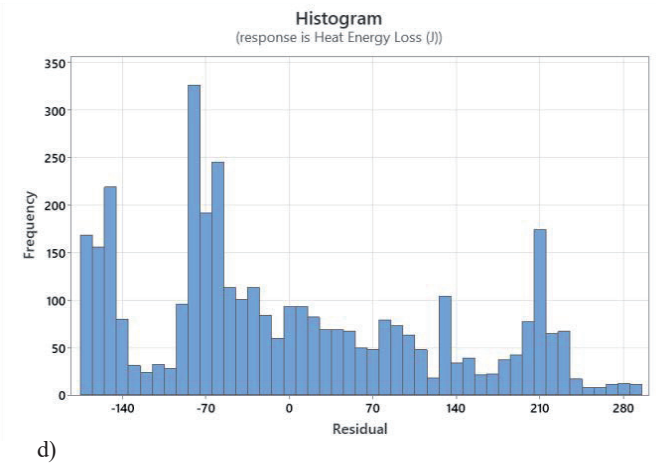

d)

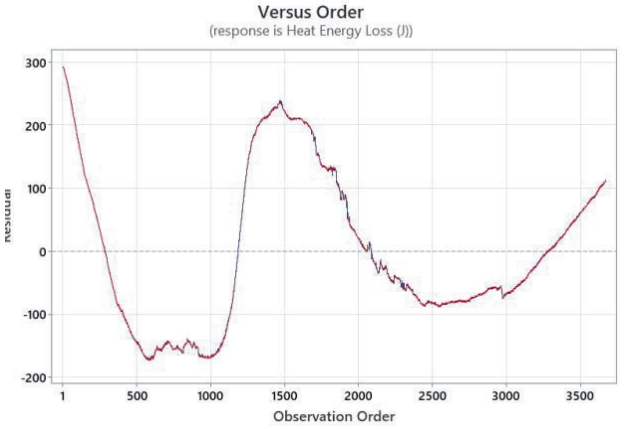

e)

Fig. 16. The Polynomial Regression Analysis: The Heat Energy Loss by non-insulated Type Gasifier Stove of the cubic regression model fit (a), Normal probability plot of residuals (b), Residuals versus fits (c), Histogram of residuals (d), and Residuals versus order (e) of the non-insulated Type Gasifier Stove.

E.3. Analysis of water Boiling Temperature

The water boiling temperature per operating time was the other parameter to determine how fast and at what temperature to boil two letters of water through insulated and non-insulated gasifier stoves. The analysis of multiple regression models for both gasifier stoves was made to determine the boiling temperatures of the water concerning operating time. The residual standard errors (RSE), the coefficient of determination (R^2), and the partial F-test are used to test or determine whether a variable can be removed or added from a model without making a model significantly better or worse to analyze the three polynomial regression models.

E.3.3.1. Water Boiling Temperature of the Insulated Type Gasifier Stove

The relationship between water boiling temperature and operating time of an insulated type gasifier stove has been analyzed using a polynomial regression model using all linear, quadratics, and cubic models. The model fits of linear, quadratic, and cubic models have been illustrated in Eqs. 25, 26, and 27, respectively. The residual standard errors of linear, quadratic, and cubic models are 22.615, 6.851, and 2.625, respectively. The smallest standard error (RSE) of 2.625 for a cubic polynomial model showed that the best measures and closest to the observed values among the predicted models, which summarizes a well-fitting model. The cubic model showed the lowest RSE, indicating an idea of how far the observed boil temperature is from the predicted model value.

$$T_w = 0.003t + 87.709\,,\ R^2 = 0.02 \tag{25}$$

$$T_w = -2.791\times10^{-5}t^2 + 0.093t + 39.487\,,\ R^2 = 0.91 \tag{26}$$

$$T_w = 1.004\times10^{-8}t^3 - 7.642\times10^{-5}t^2 + 0.156t + 2\ .718\,,\ R^2 = 0.987 \tag{27}$$

The polynomial regression models also determine whether the model fits the observed water temperature data of the insulated gasifier stove using the coefficient of determination (R^2). The R2 values of the linear, quadratic, and cubic models are 0.02, 0.91, and 0.987, respectively, revealing that the cubic model has the highest value with 98.7% of the variation of water boiling temperature observed by the model, whereas the lowest R^2 value is the linear model with only 2% of the observed data, as shown in Table 5. The ANOVA, or partial F-test, between the three models, was made for model building and variable selection to decide whether to remove a variable from a model without making it significantly worse or add a variable to the model to make it significantly better. The ANOVA between models shows a significant difference at a probability level (P) > 0.001. It also revealed that the ANOVA between cubic and quadratics with observed data of water boiling temperature is not significant at P > 0.001, but the linear model with the observed data has a significant difference. Hence, the cubic model is the best-fit model to predict the observed data of water boiling temperature. The quadratics are linear based on the RSE and R^2 determination methods, but the partial F-test indicated that both the cubic and quadratic models are the best fit.

Table V.

Polynomial Regression Summary Using Linear, Quadratics and Cubic Model (Standard Error is in Parenthesis) of Boiling Temperature of Water Within Time Elapse for Insulated Type Gasifier Stove

	Coefficients				R- Square
Model	Constant	t	t^2	t^3	
Linear	87.709*** (0. 798)	0.003*** (3.67e-04)	-	-	0.02 (22.615)
Quadratic	39.49*** (1.0e-14)	0.093*** (1.78e-17)	-2.791x10^{-5}*** (6.65e-21)		0.91 (6.851)
Cubic	- 22.718*** (1.55e-14)	0.156*** (5.178e-17)	-7.642 x10^{-5}*** (4.639e-20)	1.004x10^{-8}** (1.176e-23)	0.987 (2.625)

Significance codes: 0.0001***, 0.001**, 0.01*, 0.05, 0.1.

The graph in Fig. 17 showed that the visualizations of the polynomial model fit the boiling temperature of water in the insulated gasifier stove. As shown in Fig. 17, the maximum water boiling temperature of the insulated type gasifier stove was recorded at 124.9 oC after 1453 seconds of water boiling operation. The boiling operation was continued until 3400 seconds, even after finishing the rice husk fuel. The graph in Fig. 17, shows the cubic model (red line) is the best fit up to 3400 seconds of operation, but after the end of the observed water boiling temperature, the line of the cubic model rises in shape, so that the model fit of the cubic model is the best fit until the 3400 seconds of operation, hence the quadratic model or the blue line may be preferred. The average operation time in one batch feed of husk for insulated types of gasifier stoves was 2033.28 seconds. After this operation time, the recorded temperature was the residual temperature of the water graph of the observed boiling temperature (the green line), which continuously declined until the equilibrium condition reached room temperature.

Mersha A. Fetene, Dessye B. Tikuneh, Evaluation and Modeling the Performance of Rice Husk Gasifier Cook Stove for Household Energy Use, Journal of Energy, vol. 73 Number 3 (2024), 17–35
https://doi.org/10.37798/2024733521

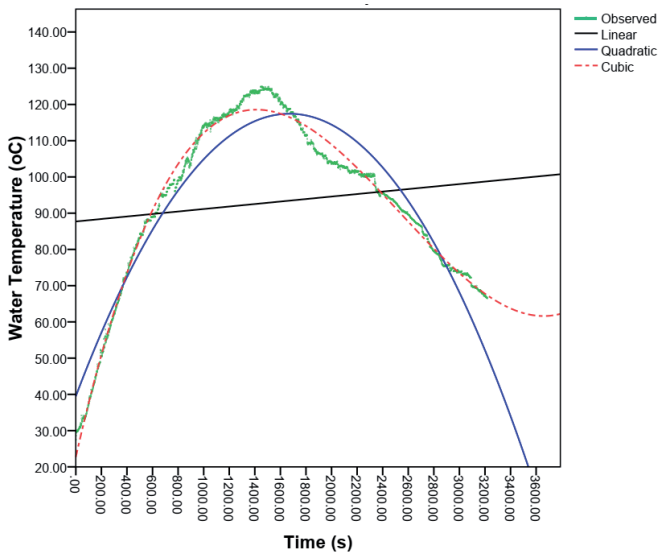

Fig. 17. Visualizations of the polynomial model fit for the water boiling temperature in the insulated type gasifier stove

As shown in Fig 18a, the study focuses on the water boiling temperature of an insulated type gasifier stove at a 95% confidence interval (CI) for fit, which provides a range of likely values for the mean response of water temperature given the specified settings of predictors of boiling time. The 95% confidence interval (PI) assesses the estimate of the fitted value for the observed values of the variables (boiling temperature and boiling time) with a 95% confidence level, ensuring that the confidence interval contains the population means for the specified values in the model. The 95% prediction interval (PI) is a range that is likely to contain a single future response for a selected determination of variable settings (boiling temperature and boiling time). The PI extends inside the acceptable boundaries, indicating that the predictions were sufficiently precise for 95% PI requirements. The prediction interval is always wider than the confidence interval due to the added uncertainty involved in predicting a single response versus the mean response (Fig 18a). The normal probability plot of the residuals as shown in Fig 18b, displays the residuals versus their expected values when the distribution is normal, verifying the assumption that the residuals are normally distributed. The graph in Fig. 18c, the residuals versus fits graph plots the residuals on the y-axis and the fitted values on the x-axis, verifying the assumption that the residuals are randomly distributed and have constant variance. The Fig. 18d, the histogram of the residuals is most effective when there are approximately 20 or more data points, ensuring that each bar on the histogram contains enough data points to reliably not show skewness or outliers.

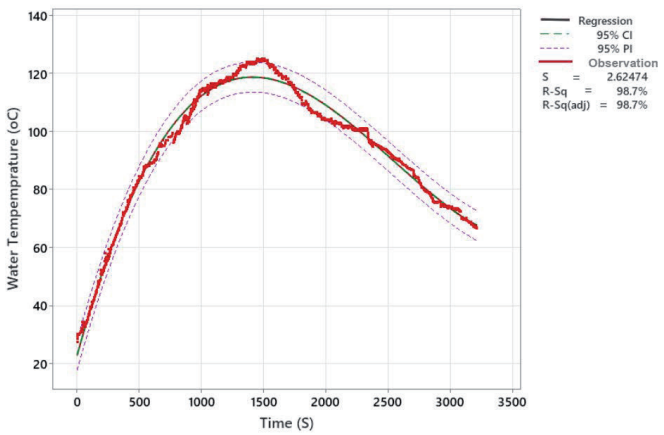

a)

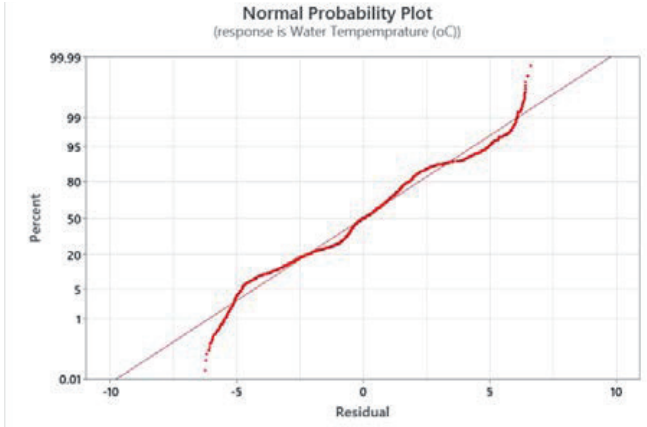

b)

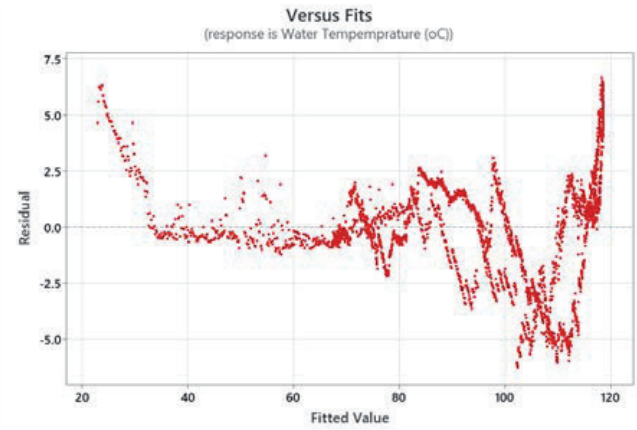

c)

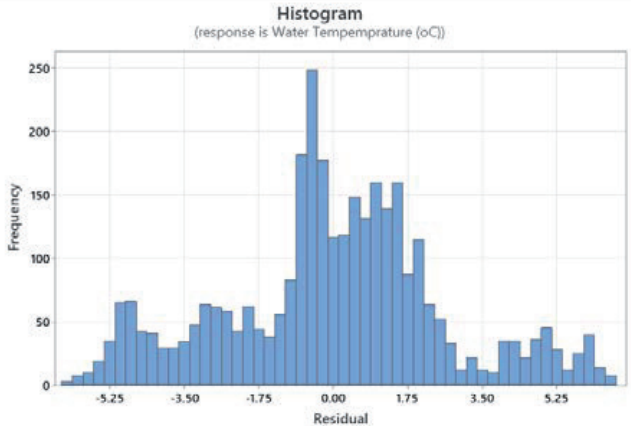

d)

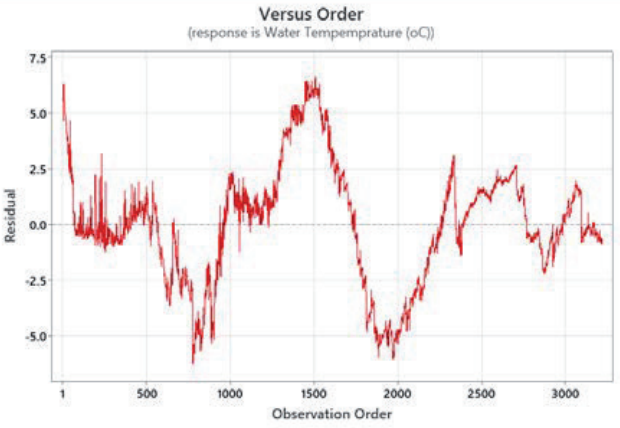

e)

Fig. 18. The Polynomial Regression Analysis: The Water Boiling Temperature of the cubic regression model fit (a), Normal probability plot of residuals (b), Residuals versus fits (c), Histogram of residuals (d), and Residuals versus order (e) of the insulated Type Gasifier Stove.

Mersha A. Fetene, Dessye B. Tikuneh, Evaluation and Modeling the Performance of Rice Husk Gasifier Cook Stove for Household Energy Use, Journal of Energy, vol. 73 Number 3 (2024), 17–35
https://doi.org/10.37798/2024733521

3.6.3.2. Water Boiling Temperature of the non-insulated type gasifier stove

The water boiling temperature of the non-insulated type of gasifier stove with the boiling or operating time was analyzed using multiple regression models. The polynomial regression model included the linear, quadratic, and cubic models presented in Eqs. 28, 29, and 30, respectively. The residual standard errors (RSE) of the linear, quadratic, and cubic models are 36.60, 20.60, and 12.383, respectively. The cubic polynomial model has the lowest value with 12.383, showing the closest among the models to predict the observed data of a non-insulated type gasifier stove of the water boiling temperature, and can be thought of as summarizing how well the cubic model fits.

$$T_w = 2.7\times10^{-4}t + 178.24, \qquad R^2 = 3.6\text{x}10^{-6} \tag{28}$$

$$T_w = -4.509\times10^{-5}t^2 + 0.136t + 110.535, R^2 = 0.683 \tag{29}$$

$$T_w = 3.225\times10^{-8}t^3 - 1.902\times10^{-4}t^2 + 031\,t + \mathbf{6}\ .911, R^2 = 0.886 \tag{30}$$

On the other hand, the coefficients of determination (R^2) of the linear, quadratic, and cubic models are 0.886, 0.683, and 3.6x10-6, respectively, as shown in Table 6 below. The cubic model is significantly higher, with 88.6% of the observed water boiling temperature of the non-insulated gasifier stove perfectly explained by the cubic predicted model fit. The percentage of prediction of the observed data in quadratics and linear models is 68.3% and 0.00036%, respectively, showing that the expression power of the linear model is almost null or worse and should be ignored, whereas the quadratic model is relatively better than the linear model but lower than the cubic model, as shown in Table 6.

Table 6.

Polynomial Regression Summary Using Linear, Quadratics and Cubic Model (Standard Error is in Parenthesis) of Boiling Temperature of Water Within Time Elapse for Non-Insulated Type Gasifier Stove

	Coefficients				R- Square
Model	Constant	t	t^2	t^3	
Linear	178.237*** (1.337)	2.70x10^{-4} (7.72e-04)	-	-	3.6x10^{-6} (36.601)
Quadratic	110.535*** (1.13)	0.136*** (0.002)	-4.509x10^{-5} *** (10^{-5})		0.683 (20.599)
Cubic	66.911*** (0.905)	0.31*** (0.003)	-1.905 x10^{-4}*** (10^{-4})	3.225x10^{-8} (10^{-4})	0.886 (12.383)

Significance codes: 0.0001***, 0.001**, 0.01*, 0.05, 0.1.

The graph in Fig. 19 shows the visualizations of the polynomial model fit for the water boiling temperature in the non-insulated type gasifier stove, where the maximum boiling temperature was recorded at 208.8 °C after 662 seconds of operation during the water-boiling test of the non-insulated type gasifier stove. As shown in the graph in Fig. 19, the observed data (green line in the graph) of water boiling temperature showed sharp increases within a 0-550 second period, then water boiling temperature was constant (in the curve, a straight line in the graph) for 1300 seconds (551 to 1850 seconds in the graph), where the average temperature was 205.83 °C. However, at the end of 1850 seconds in the straight-line curve on the graph, the temperature gradually declines to equilibrium with a room. The red, blue, and black with green line colors on the graph were cubic, quadratic, and linear models that fit with the observed data on the boiling temperature of water in the non-insulated types of gasifier stoves, respectively.

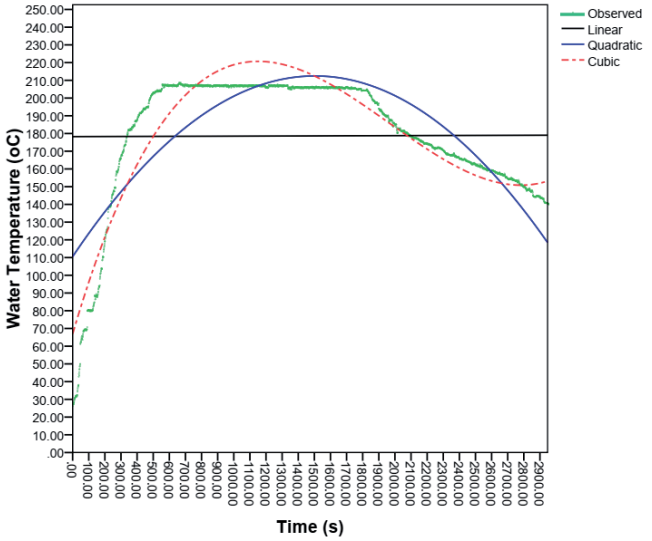

Fig. 19. Visualizations of the polynomial model fit for the water boiling temperature in the non-insulated type gasifier stove

The insulated type gasifier stove's water boiling temperature is predicted using a 95% confidence interval (CI), which evaluates the fitted value estimate for observed values of variables. As shown in Fig. 19a, this means that there is a 95% chance that the population means for the specified values are contained in the confidence interval. The principal investigator evaluated the predicted accuracy and results' applicability, finding that a single response was contained within the interval given the predictor settings or boiling time (Fig. 20a). The residuals are shown in Fig 20b against their anticipated values in a normal probability plot, confirming the premise that the residuals are normally distributed (Fig 20b). Fig 20c is the residuals versus fits graph depicting the residuals on the y-axis and the fitted values on the x-axis, confirming the assumption that the residuals are randomly distributed and have constant variance. On the other hand, Fig 20d is the residual histogram that displays the residual distribution for each observation for which the data was found to be roughly normal and satisfying the requirements of the cubic polynomial model. The best results from a histogram are obtained with at least 20 data points, as each bar on the histogram has enough data points to consistently not display skewness or outliers due to the large sample size (Fig. 20d). As shown in Fig 20e, the residuals versus order plot illustrates the residuals in the order in which the data were collected, showing that independent residuals do not exhibit any trends or patterns when presented in time order.

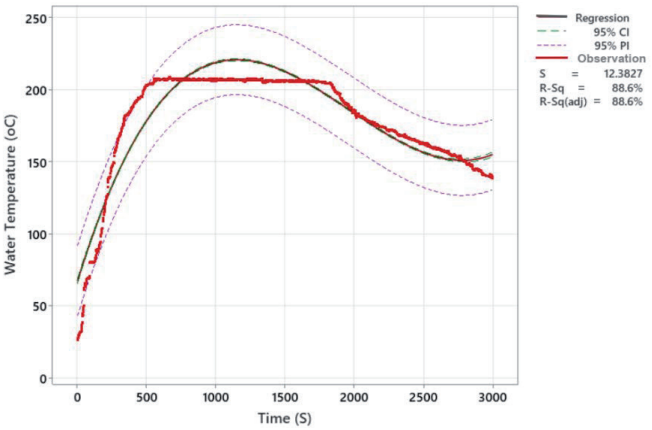

a)

Mersha A. Fetene, Dessye B. Tikuneh, Evaluation and Modeling the Performance of Rice Husk Gasifier Cook Stove for Household Energy Use, Journal of Energy, vol. 73 Number 3 (2024), 17–35
https://doi.org/10.37798/2024733521

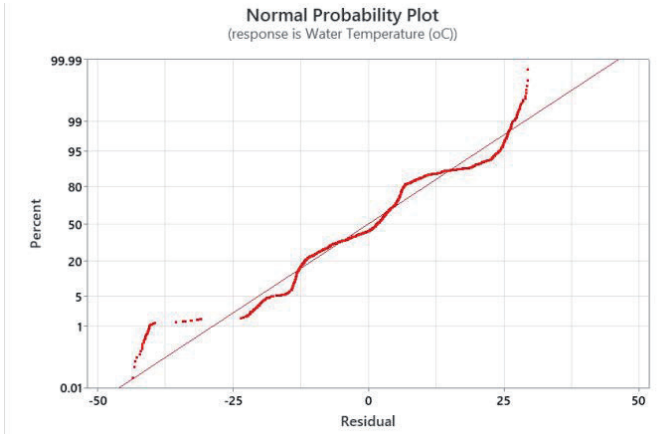

b)

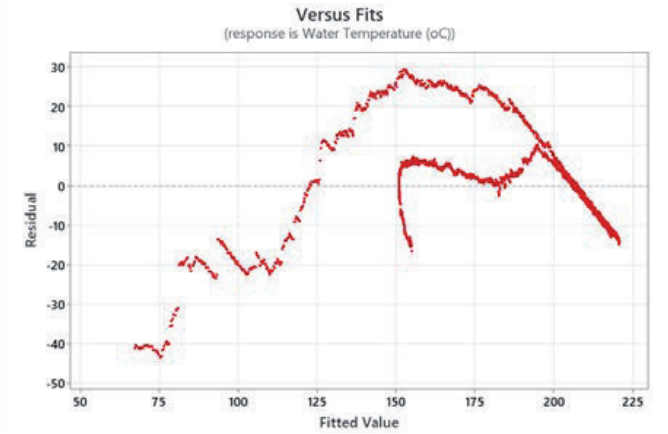

c)

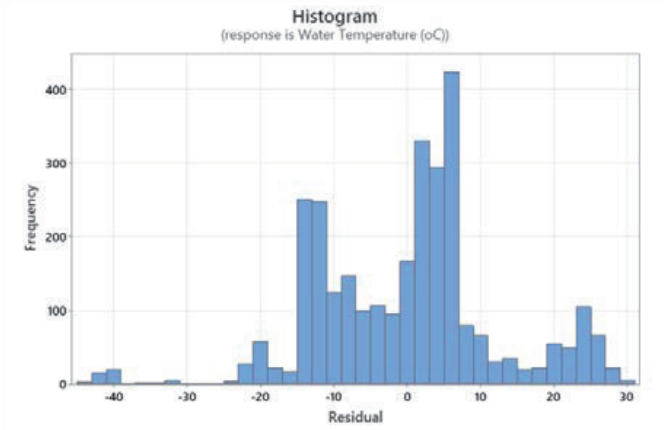

d)

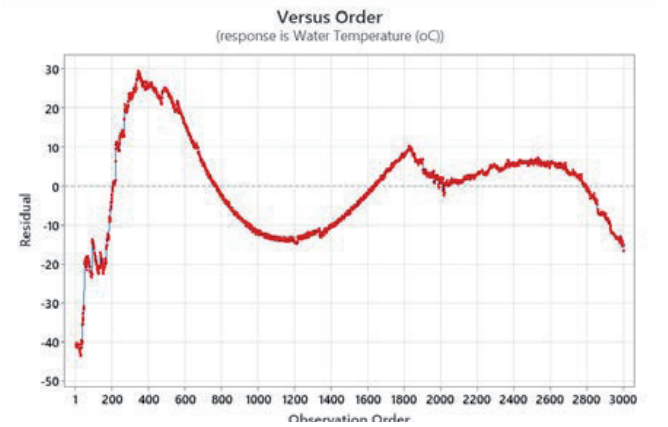

e)

Fig. 20. The Polynomial Regression Analysis: The Water Boiling Temperature of the cubic regression model fit (a), Normal probability plot of residuals (b), Residuals versus fits (c), Histogram of residuals (d), and Residuals versus order (e) of the non-insulated Type Gasifier Stove.

IV. Conclusion and Recommendation

This study aims to evaluate and model the performance of rice husk gasifier cook stoves for household energy use, a byproduct of rice milling. The study compares insulated and non-insulated gasifier stoves using rice husks, focusing on environmental issues and promoting the use of rice husks as a renewable energy source and pest repellent in stoves. The study found that the insulated stove had a lower start-up time but no significant difference at a 5% probability level. The temperature change was not significant, as heat transfer and temperature change started when the husk was ignited. The burner stoves had varying sizes and weights, with the maximum flame temperature at room temperature being 1,190.30°C, and the average temperature at 758.916°C for non-insulated gasifier stoves. Insulated gasifier stoves had maximum and average temperatures of 518.30°C and 289.014°C at room temperature. The operating time of stoves directly influences the fuel consumption rate, specific gasification rate, and combustion zone rate of stoves. The fuel consumption rate has a significant effect on the type of gasifier stove, with the maximum rates being 3.820 and 2.099 kg/hr. The time to consume rice husks to gasify them depends on the density of the rice husk, reactor volume, and fuel consumption rate. The average specific gasification rate for insulated and non-insulated stoves is 106.45 and 120.63 kg/m^{2}h, respectively. The performance of gasifier stoves varies based on the biochar conversion rate, with non-insulated stoves producing a higher biochar mass per rice husk. Multiple regression analysis was used to model the relationship between time elapse and temperature/heat energy, with the cubic polynomial model being the best predictive model fit for all variables.

Ethiopia's rural communities rely heavily on biomass fuels, with wood fuel and cow dung being the largest sources. Only 15% of Ethiopia's land is covered by forests, producing most biomass energy resources. Rice husk gasification could promote renewable energy and reduce greenhouse gas emissions. Biomass briquettes from rice husk can contribute to the energy mix and waste management options for these communities, ensuring sustainability in energy exploitation (WB, 2020). Biomass gasification is a promising technology for developing countries like Ethiopia, offering easy construction, installation, and operation. Hence, rice husk gasification can be a solution for this renewable energy promotion scheme as well as an alternative for the reduction of greenhouse gas emissions, by being an alternative to the fast-declining wood fuels, which are useful in carbon sequestration and reduction of greenhouse gas emission. Energy remains essential for development, but the exploitation of energy sources needs to be carried out with sustainability in mind. The household energy derived from rice husk can have a remarkable contribution to the energy mix and waste management options of the milling wastes so with communities in rice processing areas that largely depend on wood fuel. The study highlights the importance of maintaining local biomass supply to reduce reliance on fossil fuels and the potential benefits of distributed biomass gasifier stove technologies.

Based on the study, the following recommendations can be made:

1. To ensure the continuous and sustainable functioning of this technology using local resources, it is recommended to modify the stove for continuous feed type.
2. Conduct and highlight the need for further kitchen performance evaluations to determine fuel efficiency in typical conditions.
3. Testing revealed a thermal efficiency of approximately 31.27% for the biomass gasifier stove, indicating a need for increased efficiency through an insulation system to benefit the environment and public health compared to

Mersha A. Fetene, Dessye B. Tikuneh, Evaluation and Modeling the Performance of Rice Husk Gasifier Cook Stove for Household Energy Use, Journal of Energy, vol. 73 Number 3 (2024), 17–35
https://doi.org/10.37798/2024733521

traditional stoves.

4. Further research is suggested to develop continuous and enclosed biomass gasifier stoves for large-scale cooking, addressing future considerations in economics, technology, and the marketing system of the stove.

5. It needs to create demand by conducting a participatory demonstration of the gasifier stove at the village level. Local manufacturers need to be trained on the fabrication, maintenance, and operation of the stove so that the stove should be available to the end-users.

References

[1] The Federal Democratic Republic Of Ethiopia Central Statistics Service, "Large And Medium Scale Commercialfarms Sample Survey 2021/22(2014 EC) Results At Country And Regional Level," Addis Ababa, Ethiopia, 2022.

[2] A. Gautam, R. Batra, and N. Singh, "A Study On Use Of Rice Husk Ash In Concrete," Eng. Herit. J., vol. 3, no. l, pp. l–4, 2019, [Online]. Available: http://doi.org/10.26480/gwk.01.2019.01.04.

[3] A. Assaye and D. Alemu, "Enhancing production of quality rice in Ethiopia : Dis/incentives for rice processors," Addis Ababa, Ethiopia, 2020.

[4] P. R. Fernando, U. Karthika, K. Parthipan, T. Shandarabavan, R. Ismail, and A. Jeeva, "Designing a Cooker to Utilise the Natural Waste Rice Husk as a Cooking Gas," Adv. Recycl. Waste Manag., vol. 2, no. l, pp. 2–5, 2017, doi: 10.4172/2475-7675.1000117.

[5] N. E. Benti et al., "The current status, challenges and prospects of using biomass energy in Ethiopia," Biotechnol. Biofuels, vol. 14, no. 209, pp. l–24, 2021, doi: 10.1186/s13068-021-02060-3.

[6] B. Tamrat, B. Yilma, and M. Asfaw, "Design and Optimization of Continuous Type Rice Husk Gas Stove," ICST Inst. Comput. Sci. Soc. Informatics Telecommun. Eng., pp. 623–633, 2020, doi: 10.1007/978-3-030-43690-2.

[7] A. S. Yusuf, A. M. Ramalan, I. O. Adebayo, F. A. Makanjuola, N. F. Akpan, and K. U. Isah, "Development of Rice Husk and Saw Dust Briquettes for Use as Fuel," Am. Based Res. J., vol. 10, no. 01, 2021, [Online]. Available: https://www.researchgate.net/publication/348975115%0ADevelopment.

[8] A. T. Belonio, Rice Husk Gas Stove Handbook. Appropriate Technology Center. Iloilo City, Philippines.: Department of Agricultural Engineering and Environmental Management, College of Agriculture, Central Philippine University, 2005.

[9] R. A. Fajri and N. Hamdi, "Optimization of Making Charcoal Briquettes from Rice Husks with Variations in the Composition of Adhesive Materials and Compaction Pressure," Formosa J. Appl. Sci., vol. 2, no. 10, pp. 2265–2276, 2023.

[10] K. P. Shrestha, P. Parajuli, B. Baral, and B. P. Shrestha, "Mathematical modeling , simulation and analysis of rice grain movement for design and fabrication of low-cost winnowing machine," vol. 9, no. January, pp. 1–14, 2017, doi: 10.5897/JMER2016.0403.

[11] D. G. Mercer, "Design, Construction And Evaluation Of Performance Of Solar Dryer For Drying Fruit" September, 2015. Available: elearning.iufost.org/sites/default/files/Intermediate-Outline-1.pdf>.

[12] A. K. Gomez and A. A. Gomez, Statistical Procedures for Agricultural Research, 2nd 105 ed. John Wiley and Sons, New York, p. 97-107., 1984.

[13] S. A. Ndindeng, M. Wopereis, S. Sanyang, and K. Futakuchi, "Evaluation of fan-assisted rice husk fuelled gasifier cookstoves for application in sub-Sahara Africa," Renew. Energy, vol. 139, pp. 924–935, 2019, doi: 10.1016/j.renene.2019.02.132. Available: https://doi.org/10.1016/j.renene.2019.02.132

[14] P. Bhusal, B. B. Ale, and R. M. Singh, "Performance Evaluation of Domestic Rice Husk Gasifier Stove (Belonio Type) and Study on Modification of Design for using Different Biomass," in Proceedings of IOE Graduate Conference, 2015, 2015, pp. 55–62.

Journal of Energy
VOLUME 73 Number 3 | 2024
journal homepage: http://journalofenergy.com/

Review of Supercapacitor Equivalent Circuit Models

Karlo Kobeščak,Tomislav Baškarad

***Summary* — Supercapacitors are a promising technology for addressing the challenges faced by power systems with an increasing share of inverter-based resources. Due to their unique characteristics, supercapacitors can provide ancillary services to the grid. Understanding the behavior of supercapacitors under various conditions is crucial. Therefore, modeling and analysis are of significant interest in the research of supercapacitors for a wide range of applications. This article provides a brief overview of supercapacitor technology and presents a systematic review of five equivalent circuit models of supercapacitors.**

***Keywords* — energy storage systems, supercapacitor, equivalent circuit models, application.**

I. Introduction

THE power system (PS) with a high share of variable and unpredictable renewable energy sources (RES), which are connected to the grid through power electronics devices, and a reduced share of dispatchable fossil fuel power plants due to decarbonization goals, presents a challenge in maintaining both system stability and power quality. To ensure system stability, it is essential to have dispatchable units capable of damping disturbances caused by imbalances between electricity production and consumption due to the intermittency of RES. In the future power systems, energy storage systems and converters will play a key role in maintaining system stability. Since inverters electrically separate the RES generating unit from the grid, any kind of energy source or storage can be used to contribute to the moment of inertia of the system, for example flywheels, batteries, super-capacitors, etc [1].

According to [2], the application of energy storage can be divided into two areas, as shown in Figure 1. Energy storage systems can participate in energy management or provide ancillary services. Depending on the characteristics of the storage systems, different energy storage technologies can meet the requirements to provide various services to the power system. Several different energy storage technologies have been developed and tested to date, including pumped hydro storage, batteries, supercapacitors (SC), hydrogen, compressed air, and flywheels. A comparison of these technologies is provided in Table I, while Table II presents the required characteristics of energy storage for specific applications. From the comparison, it can be concluded that the supercapacitor technology is the most suitable for providing primary frequency control and voltage control.

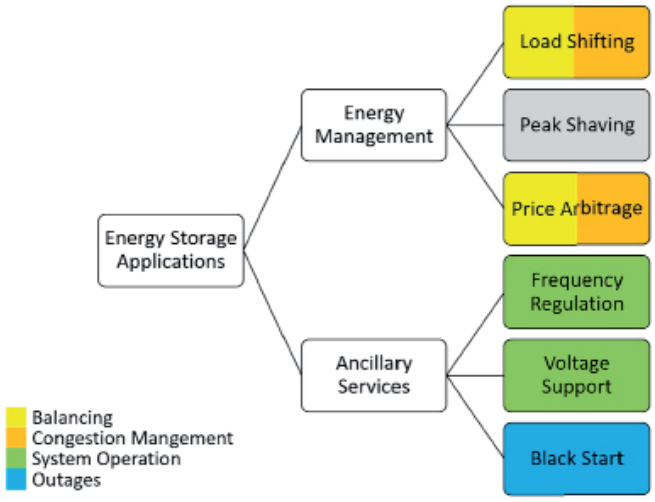

Fig. 1. Classification of energy storage application [2].

II. Types And Design Of Supercapacitors

Although Helmholtz described the electric double-layer capacitor as early as the mid-19th century, the technology of supercapacitors has developed more significantly since the mid-20th century, when the use of porous carbon materials led to the creation of the first electric double-layer capacitors. The structure of a supercapacitor is essentially the same as that of a conventional capacitor. A supercapacitor consists of two electrodes separated by a separator and impregnated with an electrolyte. The material of electrodes depends on the supercapacitor type. Separators are usually thin polymers, while electrolytes can be liquid, solid-state, or redox-active. Among liquid electrolytes, acetonitrile and propylene carbonate, or aqueous and are commonly used. Solid-state electrolytes include polymers or hydrogels. Compared to conventional capacitors, the high capacitance of SCs originates from the high specific area of the electrodes, which is largely determined by the used materials and their physical properties [3]. Voltage of the supercapacitor cell depends on the electrolyte technology. Based on the internal structure and energy storage mechanism, supercapacitors are today commonly classified into electric double-layer capacitors (EDLCs), pseudocapacitors, and hybrid supercapacitors. Characteristic comparison of supercapacitor types can be seen in Figure 2.

(Corresponding author: Karlo Kobeščak)

Karlo Kobeščak and Tomislav Baškarad are with the University of Zagreb Faculty of Electrical Engineering and Computing, Zagreb, Croatia (e-mails: karlo.kobescak@fer.unizg.hr, tomislav.baskarad@fer.unizg.hr)

Karlo Kobeščak,Tomislav Baškarad, Review of Supercapacitor Equivalent Circuit Models, Journal of Energy, vol. 73 Number 3 (2024), 36–43
https://doi.org/10.37798/2024733697

TABLE I:

APPLICATIONS OF ENERGY STORAGE SYSTEMS [2]

Application	Response Time	Power Rating (MW)	Discharge Duration	Cycles per Year
Load Shifting	10 – 30 min	1 – 2,000	Minutes - hours	> 3,000
Peak Shaving	10 – 30 min	0.1 – 10	30 – 240 min	250 – 500
Price Arbitrage	Minutes - hours	50 – 2,000	Hours	300 – 400
Primary Frequency Control	< 10 s	1 – 2,000	< 15 min	> 10,000
Secondary Frequency Control	10 – 30 s	1 – 2,000	< 120 min	< Primary Frequency Control
Tertiary Frequency Control	10 – 30 min	1 – 2,000	Hours	< Secondary Frequency Control
Voltage Support	Milliseconds	0.5 – 50(MVAr)	Seconds - minutes	> 15,000
Black Start	< 10 s	0.1 – 400	Minutes - hours	< 1

TABLE II:

CHARACTERISTICS OF SELECTED ENERGY STORAGE SYSTEMS [2]

Technology	Power Rating	Response Time	Discharge Duration	Cycles	Lifetime
Pumped Hydro	100 – 5,000 MW	Seconds	Hours - Days	> 100,000	30 – 60 years
Compressed Air	3 – 400MW	Minutes	Hours - Days	8,000 – 12,000	> 20 – 40 years
Flywheels	0.1 – 20MW	< 1 s	Seconds - Minutes	20,000 – 175,000	> 15 years
Supercapacitors	0.001 – 0.3MW	Milliseconds	Seconds - Minutes	10,000	30 years
Lithium-Ion Batteries	0 – 300MW	Milliseconds - Minutes	Minutes - Hours	1,000 – 3,000	5 – 15 years
Fuel Cells	Variable	< Seconds (LT)	Flexible	-	50,000 hours (LT)

A. Electric Double-Layer Capacitors

EDLC is most matured and commercially used technology. Electrode materials in most EDLCs are typically composed of carbon-based materials, such as graphene, graphite, carbon nanotubes or mesoporous carbon [4]. When connected to an electric source, the charges on the electrodes attract oppositely charged ions from the electrolyte, forming layers of ions parallel to the electrodes [5]. The large specific surface area of electrode materials, resulting from their porosity, enables the absorption of a greater number of ions on the electrode surface, which leads to a higher capacitance. This type of charge storing mechanism is called non-Faradic. Electrode structure does not change during this process and as a result ELDC have higher cycle life and faster time of charge and discharge than pseudocapacitors and hybrid supercapacitors.

B. Pseudocapacitors

Pseudocapacitors have metal-oxide or conducting polymer electrodes with high electrochemical pseudocapacitance material [6]. and are some of electrode materials of interest for pseudocapacitors. Pseudocapacitors have Faradic storing mechanism - reversible redox reactions happen when potential is applied, and charges are electrochemically adsorbed on the electrode surface [4]. Redox reactions typically lead to the consumption of both electrodes and electrolytes, resulting in a faster degradation of capacitance compared to EDLCs. However, they offer the advantage of a higher capacitance and energy density [7].

C. Hybrid supercapacitors

Hybrid supercapacitors combine two types of electrodes. One electrode is of electrostatic, often referred to as capacitive type, while other is electrochemical or battery type. These supercapacitors can be categorized into three types based on electrode configuration: asymmetric hybrids, battery-type hybrids, and composite hybrids [4]. Asymmetric type pseudocapacitors' electrode as a positive, and EDLC electrode as a negative electrode. Battery type combines battery electrode and SC electrode, while composite type uses electrodes that incorporates carbon-based materials with metal oxides in a single electrode [6]. Charges are stored in both Faradic and non-Faradic processes. Hybrid supercapacitors have the highest energy density and capacitance, but also the longest charging time and non-linear relationship between open-circuit voltage (OCV) and stored charge [7].

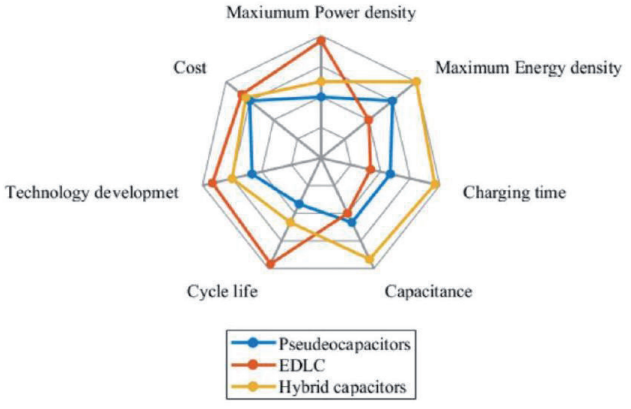

Fig. 2. Characteristics comparison of supercapacitor types [7].

III. SUPERCAPACITORS' CHARACTERISTICS

Supercapacitor characteristics vary depending on the SC type. This article focuses on EDLCs. In the literature ([2], [7]-[10]), the characteristic values of SCs differ. IEC 62391-1 classifies SCs in 5 classes depending on SCs' capacitance and internal resistance [11]. However, despite these variations, the literature agrees on the

Karlo Kobeščak,Tomislav Baškarad, Review of Supercapacitor Equivalent Circuit Models, Journal of Energy, vol. 73 Number 3 (2024), 36–43
https://doi.org/10.37798/2024733697

overall advantages and disadvantages of SCs. The main upsides of SCs include high power density (10,000-60,000 W/kg), high Coulombic efficiency (85-98%), fast response times (measured in milliseconds), fast charging/discharging times (0.3-30 seconds), a high number of cycles (up to 1,000,000), and a wide operating temperature range (-40-75 °C). On the other hand, the main drawbacks of SC technology are lower specific energy (1-30 Wh/kg) and higher self-discharge rates (up to 60% per month).

In addition to their role in providing primary frequency regulation and voltage regulation services, SCs (either standalone or as part of hybrid energy storage systems) can also be used for regenerative power harvesting (e.g., in hybrid electric vehicles), power quality enhancement, microgrid stability, UPS, and as power supplies in medicine and smart devices. Due to the low voltage per SC cell (1-3 V) and low energy density, SC cells are connected in series (to achieve higher voltage) and in parallel (to increase energy capacity) for power system applications. These interconnected cells are referred to as SC modules (or banks). It is of great importance to establish metrics and characterization techniques in order to compare different SC cells. In [12], authors presented different performance evaluations and test procedures for SCs. Commonly used metrics are cyclic voltammetry (CV), electrochemical impedance spectroscopy (EIS) and constant current charge/discharge.

A. Cyclic voltammetry

Cyclic voltammetry is a method used in electrochemistry to understand the behavior and analysis of voltage windows, specific capacitance, and cycle life [7]. The CV measurement is typically conducted in a three-electrode configuration, where the working electrode is the electrode being tested, the reference electrode has a constant electrochemical potential, and the counter electrode is an inert electrode in the tested cell that completes the circuit. During CV measurement, the potential of the working or target electrode in the system is measured against the reference electrode via linear scanning back and forth between the specified upper and lower potential limits. The current passing between the working electrode and the counter electrode can be recorded and then plotted as a function of electrode potential to yield a CV plot [13]. Comparison of SC and battery CV plot is given in Figure 3.

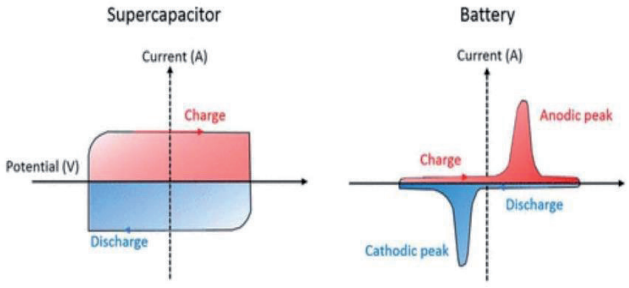

Fig. 3. Cyclic voltammetry plots of SC and battery [14]

B. Electrochemical Impedance Spectroscopy

EIS is a method for measuring supercapacitors' Equivalent Series Resistance (ESR). A sinusoidal AC excitation signal with variable frequency is superimposed on a DC potential and applied to SC and the AC response is measured. EIS is a method for frequency domain analysis of device impedance. Nyquist or Bode plots are used to illustrate the frequency dependencies of capacitance and resistance. More about EIS of EDLC can be found in [15] and physical interpretations of Nyquist plot can be seen in Figure 4. ESR is very important parameter of SC, because it restricts the rates at which the capacitance can be charged or discharged upon application of a given current or voltage [13].

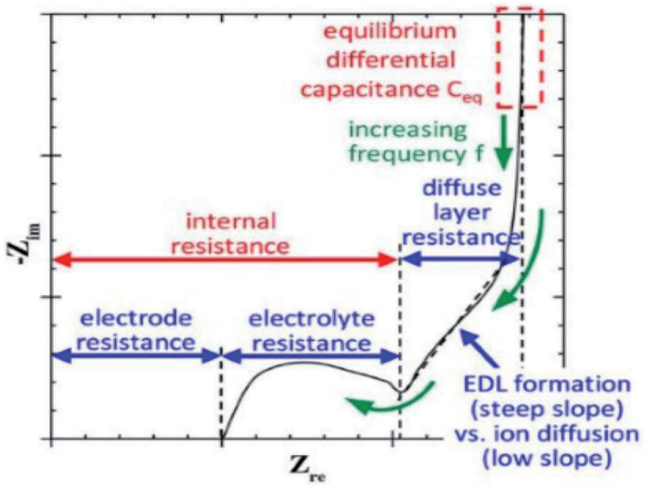

Fig. 4. Physical interpretations of EDLC Nyquist plot [15]

C. Constant current charge/discharge

Galvanostatic charge-discharge test is reliable and widely used method to determine capacitance energy density, power density, ESR and cycle life of SC. Constant cell current is applied, and cell voltage is measured as a function of charging or discharging time. Voltage – time characteristics between capacitor terminals in capacitance and internal resistance mea-surement described by IEC 62391-1 can be seen in Figure 5.

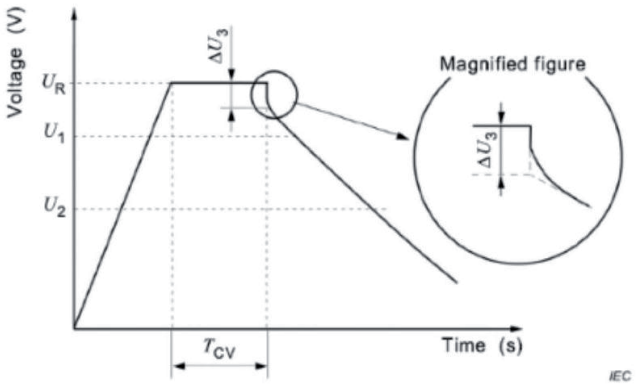

Fig. 5. Voltage - time characteristics [11]

IV. SC Modeling

To analyze a system incorporating a SC , it is crucial to establish an accurate SC model. There are several SC models presented in literature. Models differ on complexity, purpose and accuracy.

A. Overall literature review

Authors in [3] provide a review of different types of EDLC models. They present electrochemical models, equivalent circuit models (ECM), and fractional-order models as suitable for modeling the electrical behavior of supercapacitors. Electrochemical models exhibit high accuracy but low computational efficiency, making them suitable for embedded systems in realtime energy

Karlo Kobeščak,Tomislav Baškarad, Review of Supercapacitor Equivalent Circuit Models, Journal of Energy, vol. 73 Number 3 (2024), 36–43
https://doi.org/10.37798/2024733697

management and control. Fractional-order models improve modeling accuracy by incorporating fractional-order calculus. Additionally, they discuss intelligent models, such as artificial neural networks (ANN) and fuzzy logic, which can capture complex nonlinear relationships between inputs and outputs but require large amounts of training data. Equivalent circuit models, due to their structural simplicity and decent modeling accuracy, are widely accepted for real-time energy management synthesis.

The same authors, in [16], compare the complexity, accuracy, and robustness of three ECM types for SCs: the classic model, multi-stage ladder model, and dynamic model. They conducted Dynamic Stress Tests and a self-designed pulse test to collect data for model characterization and used a genetic algorithm to identify optimal model parameters. Their findings show that the most complex ladder model has the lowest accuracy and robustness, the classic model has the second-best performance, and the dynamic model provides the best compromise between model precision, robustness, and complexity. It is worth noting that none of the three models account for voltage-dependent capacitance.

In [17], the authors review ECMs and propose a new identification procedure for estimating state-space model parameters for series, parallel, and basic configurations.

A comprehensive review of SC modeling techniques is provided in [18], where the authors classify, explain, and compare these techniques, along with descriptions of the experimental methods used to measure the modeled properties. The simple RC circuit, multi-branch model, and dynamic model are briefly discussed.

Description and characterization methods for the RC model, two-branch Zubieta-Bonert model, and the dynamic SC model are presented in [19]. Some ECMs are summarized in [20], while [21] provides a literature review and simulates the two branch SC model in Simulink, which is also experimentally validated.

The comparison of EMCs is given in [22] together with a method of translating the parameters from one model to another so that the user can choose the model that best suits their particular need. The drawback of this work is that none of the compared models includes voltage dependent capacitance.

The authors of [23] address different aspects of SC models and propose small- and large-signal models for simulation and control, based on a first-order RC model. The same model is used in [24] to discuss SC module selection and design.

Krpan et al., in [25], compare the stored energy and discharge profiles of ideal and realistic SC models. In [26], a detailed RC circuit model proposed by Tironi and Musolino is simplified and used to model SC banks for power system dynamics studies.

A comparison of RC, two-branch, Zubieta, and series models is provided in [27]. In this work, the Maxwell BCAP3000 SC is tested, and measurements are used to estimate model parameters using MATLAB/Simulink's parameter estimation tool. The SC models are then compared based on their accuracy and execution time requirements for real-time simulations.

Other works discussing various SC models and parameter identification procedures include [28]-[37].

V. Supercapacitor Equivalent Circuit Models

ECMs represent a tool for estimating the electrical performance of SC. SC usually operate in two modes of charge: constant voltage (CV) and constant current (CC), and three discharge modes: constant resistance (CR), constant power (CP), and constant current. Specific energy and power densities are of interest when modeling SCs for power system applications because the mass of the storage device affects the design of the system. Compared to lithium-ion batteries, SCs have a significantly higher specific power density but a lower energy density. This section provides an overview of commonly used and proven applicable equivalent circuit models of SCs, arranged from simpler to more complex ones. ECM models can be seen in Figure 6. Models are: a) RC model, b) "classic" model, c) simplified theoretical, d) ZubietaBonert and e) Tironi-Musolino.

A. RC model

Simplest model of SC accounts only for ideal capacitance and ESR connected in series. This model is used by manufacturers in datasheets. The model parameters are obtained by the constant current charge-discharge method described in IEC 62391-1 [11]. Since parameters are available in manufacturers datasheet, it is not necessary to perform any tests on cells in order to use a model in simulations. Charging and discharging times depend on time constant . In CP discharging mode, time of discharge is described with:

$$t = (\mathrm{V}_0 - V)\frac{C}{I_C} \tag{1}$$

where

$$V = V_0 - \frac{I_C}{C}t \tag{2}$$

V_0 is initial voltage and is constant current of discharge. Specific energy density in Wh/kg and specific power density in W/kg are given in Eqs. 3 and 4, where is SC cell mass.

$$E_d = \frac{1}{2}\frac{CV^2}{m} \tag{3}$$

$$P_d = \frac{1}{4}\frac{V^2}{mR_{ESR}} \tag{4}$$

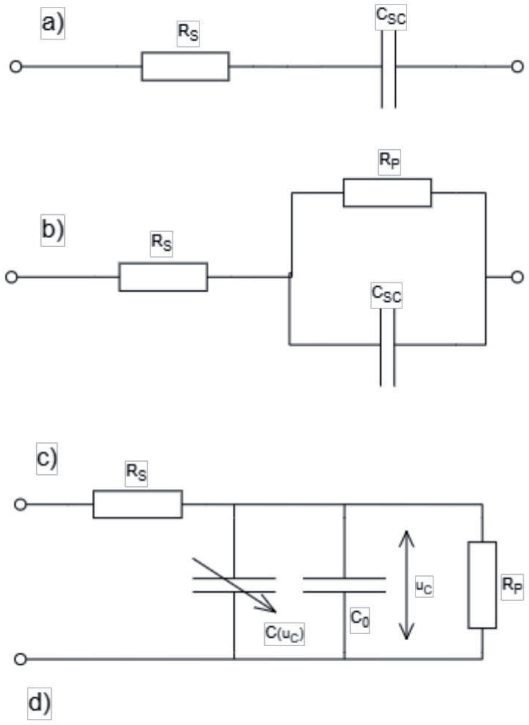

Karlo Kobeščak,Tomislav Baškarad, Review of Supercapacitor Equivalent Circuit Models, Journal of Energy, vol. 73 Number 3 (2024), 36–43
https://doi.org/10.37798/2024733697

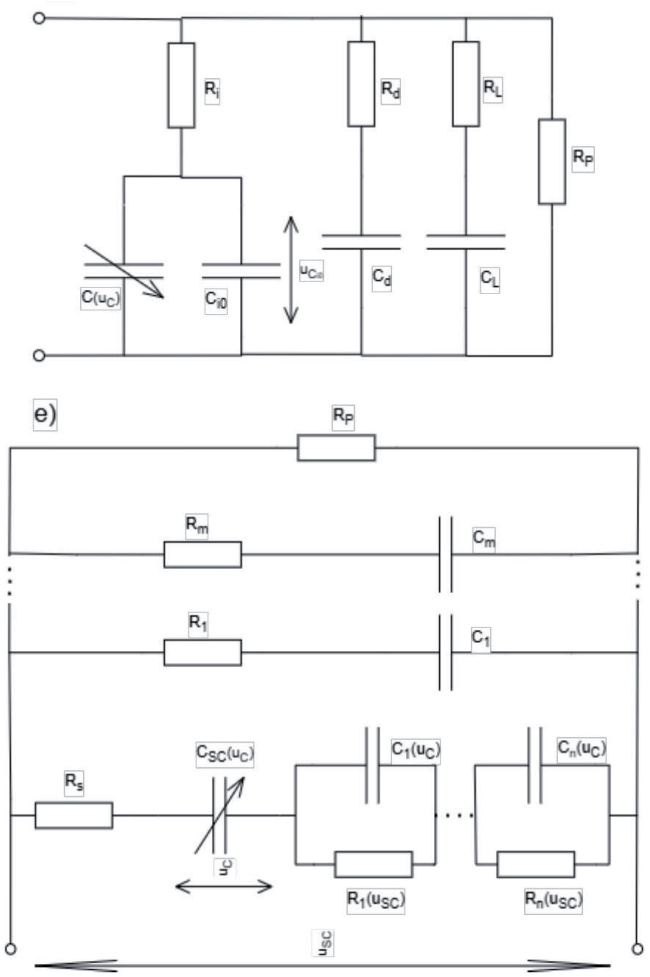

Fig. 6. SC models: a) RC model b) classical c) simplified theoretical model d) Zubieta-Bonert e) Tironi-Musolino

B. Classic model

Since RC model does not model self-discharge phenomena of SC, an additional resistance R_p was connected in parallel with capacitance to take self-discharge in account. is sometimes also referred as - Equivalent parallel resistance and can be either found in manufacturer datasheet, determined through EIS or by constant current charge/discharge and calculation described in [32]. R_p value is usually much greater than R_{ESC}, and can be omitted if charging and discharging is done at a fast rate. When SC cell is discharged in CC mode, voltage cell can be expressed by Eq. 5.

$$V = -I_C R_{ESR} + V_0 - (V_0 + I_C R_p)\left[1 - \exp\left(-\frac{t}{R_P C_{SC}}\right)\right] \quad (5)$$

Time required for SC to be fully discharged is then:

$$t = C_{SC}\frac{(V_0 - I_C R_{ESR})}{I_C} \quad (6)$$

The equation for specific energy density is same as for RC model (Eq. 3) and change in models is included in Eq. 5. It is worth noting that quadratic drop in potential means that of stored energy is depleted before voltage reaches the usable range of .

Power density can be expressed as Eq. 7:

$$P_d = \frac{I_C}{m}[-I_C R_{ESR} + V_0 - (V_0 + I_C R_p)\left[1 - \exp\left(-\frac{t}{R_P C_{SC}}\right)\right] \quad (7)$$

By increasing the time of discharge, the power density of the supercapacitor will gradually decrease. Maximum power density is obtained by deriving Eq. 7 and at t = 0 it is the same as Eq. 4. It is clear that R_{ESR} has a much stronger effect on power density than R_p.

C. Simplified theoretical model

Capacitance of EDLC is voltage dependent. Incremental change in charge dQ at certain capacitor voltage produces an incremental change in voltage dV. This change is nonlinear, however, most authors use linear expression to fit this behavior, expressing capacitance as:

$$C_{SC}(u_C) = C_0 + ku_C \quad (8)$$

is initial linear capacitance and is a constant coefficient in [F/V]. This is supported by the experiments and results presented in [38], where the authors concluded that the relationship between Helmholtz capacitance and voltage bias is linear, while the total capacitance exhibits a sublinear dependence. The change in capacitance is typically several farads within the range from zero to the rated voltage of the supercapacitor, but this varies depending on the specific supercapacitor.

In ECM presented in [23] this is represented as constant capacitance C_0 in parallel with variable capacitance $C(u_C) = ku_C$. Voltage dependent capacitance implies that stored energy also varies with voltage.

Leakage current is modeled with a shunt resistor R_p whose resistance can be determined from the criterion that SC voltage decays at 4% of V_0 after 72 hours or from an electrode metric of 2μA/F [23]. In series is connected ESR R_S.

Capacitor current is defined as:

$$i_C = \frac{\delta Q}{\delta t} = \frac{\delta[C_{SC}(u_C)u_C]}{\delta t} = \left(C_{SC}(u_C) + u_C\frac{dC(u_C)}{du_C}\right)\frac{du_C}{dt} = (C_0 + 2ku_C)\frac{du_C}{dt} \quad (9)$$

This is derived by utilizing the definition of total capacitance, which is expressed as the ratio between the total charge at a specific voltage $Q(u)$ and the voltage at that particular value , as described in Eq.10. Another possible definition of voltage dependent capacitance is the so-called "differential capacitance", which is defined as the local derivative of $Q(u)$ with respect to u, presented in Eq. 11.

$$C_{tot}(u) = \frac{Q(u)}{u} \quad (10)$$

$$C_{diff}(u) = \frac{dQ(u)}{du} \quad (11)$$

Karlo Kobeščak,Tomislav Baškarad, Review of Supercapacitor Equivalent Circuit Models, Journal of Energy, vol. 73 Number 3 (2024), 36–43
https://doi.org/10.37798/2024733697

If "differential capacitance" was used, supercapacitor current would be:

$$i_C = C_{SC}(u_C)\frac{du_C}{dt} \tag{12}$$

For linear capacitors, $C_{diff}=C_{tot.}$ The difference between differential and total capacitance can be found in [39].

Energy stored in SC can be expressed as

$$E_C = \int u_C i_C dt = \int u_C(C_0 + 2ku_C)\frac{du_C}{dt}dt = u_C^2\left(\frac{C_0}{2} + \frac{2}{3}ku_C\right) \tag{13}$$

Finally, specific energy is then:

$$E_C = \int u_C i_C dt = \int u_C(C_0 + 2ku_C)\frac{du_C}{dt}dt = u_C^2\left(\frac{C_0}{2} + \frac{2}{3}ku_C\right) \tag{13}$$

Specific power is defined as Eq.15, its maximum is again the same as in Eq. 4.

$$E_d = \frac{u_C^2\left(\frac{C_0}{2} + \frac{2}{3}ku_C\right)}{m} \tag{14}$$

Notice that in this model, Eq. 13 and Eq. 15 describe specific energy and power density stored, and not energy/power injected or extracted from the cell terminals. For that i_{sc} and u_{sc} should be used, where $i_{SC} = i_C + \frac{u_C}{R_P}$ and $u_{SC} = u_C + i_{SC}R_S$.

If SC is discharged by constant current I_0 then maximum discharge time is:

$$t = \frac{C_0V_0 + kV_0^2}{I_0} \tag{16}$$

where V_0 is the voltage of the fully charged SC.

D. Zubieta-Bonert model

One of the most commonly used, well-tested, and described models is one presented by Zubieta and Bonert in [30]. This model is even used in Matlab/Simscape SC model [40]. Variation of this model was presented in [34], so-called two branch model, where one RC branch is omitted. Different names are used for this model: parallel, multibranch, two branch, Zubieta, etc. This model achieved best accuracy for the energy stored in a SC and self-discharge [18]. The Zubieta-Bonert model consists of three RC branches and resistance to leakage R_P in parallel to those branches. Each branch has a distinct time constant. First branch or "immediate" branch is modeled as ESR R_S in series with linear voltage dependent capacitor $C_{SC}(u_C) = C_{i0} + C(u_C)$ where $C(u_C) = ku_C$. This branch models behavior of SC in time range of seconds in response to a charge action. Authors used "differential capacitance" to derive stored energy.

$$i = C\frac{du}{dt} \tag{17}$$

$$E = \int uidt = \int u_C(C_i0 + ku_C)du_C \tag{18}$$

Then for a constant charging current I and at a specified voltage V, the stored energy is:

$$E = \frac{C_{i0}}{2}V^2 + \frac{k}{3}V^3 \tag{19}$$

The second or "delayed" branch dominates terminal behavior in the range of minutes, it is composed of R_d and C_d. The third branch ("long-term" branch), consisting of R_L and C_L, determines the behavior for times longer than 10 minutes.

E. Tironi-Musolino model

Tironi and Musolino proposed a model aimed at power electronic applications in a frequency range of 0,01 Hz –1kHz [28]. The same authors presented an identification procedure for this model in [29].

This model is very similar to Zubieta-Bonert, difference is in first (immediate) branch, where Tironi and Musolino replaced it with series model proposed by Buller et al. in [41]. Transfer function Z_p (also called pore impedance) represents dynamic behavior of the device at high frequencies [28] is described by:

$$\mathrm{Zp}(j\omega, \mathrm{V}) = \frac{\tau(\mathrm{V}) \cdot \coth(\sqrt{j\omega\tau(\mathrm{V})})}{\mathrm{C}(\mathrm{V}) \cdot \sqrt{j\omega\tau(\mathrm{V})}} \tag{20}$$

Parameter $\tau(V)$ can be calculated as:

$$\tau(\mathrm{V}) = 3 \cdot \mathrm{C}(\mathrm{V}) \cdot (\mathrm{Rdc} - \mathrm{Ri}) \tag{21}$$

where R_{dc} is the resistance experimentally obtained at very low frequencies (essentially DC).

This transfer function is modeled with variable capacitance C_{SC} connected in series with n RC parallels. Parameter of first branch are:

$$C_{sc}(u_C) = C_0 + k_v u_C(t) \tag{22}$$

$$C_k = \frac{1}{2}C_{sc}, k \in \{1 \dots n\} \tag{23}$$

$$R_k = \frac{2\tau(u_C)}{k^2\pi^2 C_{sc}} \tag{24}$$

Krpan et al. showed in [26] that the significance of parallel RC groups depends on the difference between R_{dc} and R_S and that at least one parallel group should be included in the model. On the other hand, the number of RC branches (delayed and long-term) depends on the interested time scale. Cell voltage is described as:

$$u_{sc}(t) = i_{sc}(t)R_S + u_C(t) + \sum_{k=1}^{n} u_{C_k} \tag{25}$$

and first branch current is:

$$i_{sc} = (C_0 + ku_C)\frac{du_C}{dt} \tag{26}$$

Power density can then be obtained as in Eq. 15.

Karlo Kobeščak,Tomislav Baškarad, Review of Supercapacitor Equivalent Circuit Models, Journal of Energy, vol. 73 Number 3 (2024), 36–43
https://doi.org/10.37798/2024733697

VI. Conclusion and Future Work

A literature review reveals that the same models or their variations are often referred to by different names. In some studies, certain models are omitted, while others demonstrate superior suitability in terms of complexity and accuracy. Additionally, the criteria used for model comparison are frequently inconsistent and poorly defined, with model complexity often being a subjective assessment. Model parameters are typically determined based on experimental measurements, which are not always available. This lack of data makes it challenging to evaluate model accuracy in such circumstances.

In this article, five different equivalent circuit models (ECMs) for supercapacitors (SCs) are presented: the RC model, classic model, simplified theoretical model, ZubietaBonert model, and Tironi-Musolino model. Each model is accompanied by a physical explanation, and the influence of various parameters on model behavior is analyzed.

Future work should focus on experimental validation of the models, investigation of models for complete SC modules rather than individual SC cells and exploring the feasibility of incorporating SC models into control system design.

References

[1] M. Alandžak, T. Plavsic, and D. Franković, "Provision of Virtual Inertia Support Using Battery Energy Storage System," Journal of Energy - Energija, vol. 70, no. 4, pp. 13-19, 2021, [Online]. Available: http://journalofenergy.com/index.php/joe/article/view/250

[2] S. Sahoo and P. Timmann, "Energy storage technologies for modern power systems: A detailed analysis of functionalities, potentials, and impacts," IEEE Access, vol. 11, pp. 49 689-49 729, 2023.

[3] L. Zhang, X. Hu, Z. Wang, F. Sun, and D. G. Dorrell, "A review of supercapacitor modeling, estimation, and applications: A control/management perspective," Renewable and Sustainable Energy Reviews, vol. 81, pp. 1868-1878, 2018. [Online]. Available: https://www.sciencedirect.com/science/article/pii/S1364032117309292

[4] J. Zhang, M. Gu, and X. Chen, "Supercapacitors for renewable energy applications: A review," Micro and Nano Engineering, vol. 21, p. 100229, 2023. [Online]. Available: https://www.sciencedirect.com/ science/article/pii/S259000722300059X

[5] D. Vujević, "Superkondenzatori," Journal of Energy - Energija, vol. 52, no. 4, pp. 295-303., Aug 2003.

[6] N. I. Jalal, R. I. Ibrahim, and M. K. Oudah, "A review on supercapacitors: types and components," Journal of Physics: Conference Series, vol. 1973, no. 1, p. 012015, aug 2021. [Online]. Available: https://dx.doi.org/10.1088/1742-6596/1973/1/012015

[7] K. Dissanayake and D. Kularatna-Abeywardana, "A review of supercapacitors: Materials, technology, challenges, and renewable energy applications," Journal of Energy Storage, vol. 96, p. 112563, 2024. [Online]. Available: https://www.sciencedirect.com/ science/article/pii/S2352152X24021492

[8] J. Libich, J. Máca, J. Vondrák, O. Čech, and M. Sedlaříková, "Supercapacitors: Properties and applications," Journal of Energy Storage, vol. 17, pp. 224-227, Jun. 2018. [Online]. Available: https://www.sciencedirect.com/science/article/pii/S2352152X18301634

[9] K. Subasinghage, K. Gunawardane, N. Padmawansa, N. Kularatna, and M. Moradian, "Modern Supercapacitors Technologies and Their Applicability in Mature Electrical Engineering Applications," Energies, vol. 15, no. 20, p. 7752, Jan. 2022, number: 20 Publisher: Multidisciplinary Digital Publishing Institute. [Online]. Available: https://www.mdpi.com/1996-1073/15/20/7752

[10] A. G. Olabi, Q. Abbas, A. Al Makky, and M. A. Abdelkareem, "Supercapacitors as next generation energy storage devices: Properties and applications," Energy, vol. 248, p. 123617, Jun. 2022. [Online]. Available: https://www.sciencedirect.com/science/article/pii/ S0360544222005205, "IEC 62391-1:2022." [Online]. Available: https://webstore.iec.ch/en/ publication/66557

[11] J. Zhao and A. F. Burke, "Review on supercapacitors: Technologies and performance evaluation," Journal of Energy Chemistry, vol. 59, pp. 276-291, 2021. [Online]. Available: https://www.sciencedirect.com/ science/article/pii/S2095495620307634

[12] A. Yu, V. Chabot, and J. Zhang, Electrochemical Supercapacitors for Energy Storage and Delivery: Fundamentals and Applications. CRC Press, Apr. 2013, google-Books-ID: 1RWew9oy9CMC.

[13] Y. Shao, M. F. El-Kady, J. Sun, Y. Li, Q. Zhang, M. Zhu, H. Wang, B. Dunn, and R. B. Kaner, "Design and mechanisms of asymmetric supercapacitors," Chemical Reviews, vol. 118, no. 18, pp. 9233-9280, 2018, pMID: 30204424. [Online]. Available: https: //doi.org/10.1021/acs.chemrev.8b00252

[14] B.-A. Mei, O. Munteshari, J. Lau, B. Dunn, and L. Pilon, "Physical Interpretations of Nyquist Plots for EDLC Electrodes and Devices," The Journal of Physical Chemistry C, vol. 122, no. 1, pp. 194-206, Jan. 2018, publisher: American Chemical Society. [Online]. Available: https://doi.org/10.1021/acs.jpcc.7b10582

[15] L. Zhang, Z. Wang, X. Hu, F. Sun, and D. G. Dorrell, "A comparative study of equivalent circuit models of ultracapacitors for electric vehicles," Journal of Power Sources, vol. 274, pp. 899-906, Jan. 2015. [Online]. Available: https://www.sciencedirect.com/science/article/pii/S0378775314017893

[16] D. Slaifstein, F. M. Ibanez, and K. Siwek, "Supercapacitor modeling: A system identification approach," IEEE Transactions on Energy Conversion, vol. 38, no. 1, pp. 192-202, 2023.

[17] A. Berrueta, A. Ursúa, I. S. Martín, A. Eftekhari, and P. Sanchis, "Supercapacitors: Electrical characteristics, modeling, applications, and future trends," IEEE Access, vol. 7, pp. 50 869-50 896, 2019.

[18] N. Devillers, S. Jemei, M.-C. Péra, D. Bienaimé, and F. Gustin, "Review of characterization methods for supercapacitor modelling," Journal of Power Sources, vol. 246, pp. 596-608, Jan. 2014. [Online]. Available: https://www.sciencedirect.com/science/article/pii/S037877531301325

[19] W. Kai, R. Baosen, L. Liwei, L. Yuhao, Z. Hongwei, and S. Zongqiang, "A review of modeling research on supercapacitor," in 2017 Chinese Automation Congress (CAC), 2017, pp. 5998-6001.

[20] M. E. ŞahİN, F. Blaabjerg, and A. SangwongwanİCh, "Modelling of supercapacitors based on simplified equivalent circuit," CPSS Transactions on Power Electronics and Applications, vol. 6, no. 1, pp. 31-39, 2021.

[21] L. Shi and M. L. Crow, "Comparison of ultracapacitor electric circuit models," in 2008 IEEE Power and Energy Society General Meeting Conversion and Delivery of Electrical Energy in the 21st Century, 2008, pp. 1-6.

[22] Ultra-Capacitor Energy Storage Devices. John Wiley Sons, Ltd, 2013, ch. 2, pp. 22-77. [Online]. Available: https://onlinelibrary.wiley.com doi/abs/10.1002/9781118693636.ch2

[23] Ultra-Capacitor Module Selection and Design. John Wiley Sons, Ltd, 2013, ch. 4, pp. 149-215. [Online]. Available: https://onlinelibrary.wiley.com doi/abs/10.1002/9781118693636.ch4

[24] M. Krpan and I. Kuzle, "On modelling and sizing a supercapacitor energy storage for power system frequency control," in The 12 th Mediterranean Conference on Power Generation, Transmission, Distribution and Energy Conversion (MEDPOWER 2020), vol. 2020, 2020, pp. 404-409.

[25] M. Krpan, I. Kuzle, A. Radovanović, and J. V. Milanović, "Modelling of supercapacitor banks for power system dynamics studies," IEEE Transactions on Power Systems, vol. 36, no. 5, pp. 3987-3996, 2021.

[26] S. Pezzolato, "Modeling and model validation of supercapacitors for real-time simulations," Master Thesis, Alma Mater Studiorum - Università di Bologna, 2019.

[27] E. Tironi and V. Musolino, "Supercapacitor characterization in power electronic applications: Proposal of a new model," in 2009 International Conference on Clean Electrical Power, 2009, pp. 376-382.

[28] V. Musolino, L. Piegari, and E. Tironi, "New full-frequency-range supercapacitor model with easy identification procedure," IEEE Transactions on Industrial Electronics, vol. 60, no. 1, pp. 112-120, 2013.

[29] L. Zubieta and R. Bonert, "Characterization of double-layer capacitors for power electronics applications," IEEE Transactions on Industry Applications, vol. 36, no. 1, pp. 199-205, 2000.

[30] V. Castiglia, N. Campagna, C. Spataro, C. Nevoloso, F. Viola, and R. Miceli, "Modelling, simulation and characterization of a supercapacitor," in 2020 IEEE 20th Mediterranean Electrotechnical Conference (MELECON), 2020, pp. 46-51.

[31] R. Spyker and R. Nelms, "Classical equivalent circuit parameters for a double-layer capacitor," IEEE Transactions on Aerospace and Electronic Systems, vol. 36, no. 3, pp. 829-836, 2000.

[32] R. Nelms, D. Cahela, and B. Tatarchuk, "Modeling double-layer capacitor behavior using ladder circuits," IEEE Transactions on Aerospace and Electronic Systems, vol. 39, no. 2, pp. 430-438, 2003.

[33] R. Faranda, M. Gallina, and D. Son, "A new simplified model of doublelayer capacitors," in 2007 International Conference on Clean Electrical Power, 2007, pp. 706-710.

[34] D. Xu, L. Zhang, B. Wang, and G. Ma, "Modeling of supercapacitor behavior with an improved two-branch equivalent circuit," IEEE Access, vol. 7, pp. 26379-26390, 2019.

[35] C. Wu, Y. Hung, and C. Hong, "On-line supercapacitor dynamic models for energy conversion and management," Energy Conversion and Management,

vol. 53, no. 1, pp. 337-345, 2012. [Online]. Available: https://www.sciencedirect.com/science/article/pii/S019689041100063X

[36] S. V. Rajani, V. J. Pandya, and V. A. Shah, "Experimental validation of the ultracapacitor parameters using the method of averaging for photovoltaic applications," Journal of Energy Storage, vol. 5, pp. 120-126, 2016. [Online]. Available: https://www.sciencedirect.com/science/article/pii/S2352152X15300360

[37] A. Szewczyk, J. Sikula, V. Sedlakova, J. Majzner, P. Sedlak, and T. Kuparowitz, "Voltage dependence of supercapacitor capacitance," Metrology and Measurement Systems, vol. vol. 23, no. No 3, pp. 403–411, 2016. [Online]. Available: http://journals.pan.pl/Content/106345/PDF/10.15.15mms-2016-0031%20paper%2008.pdf

[38] I. Zeltser and S. Ben-Yaakov, "On spice simulation of voltage-dependent capacitors," IEEE Transactions on Power Electronics, vol. 33, no. 5, pp. 3703-3710, 2018.

[39] Supercapacitor. MathWorks. Accessed: Nov. 29, 2024. [Online]. Available: https://www.mathworks.com/help/sps/powersys/ref/supercapacitor.html

[40] S. Buller, E. Karden, D. Kok, and R. De Doncker, "Modeling the dynamic behavior of supercapacitors using impedance spectroscopy," IEEE Transactions on Industry Applications, vol. 38, no. 6, pp. 1622–1626, 2002.

Journal of Energy
VOLUME 73 Number 3 | 2024
journal homepage: http://journalofenergy.com/

Impact Of Climate Change on Transmission System Operator Assets: Experiences from Croatia and Need for Resilience Plan

Goran Levačić, Igor Lukačević, Krešimir Mesić, Mate Lasić, Petar Končar, Igor Ivanković

***Summary* — The consequences of climate change are felt everywhere, especially on power systems assets, whereby over headlines are one of its most exposed elements. It is expected that the impact of climate change, especially the effects of evident global warming, will be even more expressed in the coming decades, with increased frequency and severity of extreme weather events in the form of storms, winds, snow, ice, high temperatures, fires, etc. Therefore, it is essential to ensure the safe and stable operation of power networks. An experience with two strong storms that appeared within only two days in July 2023, affecting a larger part of the Croatian transmission network, is presented in order to discuss whether it is necessaryto change valid requirements for new overhead lines, and to consider establishment of internal resilience mechanisms for better withstand the impacts of climate change and global warming.**

***Keywords* — climate change, global warming, transmission network, OHLs, resilience, storm, wind**

I. Introduction

Over the past decade, climate change has manifested in various forms, significantly affecting power system infrastructure. Extreme weather conditions are more and more common and they have posed unprecedented challenges to the resilience and reliability of power grids. Rising global temperature shaveled to increased energy demand for cooling, placing additional stress on power generation, transmissionand distribution systems.

The impacts of climate change can reduce efficiency and alter the availability and generation potential of power plants, including both thermal and renewable facilities. For transmission and distribution networks, impacts can result in higher losses, transfer capacity change and physical damage.

These climate-induced disruptions have resulted in widespread power outages, economic losses, and compromised energy security. Infrastructure damage, prolonged downtime, and repair costs have escalated, prompting a re-evaluation of traditional approaches to power system design and maintenance. In response, there is agrowing emphasis on implementing climate-resilient technologies, enhancing grid flexibility, and diversifying energy sources to mitigate the impact of climate change on power systems. Policy makers, utilities, and industry stakeholders are now recognizing the urgency of adopting sustainable practices and investing in innovative solutions to build a more robust and adaptable power infrastructure for the future.

Figure 1 shows the change in global surface temperature compared to the long-term average from1951 to 1980. Earth's average surface temperature in 2023 was the warmest on record since record keeping began in 1880 (source: NASA/GISS). Overall, Earth was about 1.36 degrees Celsius warmer in 2023 than in the late 19th-century (1850-1900) preindustrial average.

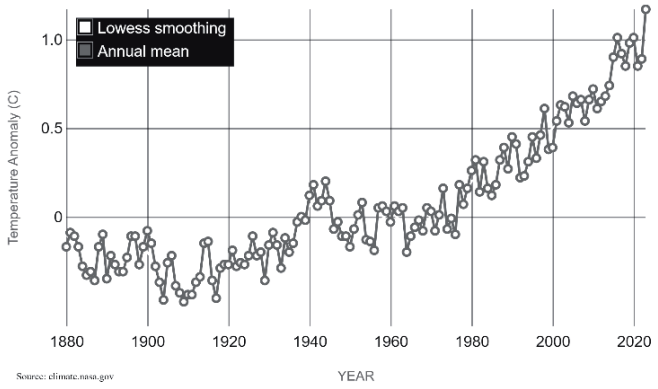

Fig.1. The change in global surface temperature compared to the long-term average from 1951 to 1980

The Mediterranean region is a recognized climate change hotspot, warming 20% faster than the global average, and as such Croatia is subjected to the most extreme climate change, and like in many other regions, they are multifaceted and can affect various aspects of the environment, economy, and society.

This accelerated warming increases the frequency and severity of extreme weather events, such as droughts and heatwaves. Additionally, precipitation is projected to decline by up to 30% in Southern Europe under higher global warming scenarios, exacerbating water scarcity and ecosystem stress. These findings highlight the vulnerability of the region compared to global averages [1-2]. The region is also experiencing ecosystem changes, including biodiversity loss and shifts in marine and terrestrial species due

(Corresponding author: Goran Levačić)

Goran Levačić, Igor Lukačević, Krešimir Mesić, Mate Lasić, Petar Končar and Igor Ivanković are with the Croatian Transmission System Operator, Zagreb, Croatia (e-mails: Goran.Levacic@hops.hr, Igor.Lukacevic@hops.hr, Kresimir.Mesic@hops.hr, Mate.Lasic@hops.hr, Petar.Koncar@hops.hr, Igor.Ivankovic@hops.hr)

Goran Levačić, Igor Lukačević, Krešimir Mesić, Mate Lasić, Petar Končar, Igor Ivanković, Impact Of Climate Change on Transmission System Operator Assets: Experiences from Croatia and Need for Resilience Plan, Journal of Energy, vol. 73 Number 3 (2024), 44–51
https://doi.org/10.37798/2024733537

to temperature rises and habitat degradation [2-3].

The Mediterranean region is currently dealing with critical challenges, including water scarcity, food and energy insecurity, and ecosystem degradation. Special Report (November 2024) [4] represents a significant step in understanding the complex relationships between water, energy, food, and ecosystems in the Mediterranean.The report offers a comprehensive assessment of the available scientific knowledge on these issues, covering the drivers of change, their cascading impacts, and response options for addressing the region's multiple climate and environmental challenges. Consequently, some notable impacts of climate change in Croatia are already visible in the energy sector. These events can have direct and indirect impacts.

There are numerous scientific and technical papers, reports, and studies that have been performed with a focus on the impact of climate change on the power systems [5-10]. Most of these works are based on real examples of extreme weather conditions and their impact on various parts of the power system, with the conclusion that there is a pronounced need for stronger resilience measures and mechanisms. Power systems need to be able to adapt and withstand different events in climate change patterns, operate under the immediate shocks, and restore the power system's function after an interruption resulting from climate hazards.

According to the IPCC WGI Interactive Atlas, Figure 2 presentsthe global warminglevel(GWL) forCroatiabasedon historical data, starting from 1900, with predictions until 2100. GWL is an analysis dimension alternative to the use of future periods across different scenarios. It translates mean temperature change and can give an answer to how far we are from reaching the global warming imit of 1.5°C (agreed upon under the Paris agreement).

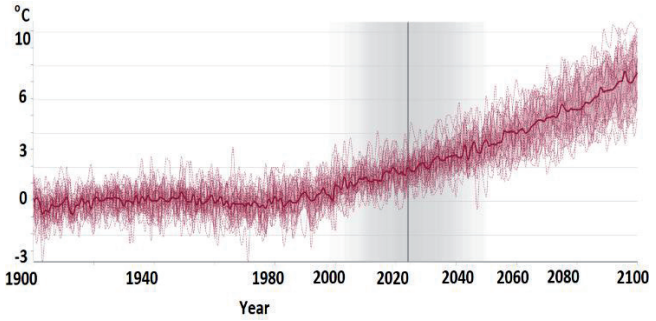

Fig. 2. Mean temperature change for 1.5 °C based on historical data from Croatia

As it can be seen, reaching the 1.5 °C limit is in fact very close. Consequently, every increment of GWL is important because it will directly impact regional changes, with climate and extremes to become more widespread and pronounced. Another evident example of global temperature rise impacting the number of natural disaster events is shown in Figure 3, based on EM-DAT data.

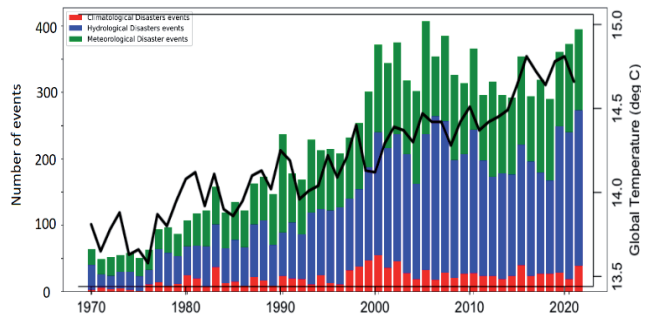

Fig. 3. Global number of events of cilmatological, hydrological and meteorological disasters vs. global temperature

Focusing on the last 20 years (2001-2020), there were 999 natural disaster events in Europe, of which 951 were weather- related, meaning they belonged to the disaster subgroups meteorological, hydrological, or climatological [11].

According to a visualization tool that enables projections of different climate factors for the future (WEMC TEAC), Figure 4 shows predictions of air temperature rise for Croatia.

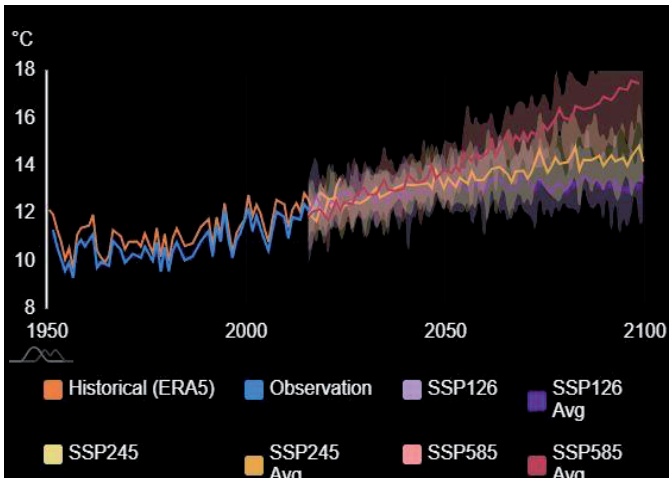

Fig. 4. Prediction of mean annual air temperatures in Croatia according to different scenarios

Temperatures have risen consistently in Europe over the last 40 years. Climate projections into the future show this difference in rates will continue, also for Croatia. Generally, climate model projections for Europe indicate major warming of about 3 to 5°C on average by 2100 for a high greenhouse gas emissions scenario. The projections indicate more frequent high-temperature extremes (e.g., heatwave events, wildfires, strong storms, etc.).

The first part of the paper gives an introtuction on evidences of global warming and climate change, overview of existing national norms and standards related to the designand engineering of OHLs (in this case, parameters related to wind).

As evidence of ongoing changes, the second part of the paper presents HOPS experiences with two strong storms that occurred in July 2023 (on the19th and 21st)on the territoryof central and eastern Croatia and caused unprecedented damage to the transmission network of HOPS, whereby in total 51 transmission line towers were damaged or completely demolished (including six interconnection OHLs with Hungary, Serbia and Bosnia Herzegovina).

For the emergency repair of the transmission network and to ensure reliable electricity supply, a modular emergency restoration towers were installed, with coordination and help provided from neighboring TSOs.

Similar events with significant impact were also recorded earlier, for example in February 2014, when ice caused significant damage to the network, in August 2018, when strong wind damage severely damaged towers and completely demolished one tower on 110 kV OHL [12], or in August 2021 (wind), when three towers of internal 400 kV OHL in a row were completely demolished [13]. The network is also often affected with salt and wildfires in coastal areas, or wind, ice, and floods in continental areas. Also, as a result of the devastating earthquakes in 2020, significant damage occurred in 7 substations in the wider Zagreb and Sisak area.

At the end, it is discussed whether changing of design parameters of OHLs could prevent future damages and their outages due to unpredictable weather phenomena. Also, the need for the establishment of resilience mechanisms is pointed out.

Goran Levačić, Igor Lukačević, Krešimir Mesić, Mate Lasić, Petar Končar, Igor Ivanković, Impact Of Climate Change on Transmission System Operator Assets: Experiences from Croatia and Need for Resilience Plan, Journal of Energy, vol. 73 Number 3 (2024), 44–51
https://doi.org/10.37798/2024733537

II. Croatian Transmission Network And Overheaed Lines Design Criteria

Croatia is a Mediterranean country located in Southeast Europe. Due to its geographical position, the Croatian power system comprises plants and facilities for electricity production, transmission, and distribution located in different climatic zones and geographical areas. The transmission network is a part of the Croatian power system and comprises transformer substations, switchyards, overhead lines (OHLs), and underground cables. The Croatian Transmission System Operator (further in text HOPS) owns 7778 kilometers of overhead lines at 400 kV, 220 kV, and 110 kV voltage levels and 187 substations.

The Croatian transmission network consists of four different areas, based on four main and biggest cities: the transmission areas are Zagreb (ZG), Split (ST), Rijeka (RI), and Osijek (OS). Each of them is located in different geographical zones with different climatic conditions and possible impacts on power system equipment.

Continental areas (parts of transmissions areas ZG and OS), especially in winter, can experience heavy snowfall and ice. Accumulation of snow and ice on OHLs and towers or substation equipment may lead to increased weight, causing sagging and potential damage. Ice accretion can also increase the risk of conductor breakage. Also, strong winter winds can exacerbate the impact of snow and ice by causing additional stress.

The area of the Adriatic Coast (parts of transmission areas ST and RI) is exposed to strong winds and salt-laden air. Salt corrosion is a significant concern for power system infrastructure, as it can accelerate the deterioration of materials, leading to equipment failure and increased maintenance needs. Also, storm surges associated with coastal storms can lead to flooding, impacting substation equipment and potentially causing electrical failures. In summer, coastal regions may also face the risk of wildfires.

Higher elevations (parts of transmission areas ST and RI), in mountainous regions, receive heavy snowfall during winter. Snow accumulation can affect power lines and transformers, and ice formation on elevated structures poses a risk of conductor breakage and equipment damage.

And, at the end, low-lying areas and river valleys may be susceptible to floodingduring periods ofheavyrainfall, which can damage substation equipment, transformers, and other infrastructure, leading to extended outages.

Understanding these regional climate-related challenges is crucial for TSOs and planners. Mitigation strategies include designing infrastructure to withstand specific environmental conditions, implementing regular maintenance and inspection programs, and employing materials that are resistant to corrosion and environmental stress. Additionally, advanced forecasting and monitoring systems can help anticipate extreme weather events and facilitate timely response and preventive measures to enhance the resilience of the power grid. The existing OHLs at HOPS are designed in accordance with the »Regulation on technical norms for the construction of overhead power lines with a a nominal voltage of 1 kV to 400 kV« [14] (hereinafter - Regulation).

The equation of wind load on a conductor or ground wire is defined as (Article 8, Regulation):

$$F_c = P_d \cdot C_{dc} \cdot L \cdot d \cdot G_c \quad (1)$$

where P_d is design wind pressure, C_{dc} is drag coefficient, L is wind span, d is diameter of conductor/ground wire and G_c is gust response factor. Similarly, equation of wind load on towers is defined as:

$$F_t = P_d \cdot C_{dt} \cdot A \cdot G_T \quad (2)$$

where P_d is design wind pressure, C_{dt} is drag coefficient, A is effective area and G_T is gust response factor for towers.

When calculating the wind load, the surface of the object is considered as the actual surface, without additional load, attacked by the wind. For cylindrical columns and for grid columns, only the surfaces facing the wind are taken into account (Article 9, Regulation).

For almost all OHLs in the continental part of Croatia, under the jurisdiction of transmission areas ZG and OS, abasic wind pressure of 600 N/m2 is assumed for design (in accordance with Article 10, Regulation). Based on Art. 10 of the Regulation, the relationship between wind speed and pressure is defined:

$$P_d = \frac{v^2}{16} \ [daN/mm^2] \quad (3)$$

where v is the maximum wind speed [m/s] for the area that appears in the period of the last 5 years (or in the longer observed period for 400 kV lines). According to the regulation, minimal wind pressure is 50 daN/m² (for basic height 40 m above ground).

The coefficients of wind action on individual parts of transmission lines are given in Art. 11 of the Regulations. Therefore, the maximum wind speed for the calculation of wind pressure is determined on the basis of several years of measurements and the application of statistical processing of measurement data.

All new building structures should be dimensioned according to the Eurocodes, and for wind loads, the proposal known also as "NNA" (the Croatian addition to the norm, which is still not approved) was created for HRN EN 1991-1-4:2012, Eurocode 1: Actions on structures - Part 1-4: General actions. - Actions of the wind - National supplement, with a wind map for Croatia [15].

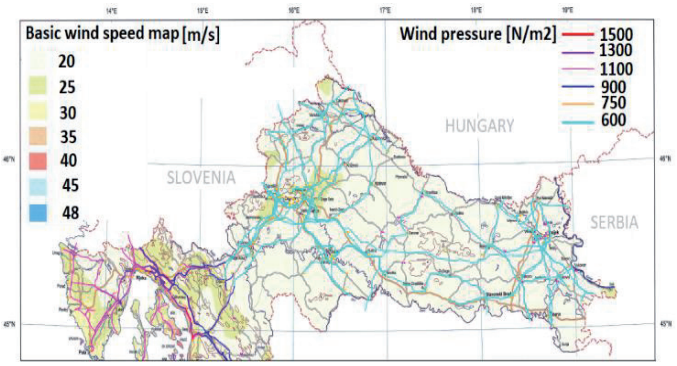

Fig. 5. Basic wind speed map of transmission areas ZG and OS, with the routes of the existing OHLs and the design wind pressures

As can be seen on the map from Figure 5, in the continental area (transmission areas ZG and OS), the basic expected wind speed 10 m above ground is 20-25 m/s, with a maximal wind gust of 40 m/s and the probability of 2% that it will be exceeded in 50 years. Also, an important parameter for the design is the basic wind pressure on sections of 110 kV, 220 kV, and 400 kV OHLs, which is for the observed area 600 N/m2.

In the coastal area, the basic expected wind speed exceeds 25 m/s, with maximal wind gusts greater than 40 m/s. Even nowadays, during the design stage of OHLs (according to the Eurocode), the loads on the structure are calculated differently in the past, it is obvious that nowadays it is more and more possible to experience extreme weather conditions. According to this, it is needed to consider whether the basic wind maps should be updated more

Goran Levačić, Igor Lukačević, Krešimir Mesić, Mate Lasić, Petar Končar, Igor Ivanković, Impact Of Climate Change on Transmission System Operator Assets: Experiences from Croatia and Need for Resilience Plan, Journal of Energy, vol. 73 Number 3 (2024), 44–51
https://doi.org/10.37798/2024733537

frequently, since they present an important input for the calculation at the OHL design stage.

Furthermore, such maps should be correlated with the most critical OHLs from the system operation state of view (according to N, N-1 or similar criteria), and based on this, TSOs can require from OHL designers consideration of stricter requirements (for towers structure and basement).

III. Example Of Climate Change Impact On OHLs In Croatian Transmission Network

On Wednesday, July 19th, 2023, northwestern and eastern Croatia were hit by a strong storm accompanied by hurricane-force winds and thunder, which caused a serious breakdown in the power system [16].

During the afternoon, a convective storm formed west of Slovenia and intensified around the border area of Italy, Slovenia, and Austria. The storm moved towards the affected areas from the west (Slovenia) towards Zagreb and further to the east. Radar images (source: State Hydrometeorological Institute - DHMZ) show the direction of the storm from 15:30 (immediately before the first driving event) until 18:30, in steps of 30 minutes (Figure 6).

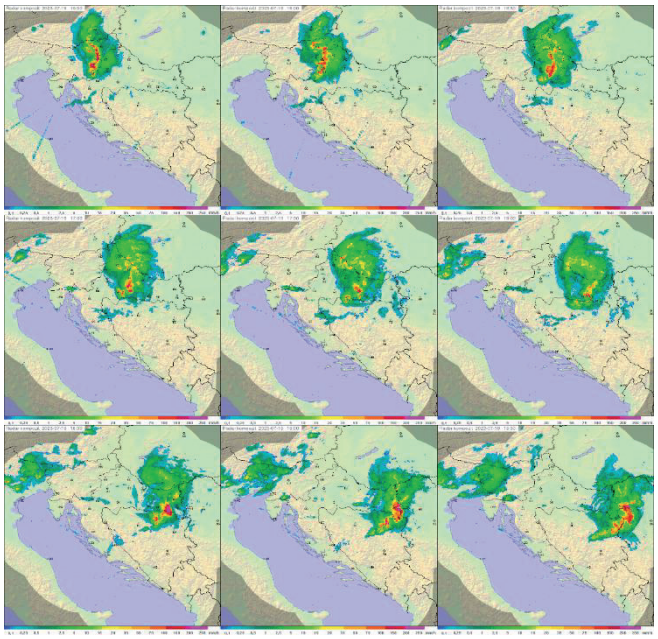

Fig. 6. The storm over Croatia from 15:30-18:30 h on radar

On its way to the east, the storm came over a plain area with ground temperatures of 28-31°C and dew points around 20°C, which enabled further strengthening in a CAPE (Convective Available Potential Energy) environment of over 1500 J/kg, in places even more than 2500 J/kg.

The storm was extremely strong and resulted in its transformation into a supercell that caused serious material damage, including hail with a diameter of about 10 centimeters, extremely strong wind shock fronts, and numerous damaged buildings in the area of Zagreb and Slavonia.

In addition to the hail, the storm was characterized by an extremely strong wind shock front (called a downburst), which, according to measurements, exceeded 20-30 meters per second at the largest number of affected measurement locations. The highest wind speed (44.7 m/s or 161 km/h) and wind gust (52.3 m/s or 188 km/h) were recorded at 17:04 int he area of the city of Kutina—as it is shown on Figures 7 and 8, which are significantly higher values than OHLs are designed for.

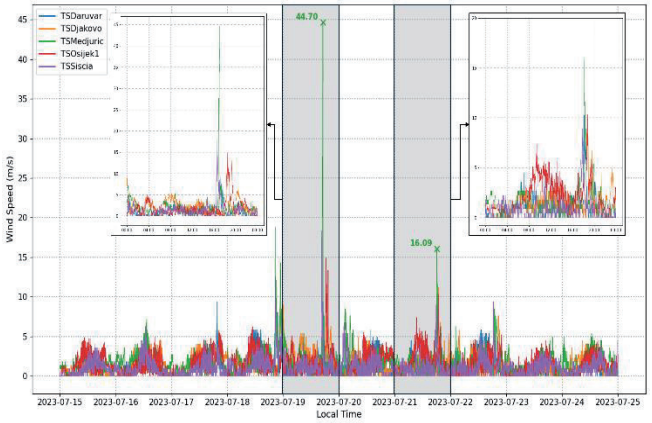

Fig. 7. Wind speed measured at several substations in the area affected by the storm from July 15th to July 24th

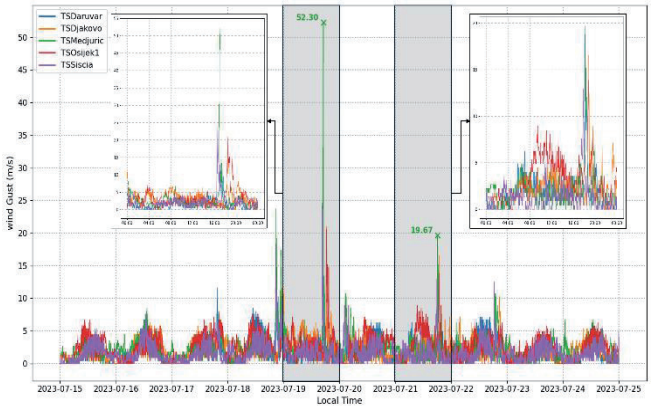

Fig. 8. Wind gust measured at several substations in the area affected by the storm from July 15th to July 24th

In parallel with the ongoing storm, numerous lightning strikes occurred in the mentioned areas of transmission areas ZG and OS, causing direct outages of nine overhead lines (Figure 9). HOPS uses a system for locating atmospheric discharges (SLAP) that provides data on lightning strikes that occurred over the observed area. The SLAP system is connected to the SCADA system and enables the correlationof lightning strikes with the indication of events in thenetwork.

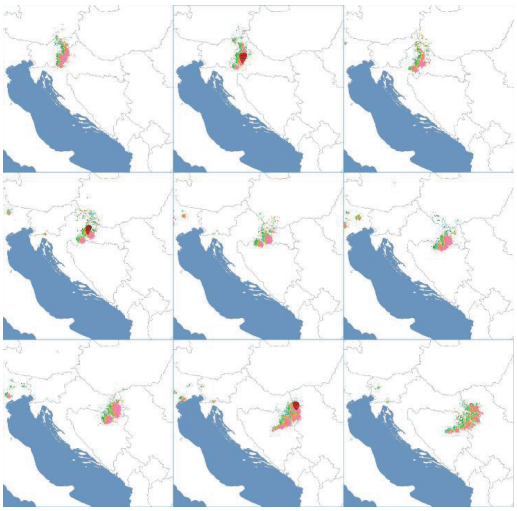

Fig. 9. Lightning strikes recorded during storm with lightning location system SLAP

Goran Levačić, Igor Lukačević, Krešimir Mesić, Mate Lasić, Petar Končar, Igor Ivanković, Impact Of Climate Change on Transmission System Operator Assets: Experiences from Croatia and Need for Resilience Plan, Journal of Energy, vol. 73 Number 3 (2024), 44–51
https://doi.org/10.37798/2024733537

In addition to the first storm, on July 21st, 2023, another storm further worsened the situation, contributing to new transmission line outages in the transmission area ZG.

An average wind speed during the storm on July 19th, 2023, was 88 km/h, and the storm encompassed a 350 kmwide area, whereby system SLAP recorded 363.872 lightning strikes (from 14:00 until 20:00), which equals 1010 strikes/min, with 9 OHL outages.

Similarly, an average wind speed during the storm on July 21st, 2023, was 94 km/h, and the storm encompassed a 470 km wide area, whereby system SLAP recorded 718.184 lightning strikes (from 14:00 until 20:00), which equals 1994 strikes/min, with 4 OHL outages.

As a consequence, due to the effects of the storm, an outage occurred on 14 overhead lines in the transmission area ZG and 8 in the transmission area OS with significant damage to towers and other equipment.

In the transmission area ZG, a total of 20 towers were damaged, 13 of which were broken, that is, the damage to the structure is such that it is not possible to correct the damage only with locksmith interventions. Looking at the km of the route, a little more than 5 km of the transmission line route was damaged in total. For the needs of temporary transmission line operation, 10 modular emergency towers were used.

In the transmission area OS, a total of 31 towers were damaged. Of these, 27 were completely demolished and 4 towers were damaged. Looking at the kilometers of the route,a total of about 12 km of the transmission line route was damaged. For the needs of the temporary operation of the transmission line, 12 modular emergency towers were installed. On the 110 kV voltage level transmission lines, modular towers were installed by HOPS, and on the interconnection (HR-RS) OHL 400 kV Ernestinovo - Sremska Mitrovica, two emergency towers were installed by the contractor.

Overview of consequences of OHLs outages, obtained from the Network Manager SCADA system (based on [16]), are shown in Table 1. The exact causes of the OHLs outages were determined subsequently by inspecting the routes according to the locations obtained from the inputs from the relay protection department.

TABLE I.

OVERVIEW OF THE CONSEQUENCES AFTER STORMS AND TOTAL IMPACT ON TRANSMISSION NETWORK

	110 kV	220 kV	400 kV
Total No. of disconnected OHLs	51	7	1
Total No.ofdisconnected OHLs due to lightning strikes	10	3	0
Total No. of damaged OHLs	14	5	3
Total No. of damaged OHL towers	40	5	6

Figures 10 and 11 shows some of damaged towers on location of transmission area ZG, while Figures 12 and 13 some of damaged towers on transmission area OS.

Fig. 10. Damages on OHL 110 kV Međurić – Daruvar located in transmission area ZG (tower no. 3) due to storm on July, 2023

Fig. 11. Damages on OHL 220 kV Međurić – TPP Sisak located in transmission area ZG (tower no. 99) due to storm on July, 2023

Apart fromthe unavailability of a large number of OHLs, asa consequenceofthetwostorms,therewasnomajorlossof consumption (EnS from 19th–21st July 2023 was <50 MWh), except during the moments of the storm in certain localities, which is significantly less than a comparable event caused by ice conditions in 2014 (in the transmission area RI, when EnS through 5 days was ≈ 100 MWh).

Fig. 12. Damage on OHL 400 kV Ernestinovo – Sremska Mitrovica located in transmission area OS (tower no. 120) due to storm on July, 2023

Goran Levačić, Igor Lukačević, Krešimir Mesić, Mate Lasić, Petar Končar, Igor Ivanković, Impact Of Climate Change on Transmission System Operator Assets: Experiences from Croatia and Need for Resilience Plan, Journal of Energy, vol. 73 Number 3 (2024), 44–51
https://doi.org/10.37798/2024733537

Fig.13. Damage of 110 kV OHL near substation

In the event of a OHL emergency, it is necessary to act immediately and to start with recovery measures, which require organized work and clearly defined procedures withthe aim of establishing the normal operating state as soon as possible.

After the accident, the most important thing was to find possible network power supplies and to perform urgent temporary or permanent recovery of the damaged OHLs, based on the realistic possibilities in the network considering the significance of their damage.

For that reason, modular towers are used. Emergency modular towers enable the establishment of temporary operation of a damaged overhead line in such a way that interruption of operation is minimal. The same is achieved in such a way that, after their installation, conductors and grounding wires are transferred to them. This enabled uninterrupted operation of the transmission line until the construction of new steel lattice towers, and the interruption of operation was limited only to the time needed to disconnect the conductors and grounding wires from the existing pole and hang them on temporary modular towers. An example of their implementation is shown in Figures 14 And 15 and previously used and elaborated [13].

Fig.14. Modular tower installation

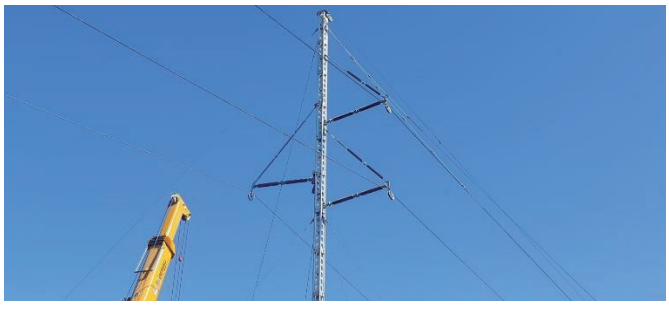

Fig. 15. View on consoles and conductors of one installed modular tower

HOPS owns modules and equipment for the formation of 110 kV, 220 kV, and/or 400 kV towers [13,16], but it is important to mention that without support from neighboring TSOs and loans of their modular towers, there wouldn't be enough of them, and the normal operation of the transmission network would not be established.

In the transmission area ZG, the next day after the storm on July 19th, preparation for damaged OHL recovery has started, and priorities for repair have been agreed upon. The priorities implied the establishment of temporary powersupply for OHL 110 kV Međurić–Daruvar (which was put back in temporary operation on 28th July), OHL 220 kV Međurić–TPP Sisak, due to the importance of the line for the 220 kV network (which was put back in temporary operation in the middle of August), and other 110 kV OHLs.

On the transmission area OS, priorities for repair implied OHLs 220 kV Đakovo–Gradačac and Đakovo–Tuzla (where temporary repair was not possible considering the major damage on the BA side), interconnection OHLs 400 kV Ernestinovo–Sremska Mitrovica (which was put back in temporary operation in the middle of August), and other 110 kV OHLs.

Final repair of the damaged OHLs lasted until the first half of 2024, due to the procurement procedure of replacement equipment etc.

IV. Recommendations and Lessons Learned

This paper shows an example of direct impact of climate change on essential TSO assets, such as power system OHLs or substations. It is shown that in areas with basic expected wind speed in the range of 20-25 m/s, a wind with strength above 50 m/s can occur and consequently, cause significant damage in a wider area, and therefore endanger the safe operation of the entire power system. From this, we can conclude that TSOs should be prepared to act immediately,and therefore:

- to consider establishment of internal resilience mechanisms (methodology and plan) based on a probabilistic risk-based method including different climate models,
- to establish a database of emergency events at the TSO level,
- to ensure availability of weather data & measurements from different platforms & tools (particularly for wind, ice, snow, wildfire, floods, lightings, saline pollution, dust, sand, and other possible weather impacts),
- to prepare risk maps based on the above-mentioned data, update them on a yearly basis, and correlate them with the most critical overhead lines from the system operation state of view,
- to prepare the "action plan for unpredictable weather phenomena" with neighboring TSOs/DSOsand other relevant institutions in the country, including determination of the OHL priority list for the returnto operation in case of emergency events,
- to ensure enough replacement equipment for unpredictable weather phenomena (i.e., modular towers, insulators, etc.),
- to ensure enough technical staff (together with machinery/vehicles) that will be in a state ofreadiness for emergency events and to educate them on how to design and mount such equipment,
- to establish an internal working group that will recognize and recommend stricter requirements according to valid standards and communicate them to the transmission line designers (i.e., NNA in Croatia).

Goran Levačić, Igor Lukačević, Krešimir Mesić, Mate Lasić, Petar Končar, Igor Ivanković, Impact Of Climate Change on Transmission System Operator Assets: Experiences from Croatia and Need for Resilience Plan, Journal of Energy, vol. 73 Number 3 (2024), 44–51
https://doi.org/10.37798/2024733537

In general, grid resilience refers to the ability of an electrical power grid to anticipate, prepare for, respond to,and recover from disruptions, whether caused by natural disasters, cyberattacks, equipment failures, or other unexpected events.It involves the grid's capacity to maintain and quickly restore reliable electricity supply in the face of such challenges.

It is obvious that the causes of OHL outages can be from different factors and that it is impossible to predict them, especially if they are being triggered by unpredictable weather events. So, it is important for TSOs, especially located in our Mediterranean region to consider establishing of Resilience mechanisms, in terms of "Resilience Methodologies and Plans", that are already implemented in other TSOs.

For instance, TERNA (IT) has integrated climate adaptation measures into its operations.Key initiatives include climate impact assessments, resilient design standards, methodology and plan, and digitalization [17-18].

IPTO (GR) has a resilience strategy [19] that emphasizes the importance of network modernization to manageincreasing renewable energy penetration and extreme weather resilience by strengthening inter-island and mainland connections to reduce dependency on vulnerable systems, deploying advanced automation and monitoring systems to anticipate and mitigate risks from climate-related disruptions, etc.

Tennet (NE & DE) integrates resilience [20] into its operations by deploying innovative offshore grid solutions. One of its key strategies includes the development of multi- purpose interconnectors, which combine the functions of connecting offshore wind farms and enabling cross-border electricity trade. This reduces the need for extensive infrastructure while ensuring reliability and adaptability to extreme weather events.

National Grid (UK) has a detailed climate change adaptation plan [21] that includes investments in flood defenses, upgradings ustations,and using predictive analytics to assess risks from extreme weather. The company allocated over £150 million to mitigate flooding risks at high-priority sites and has embedded resilience measures into its asset management strategies.

Elia (BE) focuses on grid reinforcement and the deployment of digital technologies to enhance operational resilience [22]. They conduct regular assessments of infrastructurevulnerabilityto extreme weatherandcollaborate with other European TSOs to optimize grid stability during regional crises.

Such resilience measures not only protect infrastructure, but also ensure continuous operation amidst increasing climate-related disruptions. Construction of new infrastructure is definitely the best preventive measure for increasing grid resilience, but not always possible. So, the establishment of monitoring & observability measures is also very important, and requires the implementation of smart grids, new technological solutions, digitalization etc.

V. Conclusion

In recent years, the effects of climate change have led to increasingly frequent extreme weather events. For TSOs, it means greater exposure of their infrastructure to levels of stress that could endanger service continuity. Understanding these potential impacts is crucial for designing resilient,robust, and adaptive energy infrastructure.

Due to strong storms that occurred on July 19th and 21st, 2023, and direct impact of strong wind and lightning strikes,in total, 59 OHLs were disconnected from the network.Almost half of these OHLs were significantly damaged. In total, 51 transmission towers were damaged, which is equal to approximately 17 km of transmission route. In order to immediately restore the damaged part of the transmission network, in total, 22 modular emergency restoration towersare used. Other damages require more time for repair.

This fact led us to the conclusion that detailed planning and preparation in advance are necessary, together with the determination of critical OHLs that will likely remain undamaged and, as such, help in restoring the network as soon as possible.

Also, based on example from this paper, it would be beneficial for TSOs to ensure enough modular emergency restoration towers and other equipment, in order to cover at least a 25-30 km route of transmission line corridor.

Taking into account all the events of the last few years, it is evident that the impact of climate change is gaining momentum. Although the number of OHL outages and damages cannot be immediately visible in the statistics of operating events, TSOs should consider stricter OHL design requirements in order to adapt to the newly created circumstances. It can be beneficial for the design of new OHLs, especially if they are located in areas sensitive to some of the above-mentioned climate factors.

At the end, as climate change continues to present new challenges, the resilience of power networks is playing an increasingly vital role in ensuring reliable and sustainable energy supplies. So, in the new circumstances, TSOs should consider the establishment of resilience mechanisms. By adopting a holistic approach that includes technological innovation, infrastructure upgrades, policy support, and community engagement, power networks can be better prepared to face the impacts of climate change and maintain continuity of service in the face of growing uncertainties.

References

[1] United Nations Environment Programme (UNEP), "Climate change in the-Mediterranean," UNEP/MAP, 2021. [Online]. Available:https://www.unep.org/unepmap/resources/factsheets/climate-change.

[2] IPCC, "Mediterranean Region: Climate Change 2022: Impacts, Adaptation,and Vulnerability," Sixth Assessment Report, 2022. [Online]. Available:https://www.ipcc.ch/report/ar6/wg2.

[3] MedECC, "Climate and Environmental Change in the Mediterranean Basin:Current Situation and Risks for the Future," Union for the Mediterranean(UfM), 2020. [Online]. Available: https://www.ufmsecretariat.org/medecc-report.

[4] Mediterranean Experts on Climate and environmental Change (MedECC),"Interlinking climate change with the Water - Energy - Food - Ecosystems(WEFE) nexus in the Mediterranean Basin Summary for Policymakers",2024 ISBN: 978-2-493662-09-5 doi: l0.5281/zenodo.13365388

[5] Dowling P., "The Impact of Climate Change on the European EnergySystem", ENERGY POLICY 60; 2013. p. 406-417. JRC76197

[6] K. Sullivan, A. Mehos, R. Jones, and J. Reese, "The impact of climatechange on EU energy system resilience", Published in: Climatic Change(2015)

[7] Cronin, J., Anandarajah, G. Dessens, O., "Climate change impacts on the energy system: a review of trends and gaps", Climatic Change 151, 79–93(2018),https://doi.org/10.1007/s10584-018-2265-4

[8] P. Vassolo, L. Ganbat, and T. H. C. Zeyer, "Climate change impact assessment on energy infrastructure with focus on the water-energy nexus,Published in: Environmental Research Letters (2019)

[9] IEA, "Power systems in transition - Challenges and opportunities ahead forelectricity security", 2020

[10] G. Marco Tina, Claudio F. Nicolosi, "Assessment of the Impacts ofClimateChange on Power Systems: The Italian Case Study", Appl. Sci. 2021,11(24), 11821; https://doi.org/10.3390/app112411821

[11] CRED,"Extreme weather events in Europe",IssueNo.64,2021.

[12] S. Vinter, I. Lukačević, K .Horvath, K. Pavić, "Analysis Of The OHL 110kVNašice–Donji Miholjac Breakdown",14th colloquium HROCIGRE, Šibenik,2019

[13] S. Vinter, H: Didak, Z. Bošnjak "Application Of Emergency Restoration-Towers For The OHL 400 kV Ernestinovo – Žerjavinec EmergencyOperation", 16th colloquium HRO CIGRE, Šibenik, 2023

[14] NN 24/l997 (28.2.l997.), “Modifications of Regulation on technical norms for the construction of overhead power lines with a nominal voltage ofl kVto 400 kV”

[15] HRNENl99l-l-4:20l2,Eurocodel:Actionsonstructures

[16] HOPS, “Internal analysis of the storm occurred on 07/2023 on the area of north-western and eastern Croatia and its impact on power system”, December,2023

[17] TERNA, RSE, “Metodologia per il calcolo dell’incremento della resilienza-della Rete di Trasmissione Nazionale”, Allegato A.76, 2022.

[18] TERNA,“PianoResilienza2022”,2022.

[19] IPTO,“Resiliencestrategiesandgridmodernization,”2023.[Online]. Available:https://www.admie.gr

[20] TenneT,“TenneToffshoreprojects,”2024.[Online].Available:https://www.tennet.eu

[21] NationalGrid,“ClimateChangeAdaptationReport,”2021.[Online]. Available:https://www.nationalgrid.com

[22] EliaGroup,“Strengtheninggridresilience,”2023.[Online].Available:https://www.eliagroup.eu

Goran Levačić, Igor Lukačević, Krešimir Mesić, Mate Lasić, Petar Končar, Igor Ivanković, Impact Of Climate Change on Transmission System Operator Assets: Experiences from Croatia and Need for Resilience Plan, Journal of Energy, vol. 73 Number 3 (2024), 44–51
https://doi.org/10.37798/2024733537

ENERGIJA